TRW REPORT NO. 36186-6016-UE-00
March 10, 1981
NASA CR165442

FINAL REPORT

IMPLICATIONS OF ARCING DUE TO SPACECRAFT CHARGING ON SPACECRAFT EMI MARGINS OF IMMUNITY

George T. Inouye

Prepared for

NASA/LEWIS RESEARCH CENTER
Cleveland, Ohio 44135

Under Contract No. NAS3-21961

TRW

Defense and Space Systems Group
One Space Park, Redondo Beach, CA

1 Report No	2 Government Accession No	3 Recipient's Catalog No
NASA CR-165442		

4 Title and Subtitle	5 Report Date
FINAL REPORT - IMPLICATIONS OF ARCING DUE TO SPACECRAFT CHARGING ON SPACECRAFT EMI MARGINS OF IMMUNITY	March 10, 1981
	6 Performing Organization Code

7 Author(s)	8 Performing Organization Report No
G T Inouye	36186-6016-UE-00
	10 Work Unit No

9 Performing Organization Name and Address	11 Contract or Grant No
TRW Systems, Inc One Space Park Redondo Beach, California 90278	NAS3-21961
	13 Type of Report and Period Covered
12 Sponsoring Agency Name and Address National Aeronautics and Space Administration Lewis Research Center 21000 Brookpark Road, Cleveland, Ohio	October 1979 - March 1981
	14 Sponsoring Agency Code 5532

15 Supplementary Notes

Project Manager, Carolyn K Purvis, NASA/Lewis Research Center, Cleveland Ohio

16 Abstract

An analytical and experimental study was performed to determine the implications of arcing due to spacecraft charging on spacecraft EMI margins of immunity The configuration of the P78-2 spacecraft of the SCATHA program was analyzed and two elements, one of the short booms and the large aft closure dielectric area, were selected for further study as being representative of the most hazardous components

A brushfire arc discharge model was developed and many features of the model such as the brushfire propagation velocity and the discharge waveform (risetime duration and magnitude) were confirmed experimentally A technique for initiating discharges with a "spark plug" trigger was developed and used to obtain data which would otherwise have been difficult to obtain

Combining the results of the analysis (including published data from other workers) and the experimental study, a set of best estimate arc discharge parameters was defined The effects of (positive) spacecraft potentials in limiting the discharge current blowout component were included Arc discharge source models were incorporated into a SEMCAP EMI coupling analysis code for the DSP spacecraft The results of the SEMCAP analysis were that no mission-critical circuits would be affected Negative EMI margins of immunity were obtained on a few housekeeping telemetry lines, but these represented the exceeding of detection thresholds rather than the approaching of component burnout levels

17 Key Words (Suggested by Author(s))	18 Distribution Statement
Spacecraft Charging, Electrostatic Discharges, Brushfire Arc Discharge Model, Arc Discharge Trigger Circuit, Best Estimate Arc Discharge Parameters, SEMCAP, EMI Coupling Analysis	

19 Security Classif (of this report)	20 Security Classif (of this page)	21 No of Pages	22 Price*
Unclassified	Unclassified	170	

* For sale by the National Technical Information Service Springfield Virginia 22161

TRW REPORT NO. 36186-6016-UE-00
March 10, 1981
NASA CR165442

FINAL REPORT

IMPLICATIONS OF ARCING DUE TO SPACECRAFT CHARGING ON SPACECRAFT EMI MARGINS OF IMMUNITY

George T. Inouye

Prepared for

NASA/LEWIS RESEARCH CENTER
Cleveland, Ohio 44135

Under Contract No. NAS3-21961

Defense and Space Systems Group
One Space Park, Redondo Beach, CA

CONTENTS

CONTENTS (Continued)

APPENDICES

ILLUSTRATIONS

ILLUSTRATIONS (Continued)

ILLUSTRATIONS (Continued)

TABLES

TABLES (Continued)

1. INTRODUCTION AND SUMMARY

The data on many aspects of the spacecraft charging phenomena generated on the ground by the Spacecraft Charging at High Altitudes (SCATHA) program and in-flight aboard the P78-2 spacecraft (launched January 30, 1979) offers an opportunity for verification of many of the notions about the hazards of spacecraft charging that have been promulgated in recent years. For example, in our TRW study, "Effects of Arcing Due to Spacecraft Charging on Spacecraft Survival," for NASA/LeRC, we reviewed the state-of-the-art (final report dated November 4, 1978) and concluded that much of the data available was of questionable applicability to spacecraft design, and that additional data was required to make a quantitative determination of the hazardous effects of spacecraft charging on typical space systems.

In particular, the prevalent technique for the grounding of test samples in laboratory measurements with a small resistance (typically 1 to 50 ohms) to measure arc discharge currents was criticized in that an unlimited source of replacement currents, the system ground, was not available in the in-flight configuration. The resulting increased (more positive) spacecraft potential would limit the amount of electron charge that could be ejected during an arc discharge. The ratio of blowoff currents to flashover current, G', was demonstrated to have a crucial role in determining the magnitude of electromagnetic interference (EMI) coupled into spacecraft electrical subsystems. The possible range of values for G' could range from about 10^{-5} to unity, but data on realistic values was not available and analytical estimation techniques were not developed.

In this study, the SCATHA program data was used as a baseline to investigate the "Implications of Arcing Due to Spacecraft Charging on Spacecraft EMI Margins of Immunity." Because the computerized Specification and Electromagnetic Compatibility Analysis Program (SEMCAP) was not available for the P78-2 spacecraft, a SEMCAP model of the Defense Support System (DSP) spacecraft was used for the purposes of this study. The SEMCAP model was modified to incorporate two selected elements, one of the short booms and the large flat dielectric area on the aft end of P78-2. The resulting data was not applicable directly to either DSP or P78-2. However, since both preflight ground test data as well as in-flight data

were available for P78-2, this information provided a valuable insight into how a typical spacecraft system, as exemplified by DSP, would react to the geosynchronous orbit energetic plasma environment. Furthermore, various aspects of this study provided an insight into the behavior of the P78-2 spacecraft in response to its environment. The flow diagram of tasks performed in this study is shown in Figure 1-1. The tasks are listed in Table 1-1.

1.1 SUMMARY OF THE MAJOR CONCLUSIONS OF THIS STUDY

The major conclusions reached in this study are as follows:

- The in-flight P78-2 spacecraft performance is generally consistent with the results of the analyses and experimental studies performed in this study.
- An initial formulation of a propagating arc discharge model has been made. Many improvements are necessary:
  - Include more physical processes
  - Improve the mathematical analysis methods
  - Define the arc breakdown processes.
- A concurrent experimental program is essential to guide the analytical work as well as to verify the analytical predictions. Many features of the brushfire arc discharge model were verified experimentally during this study.
- It is essential that the effects of the in-flight spacecraft configuration on the arc discharge blowout currents be taken into account.
- Large area dielectric surface arcs directly to cables must be prevented by routing. If this is not possible, appropriate EMC measures must be implemented.
- High voltage breakdown effects on nominal (low voltage) component parameters must be included as a part of the EMC analysis process.
- SEMCAP coupling analyses are useful procedures for evaluating the design of a spacecraft for immunity to arc discharges. More work needs to be performed to validate the accuracy of the discharge source models developed in this study.

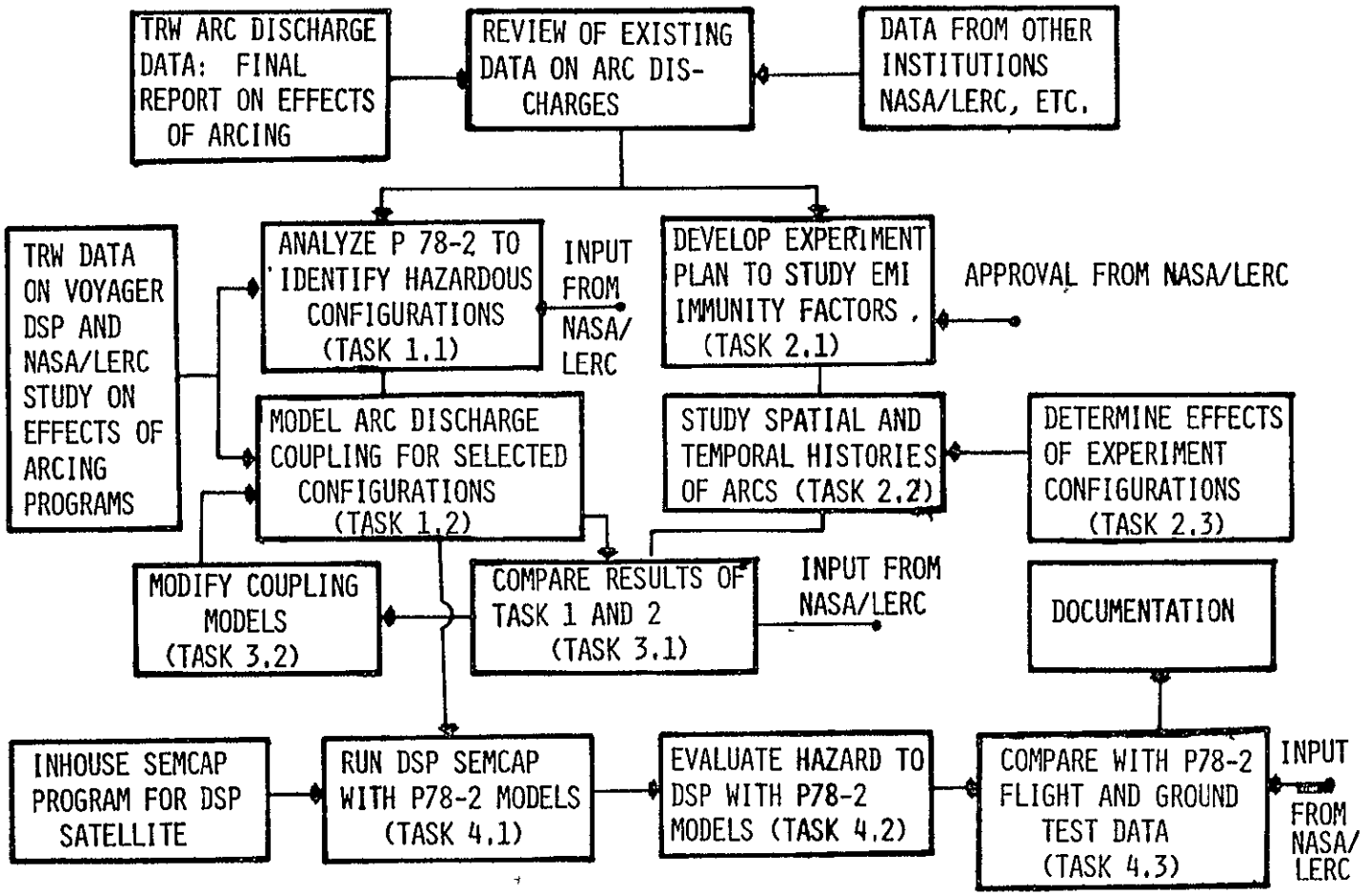

Figure 1-1. Approach in Determining Factors Impacting EMI Margins of Immunity of Arcing Due to Spacecraft Charging

Table 1-1. Tasks Performed in "Implication of Arcing Due to Spacecraft Charging on Spacecraft EMI Margins of Immunity"

Task 1:	Analytical Study of EMI Immunity Factors
Task 1.1	Analysis of the P78-2 Spacecraft Configurations - Meeting at SAMSO to select specific elements for further study
Task 1.2	Coupling Model Analysis of ARC Discharges
Task 2:	Experimental Study of EMI Immunity Factors
Task 2.1	Development of an Experimental Study Plan Submit to NASA/LeRC for Approval and Modifications
Task 2.2	Development of Diagnostics and Instrumentation
Task 2.3	Effects of Chamber Walls and Nearby Metals
Task 3	Comparative Study of Analytical and Experimental Results
Task 3.1	Comparison of Analytical and Experimental Study Results - Present Results at SAMSO Meeting
Task 3.2	Modify Arc Coupling Models as Indicated by Comparative Study
Task 4:	SEMCAP Study and P78-2 Results Comparison
Task 4.1	Run SEMCAP on DSP Model with Arc Sources
Task 4.2	Evaluate Hazard to DSP with these Sources
Task 4.3	Compare these Results with P78-2 Flight and Ground Test Results

1.1.1 Summary of Analytical Study Results, Task 1

The analytical study of the implications of arcing due to spacecraft charging on spacecraft EMI margins of immunity first focused on the configuration of the P78-2 spacecraft. Differences between that spacecraft and typical communications spacecraft were noted such as the presence of a large number of booms and the relatively small surface area covered with thermal blankets. The design was such as to minimize the effects of arcing with a good Faraday cage design and good shielding practices. For the purposes of the remaining analytical study as well as the experimental

study and EMI coupling study, two elements of the P78-2 spacecraft were selected for further study from a list of potentially hazardous configurations identified on the P78-2 spacecraft.

In the second portion of the analytical study a brushfire arc discharge propagation model was developed to account for the large area wipeoff of charge from a thin dielectric surface layer over a conducting substrate. The effects of the in-flight configuration as opposed to the laboratory test configuration were studied in terms of a blowout current and a flashover current component. Summary of the brushfire model results is found in Appendix 4. Highlights of the brushfire analysis and the P78-2 configuration results are summarized in Table 1-2.

Table 1-2. Highlights of the Analytical Study Results

- The P78-2 spacecraft was designed to minimize the effects of arcing.
- The P78-2 spacecraft differs significantly from typical communications satellites:
  - More booms
  - No large area dielectric surfaces likely to arc.
- Two elements of the P78-2 spacecraft were selected for further study from a list of possibly hazardous arcing sources:
  - One of the booms
  - The aft closure dielectric area.
- A brushfire arc discharge model was developed with the following features:
  - Propagation velocity = $2.45 \cdot 10^7$ cm/sec
  - Flashover surface current density = 3.18 amp/cm
  - Blowout surface current density = 1.86 amp/cm
  - G', the blowout to flashover current ratio = 58.5 percent
  - Blowout current is directed towards the arc initiation point
  - Blowout current is limited, cut off, by the rising spacecraft potential

1.1.2 Summary of Experimental Study Results, Task 2

The Experimental Study, Task 2, provided a number of unique results which were used to evaluate the implications of arcing due to spacecraft charging on spacecraft EMI margins of immunity. Table 1-3 lists the highlights of the experimental study results. The direct determination of the brushfire propagation velocity, $2.3 \cdot 10^7$ cm/sec, was made possible with the development of the arc discharge trigger. Without the trigger it would have been nearly impossible because the location, direction and timing of the discharges would have been undetermined. The determination of the spatial distribution of blowout currents was made possible by the 2-dimensional array of collectors, and the results also verify the predictions of the analytical brushfire model. The importance of the high voltage feedthrough for the sample grounding resistor, outside the vacuum system, was revealed by the inconsistent results obtained initially.

The high sample substrate voltage, ~20 kV, observed with grounding resistances greater than 1000 ohms, verified the rapid cutoff of the blowout electron current. The subsequent positive ion current arriving at the collectors, although not anticipated initially, was consistent with the high positive sample voltage. Looking at any single collector, one might expect that the sample voltage should drop back to near zero as quickly as it rose to ~20 kV. The fact that the sample voltage remained high for the duration of the brushfire discharge process indicated that the net ejected current must be neutral after the initial chargeup period of less than 100 ns. At the end of the brushfire process, electron ejection ceased, and the positive ion current predominated until the sample voltage was brought back to zero.

In addition to verifying the qualitative features of the analytical brushfire arc discharge model, the arc discharge parameters were quantified for both low and high sample substrate grounding impedances as summarized in Table 1-4 below.

Table 1-3. Highlights of the Experimental Study Results

1. Development of Diagnostics and Instrumentation
   - Arc discharge trigger
   - Blowout particle spatial distribution
   - Brushfire propagation velocity sensors
   - Importance of high voltage feedthrough
2. Measurements
   - Brushfire propagation velocity = $2.3 \cdot 10^7$ cm/sec
   - Electrons are blown off the surface, but in the direction of the discharge initiation point (≈45 degrees). The maximum-to-minimum ratio for different collectors is ≈10:1.
   - Flashover currents are ≈20 percent of blowout currents for low sample grounding impedance
   - Blowout electron currents are cut off early in the discharge with high sample grounding impedance
   - Brushfire propagation persists independent of grounding impedance
   - Sample voltage ≅20 kV when sample grounding impedance >1000 ohms
   - Ions are detected on collectors at later times during the discharge

Table 1-4. Experimentally Determined Arc Discharge Parameters

1. Brushfire propagation velocity: $2.3 \cdot 10^7$ cm/s
2. Low sample grounding impedance ($\sim$1 ohm)
   - Peak current $\cong$ 0.65 • area (cm^2) amperes
   - Current pulse waveform nearly triangular: $t_r \cong t_p \cong 40$ • side (cm) ns
   - Flashover current (to sideplate) $\cong$ 20 percent of replacement current
3. High sample grounding impedance (>1000 ohms)
   - Peak sample voltage $\cong$ 20 kV
   - Sample voltage resistive $\cong$ 100 ns
   - Sample voltage decay time $\cong$ 300 ns
   - Electron current to collector pad cut off in $\sim$200 ns

Many of the quantitative features of the arc discharge parameters were reevaluated in light of the analytical predictions and other available data in the comparative study, Task 3. For example, although the three data points on peak discharge amplitude variation with sample area seemed to indicate a linear dependence with area, both the analysis and other experimental data over a much wider range of areas indicated that the dependence should be as the square-root of the area. It turns out that there was no inconsistency in the amplitude results if they were interpreted as data applicable over a restricted range of areas.

1.1.3 Summary of Comparative Study Results

The comparative study of the analytical study, Task 1, and the experimental study, Task 2, resulted in a quantitative best estimate characterization of arc discharges which differed from previous concepts in many ways. Early predictions of arc discharge effects on spacecraft electrical systems were based on laboratory measurements with low test sample grounding impedances. The analytical study predicted and the experimental study confirmed that the large blowout electron currents observed with low sample grounding impedances did not apply when the impedance was greater than

1000 ohms. For a spacecraft in orbit, its ability to gather in replacement electrons was limited and its potential rose to collect more electrons. Also, in the process, a displacement current flowed to charge up its capacitance to space. This positive spacecraft potential cuts off the blowout current. Highlights of the comparative study are shown in Table 1-5.

Table 1-5. Highlights of the Comparative Study Results

- The best estimate low grounding impedance currents are

  I_{peak} (blowout) = 7.30 s(cm) amperes

  I_{peak} (flashover) = 12.5 s(cm) amperes

  Where s is the side of a square arcing source or the square root of the area of any large area source

- The best estimate G' value is 58.5 percent for a low grounding impedance

- The best estimate low impedance flashover current waveform is nearly triangular and is defined by

  $t_r = s/(2v_b)$, $t_p = 2\ t_r = 4.08 \cdot 10^{-8}$ s(cm) seconds

- G' does not apply in the in-flight situation

- The blowout current is independent of the size of the arcing source

  - For DSP I_{peak} (blowout) = 12.6 amperes
  - For DSP τ (cutoff) = 92 nanoseconds

- The low impedance flashover current waveform for a long narrow source such as a boom is nearly rectangular and is defined by

  t_r = (circumference)/(2 v_b); $t_p = L/v_b$.

- The low impedance flashover peak boom current is given by.

  $I_{peak} = (\text{diameter}) \cdot \pi^2 J_s/2$.

The best estimate arc discharge characteristics applicable to the in-flight situation was based on both low and high impedance analysis and test results. For a low grounding impedance the peak blowout current for a roughly square area was

$$I_{peak}\ (\text{blowout}) = 7.30\ s(\text{cm})\ \text{amperes}.$$

This peak current corresponded to a blowout surface current density, J_{sz}, of 7.96 A/cm instead of the 1.86 A/cm value derived analytically. Assuming that the analytically derived flashover surface current density, J_s, of 3.18 A/cm was correct, the peak flashover current was

$$I_{peak}\ (\text{flashover}) = 4.99\ s(\text{cm})\ \text{amperes}.$$

The best estimate ratio of blowout to flashover currents, G', was

$$G' = 1.46 \text{ or } 1.46 \text{ percent}.$$

This was 2.50 times greater than the analytically derived value of 58.5 percent. The fact that G' was greater than 100 percent was not disturbing because the analysis showed that a far larger number of free electrons were generated in the discharge process than were originally stored in the chargeup process.

For the high sample grounding impedance situation the best estimate blowout current was independent of the size of the arcing source provided its side, s, was greater than 4.35 centimeters. The cutoff time, τ, varied as the square root of the spacecraft diameter and was 92 nanoseconds for the 3-meter diameter of the DSP spacecraft. The peak blowout current also varied as the square root of the spacecraft diameter and was 12.6 amperes for the DSP spacecraft.

Finally, the analytical prediction and the experimental verification of the waveforms of the low impedance current pulse, triangular for the square sample and rectangular for the long narrow sample, was a very satisfying and unique result.

1.1.4 Summary of the SEMCAP Study and P78-2 In-Flight Results, Task 4

The conclusions of the SEMCAP study and P78-2 in-flight results comparison are highlighted in Table 1-6. The fact that SEMCAP predicted no problems and the fact that no serious in-flight anomalies were

Table 1-6. Highlights of the SEMCAP Study and the P78-2 Results Comparison

- SEMCAP predicted that no anomalous events would be detected on the (fictitious) DSP/P78-2 spacecraft model.
- This was consistent with the in-flight performance of P78-2 except for the failure of the two SC2 plasma voltage probes.
- A simple explanation for the SC2 probe failures was that the series 10 kΩ resistor broke down under arc discharge conditions.

observed on P78-2 were consistent. The failure of the two SC2 plasma voltage probes during electron gun operations on March 30, 1979 were simply explained by assuming a high-voltage breakdown across a 1/4-watt 10-kΩ resistor. It was unfortunate that the design of the P78-2 was not such as to permit large area arc discharges to occur, which was of concern in the design of operational spacecraft. The engineering experiments were unable to localize the arc discharges that did occur, thus making it impossible to make any quantitative evaluations.

The SEMCAP study result highlights are summarized in Table 1-7. Five different types of arc discharge sources were modeled:

- Localized inductive and capacitive sources
- Arc-to-cable shield
- Conductive replacement current (blowout)
- Capacitive replacement current
- Blowout current H-fields.

These sources were modeled for a large area at the aft end of the spacecraft and for a boom. A subset of transient sources (t_p = 10 ns) was included for each type.

Table 1-7. Summary of the SEMCAP Study Results

- Satellite circuits had safety margins ranging from +5 dB to +139 dB.
- Housekeeping telemetry lines had margins from -44 dB to +58 dB but no problems were expected.
- Arc-to-cable shields were the most likely source of problems. Cables should be routed to avoid dielectric surfaces likely to arc or be protected.
- Replacement currents due to blowout electrons were not a problem. Capacitive replacement currents was ≈40 dB smaller.
- Transients less than 10 ns were not a problem.

The response of the DSP receptor circuits had immunity margins of +5 dB to +139 dB, and the most probable values were 9 dB greater. Housekeeping telemetry lines had margins ranging from -44 dB to +58 dB, but no problems were expected because of the low-duty cycle at which these lines were telemetered. No burnout problems were expected for the type of interface circuits used.

1.2 RECOMMENDATIONS FOR FURTHER WORK

The work performed in the present study, "Implications of Arcing Due to Spacecraft Charging on Spacecraft EMI Margins of Immunity," provided an improved analytical and experimental basis for the formulation of arc discharge models for the SEMCAP electromagnetic analysis code. It was our premise that once the discharges were properly modeled, SEMCAP was the most efficient method of evaluating the design of a spacecraft system for immunity to arc discharges. Working backwards from the SEMCAP analysis, then, the recommendations for further work in improving the capability and confidence in minimizing arc discharge hazards to spacecraft systems are given in Table 1-8.

1.2.1 Validation of SEMCAP Arc Discharge Source Models

The source models generated in the present study incorporated best estimate arc discharge parameters, but lacked any validation of their accuracy. In the Voyager program, the SEMCAP models were updated as a result of several system level tests with diagnostics as well as stimulus

Table 1-8. Recommendations for Further Work in Improving Arc Discharge EMI Immunity

(1) Validation of SEMCAP arc discharge source models:
- Perform on-line SEMCAP analyses of simplified typical configurations
- Validate analyses experimentally with test configurations similar to those analyzed
- Document results for application to the design and verification of typical spacecraft systems
(2) Perform more extensive arc characterization tests
- Different materials (Mylar, Teflon, Kevlar)
- Different thicknesses
- Different configurations (area, shapes)
(3) Improve analytical model of arc discharges:
- Include more physical processes
- Improve mathematical analysis techniques
- Investigate arc discharge breakdown thresholds.

sources. What is recommended here is that simple models be constructed (conceptualized) and analyzed on an on-line version of SEMCAP. With such a technique source parameters such as geometry as well as pulse shape can be varied over a wide range of values. The effects of receptor characteristics such as input filter paprameters and threshold sensitivities may also be investigated in a systematic manner.

The experimental validation and the documentation of these results would provide a useful tool to be used in the early design phases of a new spacecraft system. Subsequently, as the design and fabrication progresses, the usefulness and confidence in the applications of SEMCAP will be reinforced with the backup data provided by this task.

1.2.2 Perform More Extensive Arc Characterization Tests

The experimental work performed in the present study gave confidence in the analytical work and also provided data which could not be obtained

easily by analysis. Because of the limitations of time and funding many aspects of the experimental work had to be curtailed. The effects of different dielectric materials, thicknesses, areas, and shapes should be investigated.

1.2.3 Improve Analytical Model of Arc Discharges

The analytical brushfire arc discharge model as developed in the present study provided an insight into many aspects of an arc discharge with first-cut quantitative values for flashover and blowout surface current densities. Many features of the present model need to be improved to provide a more cohesive and comprehensive model. Physical processes such as ablation and ionization need to be examined more carefully. The 1-dimensional mathematical analysis was simplified to provide crude answers, and should be approached in a more self-consistent manner using a computer.

Finally, the problem of the initiation threshold for arc breakdown has been passed over too lightly. Because of the many ways in which dielectric surfaces are installed in real spacecraft, the definition of a breakdown threshold is a difficult problem. We assume here that breakdown will be initiated at edges or stitching where the local electric fields are greatly enhanced. A realistic and believable breakdown initiation model must be developed and verified experimentally. One of the paradoxes that has developed in the spacecraft charging arena is that charging analyses tend to predict maximum differential potentials in the order of 3 to 4 kV on many different spacecraft configurations. In the laboratory, breakdown thresholds typically have been found to be 8 to 20 kV for many different kinds of sample materials. The reason for this difference by a factor of greater than 2 has not been resolved and needs to be investigated.

2. TASK 1: ANALYTICAL STUDY OF EMI IMMUNITY FACTORS

In this task, the P78-2 geometry and circuit layout were analyzed to identify hazardous arc discharge configurations. The results of this analysis was presented at a meeting at SAMSO at which the two potentially most hazardous configurations were selected for further analysis. The two P78-2 elements selected were one of the short booms and the large flat dielectic surface at the aft end of the spacecraft. Analytical models of the arc discharge sources were developed for incorporation into the DSP SEMCAP model. The flow of subtasks for Task 1 is shown in Figure 2-1.

2.1 TASK 1.1 ANALYSIS OF THE P78-2 SPACECRAFT CONFIGURATIONS

The purpose of this subtask was to provide familiarization with the P78-2 spacecraft and to provide a "shopping list" of potentially hazardous configurations from which the two most dangerous could be selected for further study in the remainder of this contract. Table 2-1 lists the documents which were studied. Figures from these documents have been extracted for various parts of this task and are referenced according to the numbering of Table 2-1.

2.1.1 P78-2 Spacecraft Exterior Surface Analysis

The most complete documentation of the P78-2 spacecraft configuration is given in References 1 and 2. Figure 2-2 from these references identifies the location of the various experiments, and Figure 2-3 from the same references identifies the materials on the exterior surfaces. A crude analysis of the constituents of the external surfaces of P78-2 has been made from the data shown in Figure 2-2. Table 2-2 lists the metallic and dielectric surface areas and their relative amounts in sunlight and in the dark.

The 18.8 percent exposed metal is rather high compared with the DSCS-II spacecraft, also a spin-stabilized spacecraft, where the proportion was less than 9 percent. The difference here is that P78-2 is a scientific spacecraft with requirements for large metallic areas to accommodate the on-board experiments, whereas DSCS-II is an operational communications satellite in which thermal control requirements, in a large measure, dictated the external surface materials. The percentage of metallic

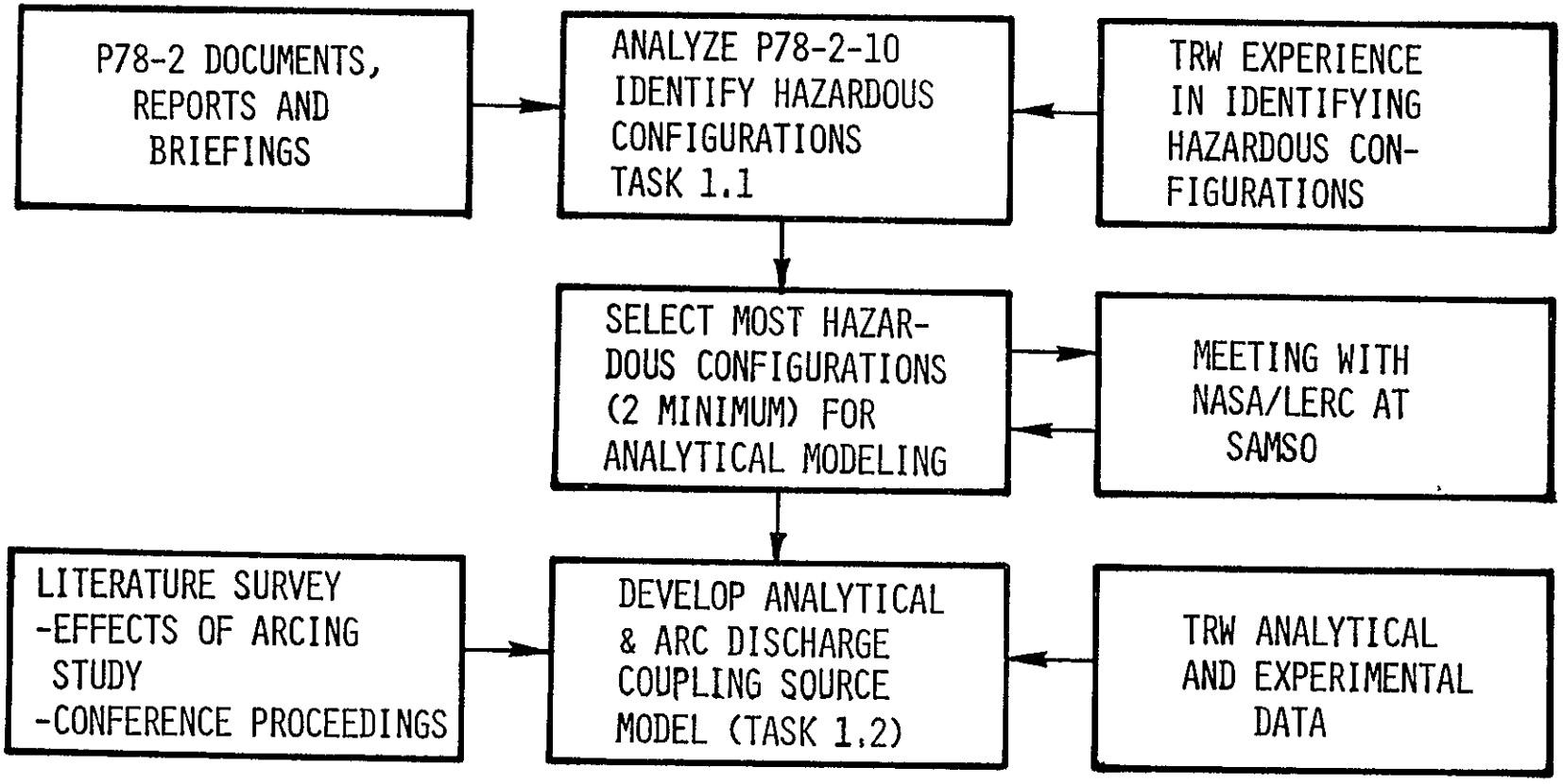

Figure 2-1. Task 1· Analytical Study of EMI Immunity Factors

Table 2-1. SCATHA-Related Documents Studied

(1)	SAMSO TR-78-24 "Description of the Space Test Program P78-2 Spacecraft and Payloads," 31 October, 1978
(2)	SAMSO/Martin-Marietta MCR-78-1207 "Preliminary Report of the Implementation of IEMCAP (IDIPR and TART) to the P78-2 Space Vehicle Program," 15 December, 1978
(3)	Report No. TOR-0079 (4505-02)-1 by P.F. Mizera, Aerospace Corp., "Preliminary Natural Charging Results from the P78-2 Satellite Surface Potential Monitors During the April 24, 1979 Event
(4)	Science Applications, Inc., LAC-171-80-128 "Minutes of the Spacecraft Charging Coupling Validation Meeting (SAMSO - 9 July, 1979)," 10 July, 1979
(5)	JPL ESD Workshop (October 2-4, 1979), "Viewgraphs as Made Available by Various Speakers"
(6)	IRT/J. Wilkenfeld "Internal Response of a Complex Satellite Model to Two Electron-Induced Discharge Simulation Techniques" IRT Document 4321-004 September, 1979, also presented at IEEE Conference on Nuclear and Space Radiation Effects, July 17-20, 1979

surface area in the dark, 82 percent of the total metallic area, implies that structure potential will tend to go negative during substorms. Our experience on tests of the TDRSS solar array, however, indicates that structure potentials cannot go much further negative in sunlight than 500 to 1000 volts before other effects such as secondary and high field emission of electrons limit potential excursions of this polarity.

The percentage of exterior dielectric surface area always in the dark, 8 percent of the total exterior surface area, is quite small. This excludes the solar array and miscellaneous bellyband dielectrics which go in and out of sunlight with each spacecraft rotation. Of this 8 percent, the major portion is the 0.87 m^2 of nonconducting white paint on the aft surface. This is one of the two elements selected for further study on the project. NASCAP identifies this paint as "whiten," of 2-mils thickness, and lists its dielectric constant to be 3.5 and its resistivity as $1.7 \cdot 10^{5}$ Ω/cm ($5 \cdot 9 \cdot 10^{-14}$ mho/m).

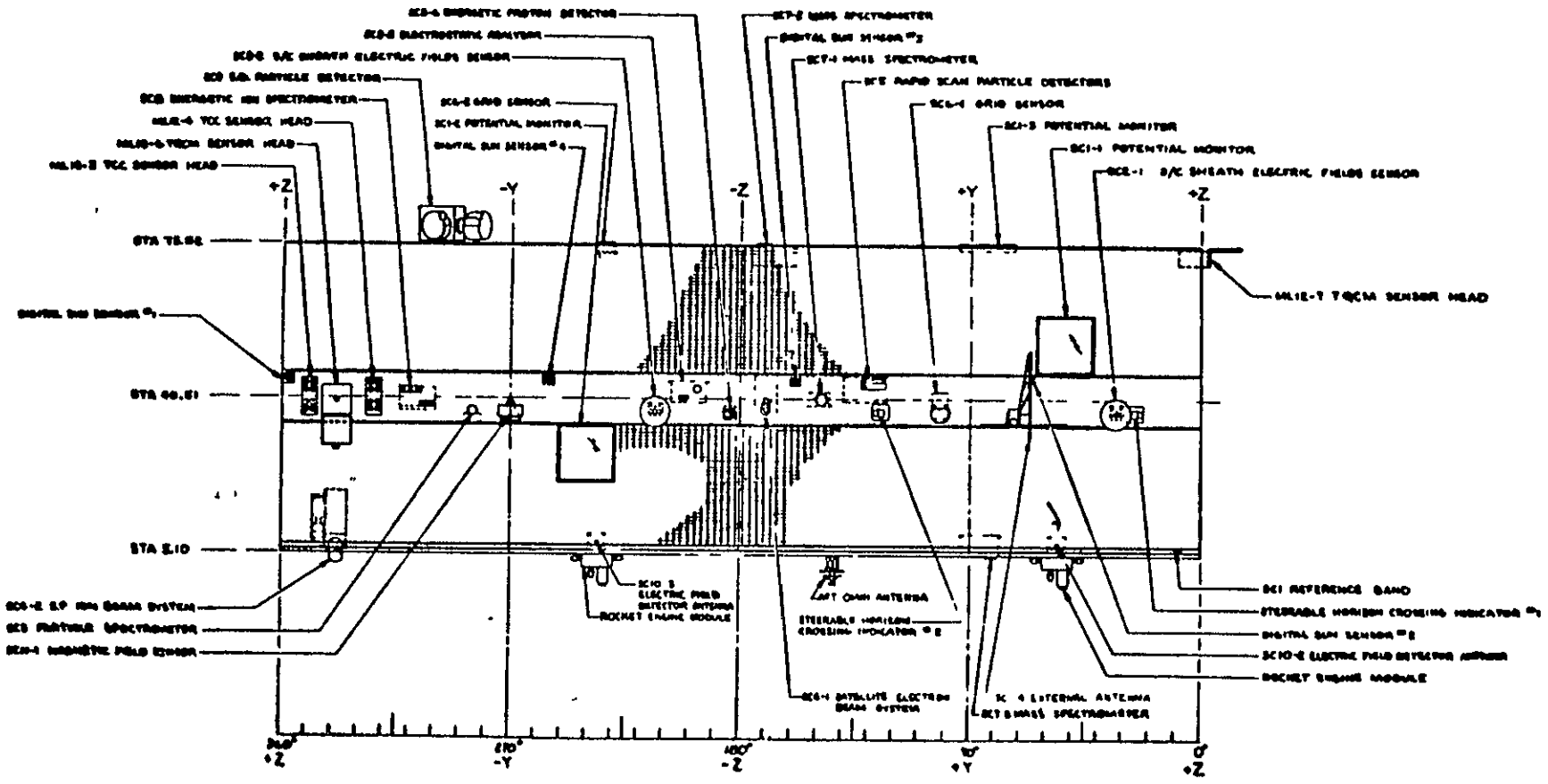

Figure 2-2. SCATHA Cylindrical Surface Features

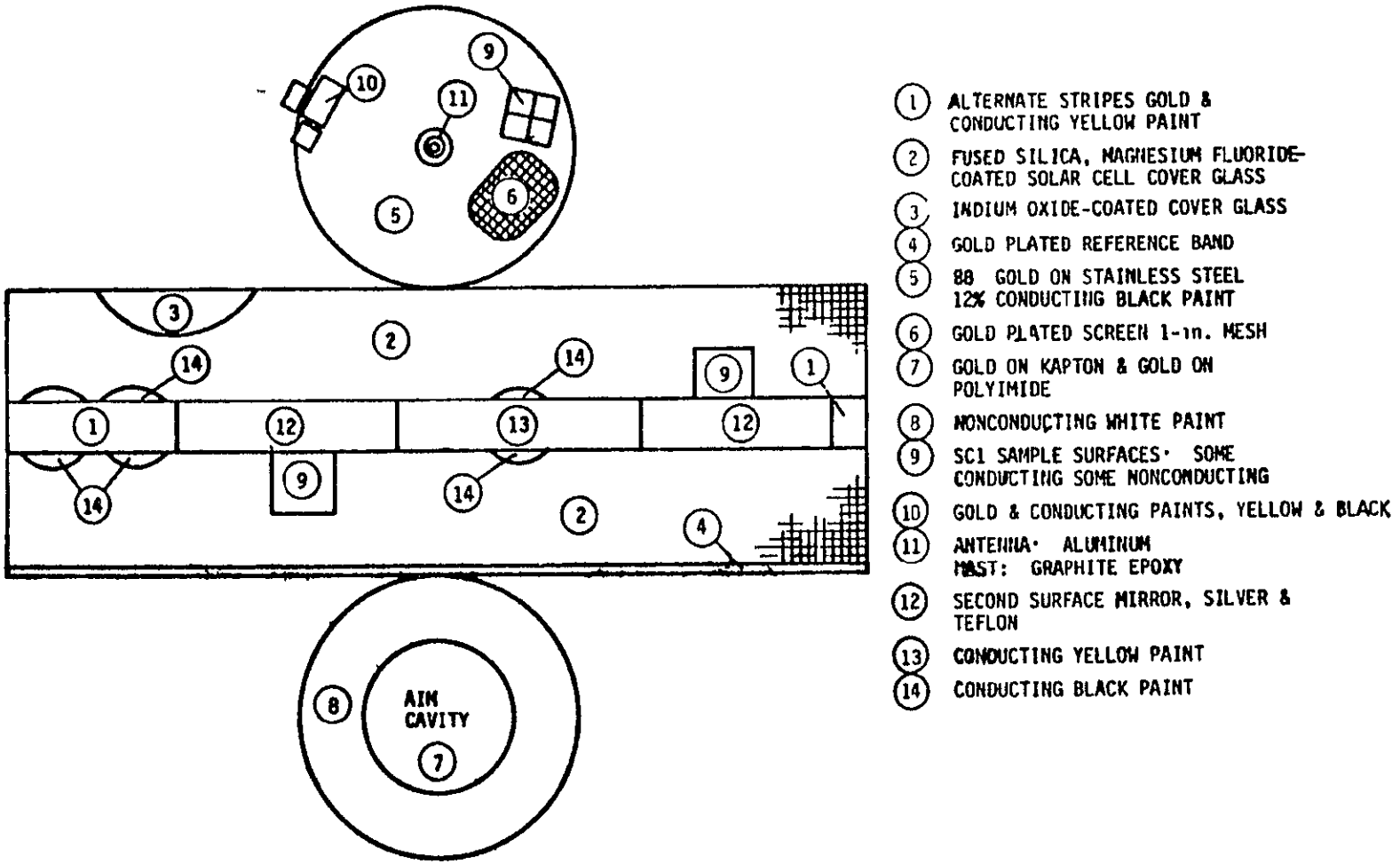

Figure 2-3. Identification of SCATHA External Materials

Table 2-2. Gross Surface Configuration of P78-2 Spacecraft (Excludes Booms)

	Sunlit Area	Dark Area	Total Area	Percent of Total
Solar Array	3.99 m^2	4.00 m^2	7.99 m^2	66.4
Bellyband Teflon SSM	0.41 m^2	0.41 m^2	0.82 m^2	6.8
Bellyband Metallic	0.41 m^2	0.41 m^2	0.82 m^2	6.8
Forward Metallic	-	1.11 m^2	1.11 m^2	9.2
Forward Dielectric	-	0.10 m^2	0.10 m^2	0.8
Aft Metallic	-	0.34 m^2	0.34 m^2	2.8
Aft Dielectric	-	0.87 m^2	0.87 m^2	7.2
	4.81 m^2	7.24 m^2	12.05 m^2	100

Total dark metallic area = 1.86 m^2 = 15.4 percent of total surface area

Total sunlit metallic area = 0.41 m^2 = 3.4 percent of total surface area

Total sunlit dielectric area = 4.40 m^2 = 36.5 percent of total surface area

Total dark dielectric area = 5.38 m^2 = 44.7 percent of total surface area

All sunlit exterior surfaces are in the dark for half of each spin period (~1 minute) because of the orientation of the spin axis in the orbit plane normal to the sun line. No seasonal changes in sunlit/dark ratios occur because of spin axis orientation. This situation is different from that for the DSCS-II spacecraft in which the spin axis is parallel to that of earth's. In that case the forward and aft ends are alternately sunlit and dark as the equinox crossings are passed.

2.1.2 In-Orbit Experiment Suggestion for the P78-2 Spacecraft

An experiment that can easily be performed on the P78-2 spacecraft, if sufficient attitude control gas is available, is to offset the spin axis from the sun-line normal by about 30 degrees for several days during a geomagnetically active period. Tilting the axis to let the sun shine on

the forward surface would change the sunlit metallic surface area from 3.4 percent to 12.8 percent of the total exterior surface area, and from 18 percent to 68 percent of the total metallic surface area. Tilting the spin axis in the other direction so that the aft end is sunlit, the dielectric area always in the dark is reduced from 8 percent of the total exterior surface area to 0.8 percent. Thus, the charging characteristics of the P78-2 spacecraft should be drastically changed, and these changes would provide additional data on material parameters as well as further validation of the charging analysis programs such as the NASA Charging Analyzer Program (NASCAP) and TRW's Spacecraft Charging Analysis Technique (TSCAT). The seasonal effect on the DSCS-II configuration, which this axis tilting on the P78-2 would simulate, has resulted in a very noticeable seasonal dependence on the frequency of occurrence of anomalies that may be attributed to spacecraft charging. This feature is shown in Figure 2-4. Also shown in Figure 2-4 is a plot of the magnetic activity index, A, for Fredericksburg, Virginia, over the same 5 year period. The correlation of anomalies with geomagnetic activity is not clear; however, the clustering of anomalies during the winter months is very evident. This effect has been demonstrated to be consistent with the DSCS-II configuration and sun-orientation by means of a charging analysis using the TSCAT analysis program.

2.1.3 General Comments on P78-2 Spacecraft Configuration

The general comments on the P78-2 spacecraft configuration in regards to spacecraft charging effects are summarized in Tables 2-3 and 2-4. Basically, the Faraday cage design and the double shielding of all exterior cabling should provide high immunity to arc discharges. The in-orbit data to date indicating only minimal arc discharging and even fewer spacecraft anomalies tends to validate this conclusion. The only real anomaly, the failure on March 30, 1979 of the SC2-1 and SC2-2 plasma potential sensors at the ends of two of the short booms, is clearly attributable to the operation of the electron gun. Data on the sequence of events on this day is shown in Table 2-5 which is taken from Reference 4 of Table 2-1. One of the short booms is the other element of the P78-2 spacecraft which was selected for further analysis in this present study.

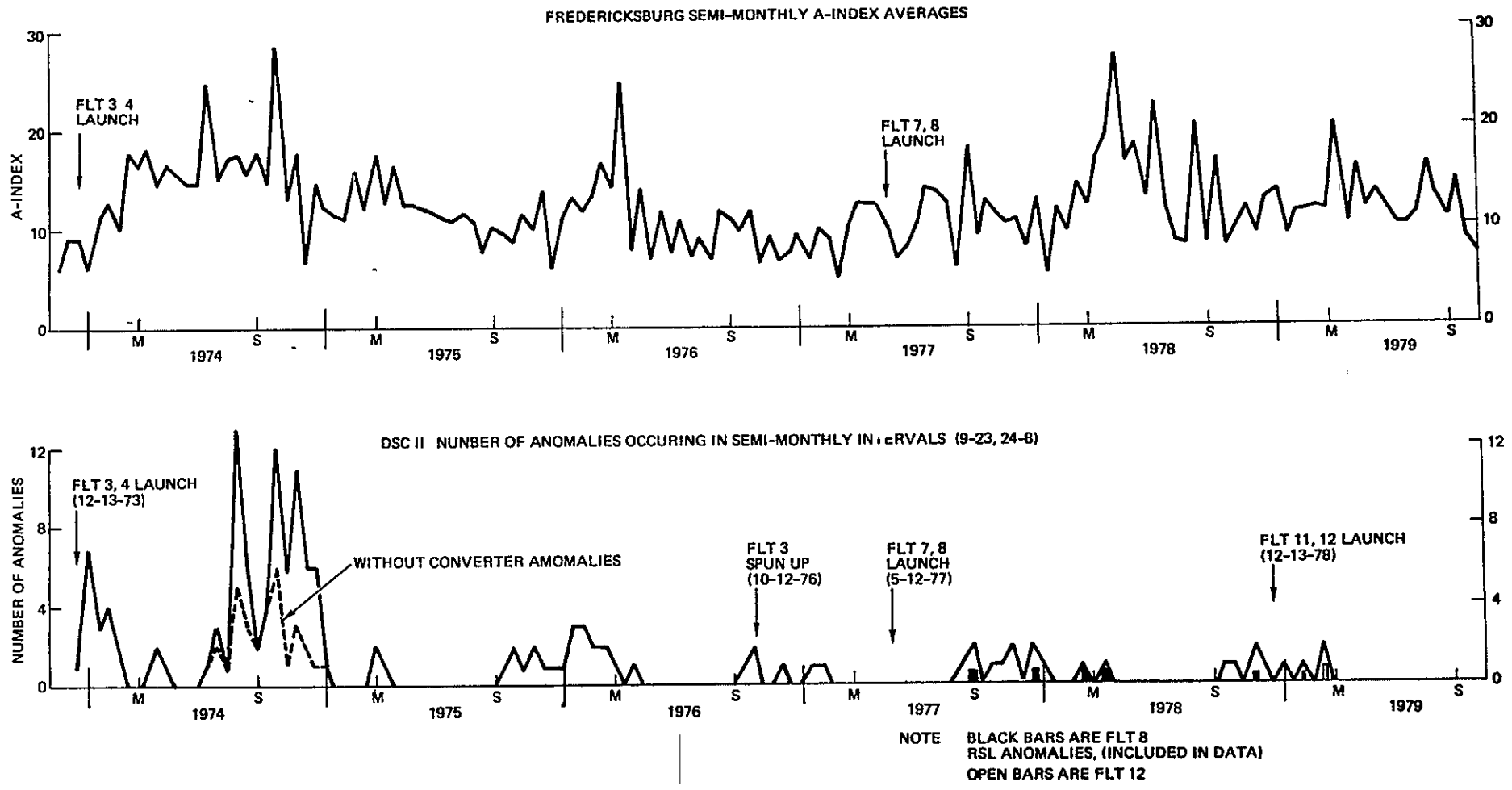

Figure 2-4. DSCS II Anomalies and the Fredericksburg, Va. Magnetic Activity Index (Semimonthly Intervals)

Table 2-3. General Comments on the P78-2 Spacecraft Configuration

- The Faraday cage design and the double shielding of all exterior cabling should provide high immunity to arc discharges
- The P78-2 configuration has many features that do not reflect an operational communications spacecraft:
  - Many booms
  - Electron and ion beam system
  - More metallic surface areas
  - Sensitive electric and magnetic field and particle sensors
- Thermal blankets are not used except for experiments
  - SC-1 thermal blanket configuration is not conventional
- Second surface mirror and thermal blanket areas are not comparable to those in operational spacecraft
  - Large area effects may not be reflected in the data
  - Need to put diagnostics on operational spacecraft

Table 2-4. Further Comments on the P78-2 Spacecraft Configuration

- 82 percent of metallic area is in the dark: structure potential will charge negatively
- Dark dielectrics may charge to more negative potentials than structure
  - Spacecraft spin affects cylindrical area dielectric potentials
  - Forward and aft dielectrics are always in the dark
- Sunlit dielectric potentials will be spin-modulated
- Platinum rings on the short booms are isolated metals
  - May charge more quickly due to small capacitance
  - Smaller charge storage because of small capacitance
- SC-1 thermal blanket samples probably will not arc because of framing -- except for those with a 1/4 inch hole in the middle

Table 2-5. P78-2 Electron Gun Operations - March 30, 1979

UT	Remarks
54728	Operation of SC4-1 at -1.5 kV and 6 mA, no observed deleterious effects
54728	SC4-1 commanded to -3 kV. TPM records 8.4 V negative pulse on Lo-Z sensor
54729	TPM records 7.0 V negative pulse on Lo-Z sensor
54730	SC2-1 plasma potential sensor fails
54736	P78-2 data system begins scrambled operation
54749	P78-2 data system corrects itself (at main frame 0)
54760	SC2-2 plasma potential sensor fails
54728-809	TPM records numerous pulses in the 6 V to 15 V range. Pulse characteristics measured by SC1-8B
54809	SC4-1 commanded to -1.5 kV. Pulses drop to 1 V to 3 V range
55056	SC4-1 current lowered to 0.01 mA, pulses cease
55122	SC4-1 commanded to -3 kV
55548	SC4-1 current raised to 0.1 mA
55570	TPM records 4.6 V negative pulse
55658	Beam voltage lowered to 0.3 kV; pulses cease

There are many features of the P78-2 configuration that do not reflect an operational communications spacecraft, mainly because of the scientific nature of its mission requires many environmental sensors. As a result, there are many booms and the percentage of metallic exterior surface area is much higher. The lack of thermal blankets and second surface mirrors for thermal control is immediately noticeable. The thermal control materials that exist are relatively small patches in the experimental sensors, and these are carefully configured to minimize the probability of arcing. Thus, as has been the in-flight experience, data on arc discharges has not been extensive. In particular, effects of large area discharges cannot be obtained.

The platinum rings on the short fiberglass booms could be sources of metal-dielectric-metal arcs because of their electrical isolation and low effective capacitance to the cabling running along the length of the boom. Arc discharges from these metallic rings should be frequent because of their low capacitance, but also of small magnitude because of the small stored charge. Their proximity to the boom cabling, however, is a source of some concern.

2.1.4 Potentially Hazardous Arcing Configurations on P78-2

The potentially hazardous arcing configurations on the P78-2 spacecraft are summarized in Table 2-6. These have been grouped according to whether the spacecraft potential is highly negative or near zero potential. As indicated previously, the situation in which the spacecraft potential is negative by many kilovolts is highly unlikely because of the high field emission and secondary emission of electrons which occurs before a ∿1 kilovolt negative potential is reached. Nevertheless, such low voltage arc discharges are a possibility.

Table 2-6. Potentially Hazardous Arcing Configurations on P78-2 Spacecraft

Spacecraft Potential Highly Negative
• Solar array
• Sunlit second surface mirrors teflon on bellyband, SC-1 samples
• Platinum rings on fiberglass epoxy base, five short booms
• Reference band at aft end
• Other dielectrics in sunlight, e.g., insulating standoffs and collars
• Shielded cables near above items
Spacecraft Potential Near Zero
• Second surface mirrors on forward end
• Nonconducting white paint on aft end
• Other dielectrics in dark; e.g., insulating standoffs and collars
• Shielded cables near above items

The second category of hazards is that in which the spacecraft potential is more positive than the arcing dielectric surface. This polarity of differential stress corresponds to that which is obtained in most of the laboratory tests where dielectic surfaces are irradiated with an electron beam and the underlying substrate is grounded. On P78-2 the dielectric surfaces on the front and aft ends, always being in the dark, fall into this group. Because of the relatively slow spin rate of ~1 rpm, dielectric surfaces on the cylindrical surface have about 30 seconds to charge up before photoemission takes over. This would appear to be a marginal time span for full chargeup.

In regards to miscellaneous small insulators such as standoffs and collars, the possibility of generating appreciable positive differential potentials relative to large surrounding areas is small because of the retarding potential barrier for low-energy electron emission generated off-surface. For the opposite polarity situation of small surfaces charging negative with respect to the surrounding areas, it appears that the usual Langmuir-Mott-Smith equations would tend to overestimate the actual differential potentials that could be attained. This is because of the increased density of equipotential and electric field lines near the edges of the dielectric as compared to the density which would be obtained for a sphere in space. The problem is one that could be solved by NASCAP just as easily as the former one of positive polarity was solved by NASCAP.

Table 2-7 lists some additional considerations that must be taken into account in evaluating the potential hazards to a spacecraft system from electrostatic discharges (ESD). SEMCAP, for example, has tabulated within its model of the spacecraft a threshold voltage at which anomolous voltage spikes could be detected for each wire modeled. There are, however, higher thresholds for upsetting an associated logic circuit, and even higher thresholds at which component damage or burnout could occur. The effects of possible consequences of arc discharges must, then, be evaluated in the context of the criticality of the function that an anomolous pulse might cause. Table 2-7 also lists examples of critical and noncritical spacecraft functions that could be affected.

Table 2-7. ESD Susceptibility Considerations

- Thresholds for detection
- Thresholds for upsets
- Thresholds for damage or burnout
- Partial or temporary malfunctions (some are correctable by command)
- Criticality to mission

Critical	Noncritical
Transmitter	Temperatures
Receiver	Voltage monitors
Experiments	Current monitors
Power system	Boom deployment indicators
Command system	Mode/status indicators

2.1.5 Preflight and In-Flight Test Locations for P78-2

Figure 2-5 taken from Reference 6 of Table 2-1 shows the test points at which arc discharge stimuli were injected during preflight tests. Figure 2-6 taken from Reference 2 of Table 2-1 shows the test configurations used. SCATHA refers to the P78-2 spacecraft and SCATSAT refers to a 2/3 scale model of P78-2 on which some additional tests are being performed by IRT Corporation (J. Wilkenfeld). Figure 2-7 and Table 2-8 taken from the same references indicate diagnostic test points for the preflight test. Figure 2-7 also shows some of the in-flight diagnostics. The purpose of showing these figures and Table 2-8 is that they indicate those points which were considered by others to be the most susceptible to arc discharging and to coupled EMI signals.

2.1.6 P78-2 Elements Selected for Further Study

After our presentation at SAMSO on December 4, 1979, NASA/LeRC selected two elements of the P78-2 spacecraft for further analysis. As indicated previously, these were the large flat nonconducting painted surface on the aft end and one of the short booms. These two configurations exist on many spacecraft, and each represents a potential hazard. The large

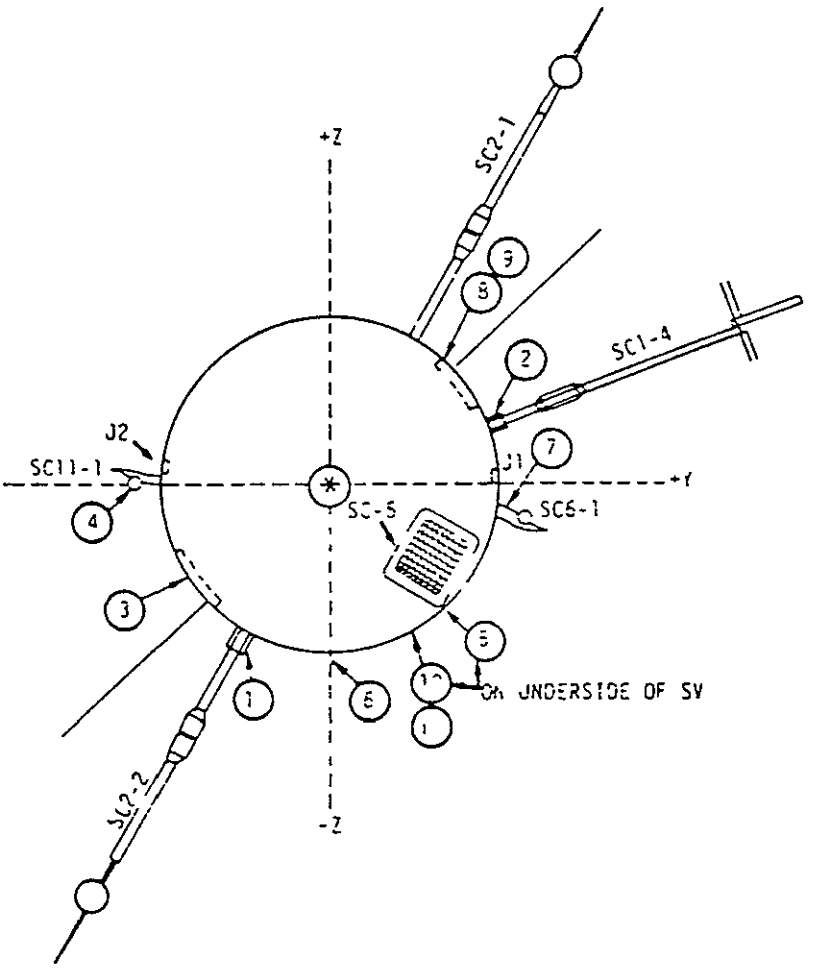

ARC	LOCATION
1	SC2-2 BASE TO SHOULDER
2	SC1-4 BASE TO SHOULDER
3	6 INCHES FROM SC10-3 EXIT HOLE
4	SC11 THERMAL BLANKET
5	BASE OF AFT OMNI ANTENNA
6	STRUCTURE ADJACENT TO SC4-2 APERTURE

ARC	LOCATION
7	BASE OF SC6-1 BOOM TO SHOULDER JOINT
8	SOLAR ARRAY ADJACENT TO SC1-1 BB COVER
9	SOLAR ARRAY ADJACENT TO SC1-1 BB COVER
10	NEAREST POINT TO CONDUCTIVE RING (SC7)
11	SC7 AFT CLOSURE SCREW CLOSEST TO SC7 APERTURE

Figure 2-5. SCATHA and SCATSAT Arc Injection Locations

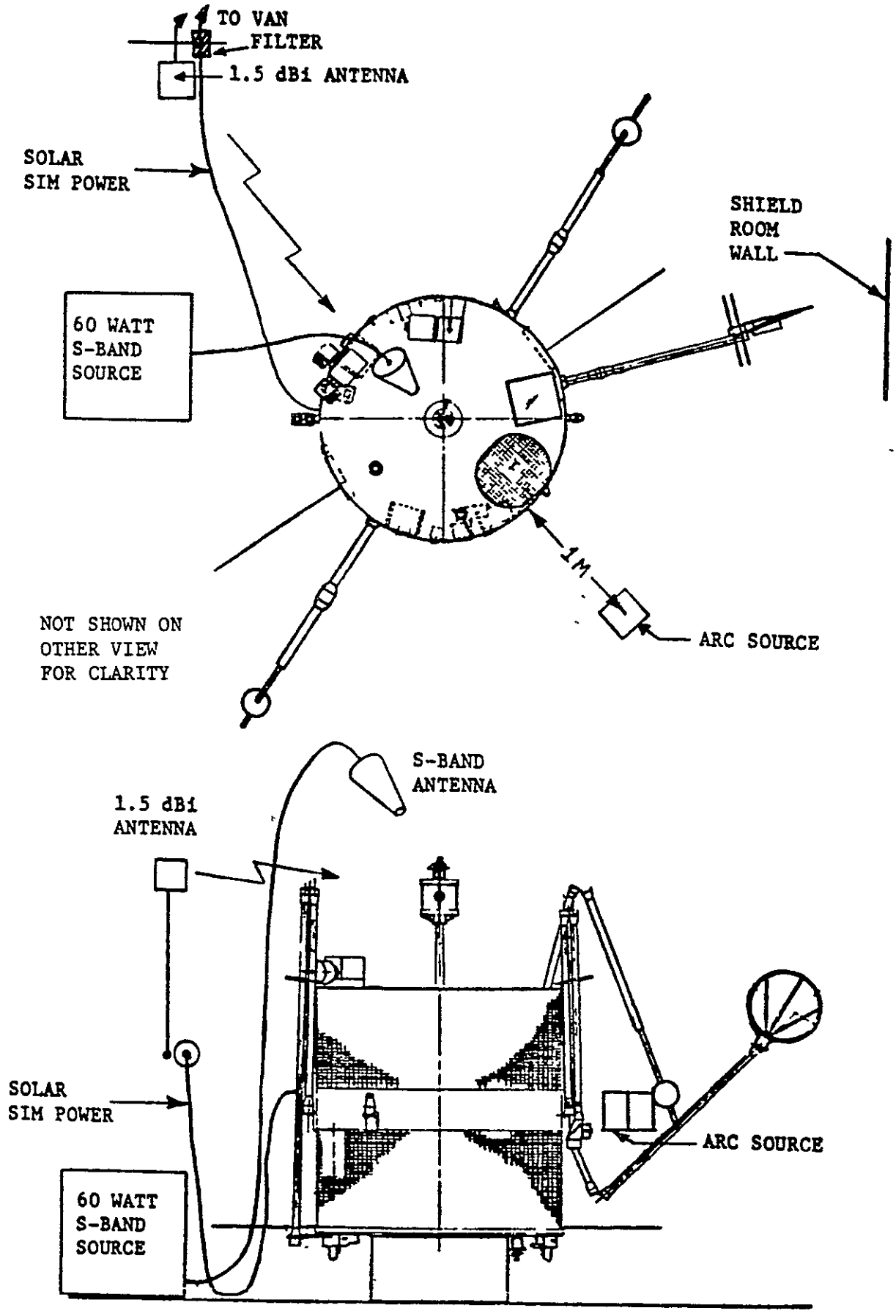

Figure 2-6. SCATHA Arc Discharge and Radiated Susceptibility Test Configuration

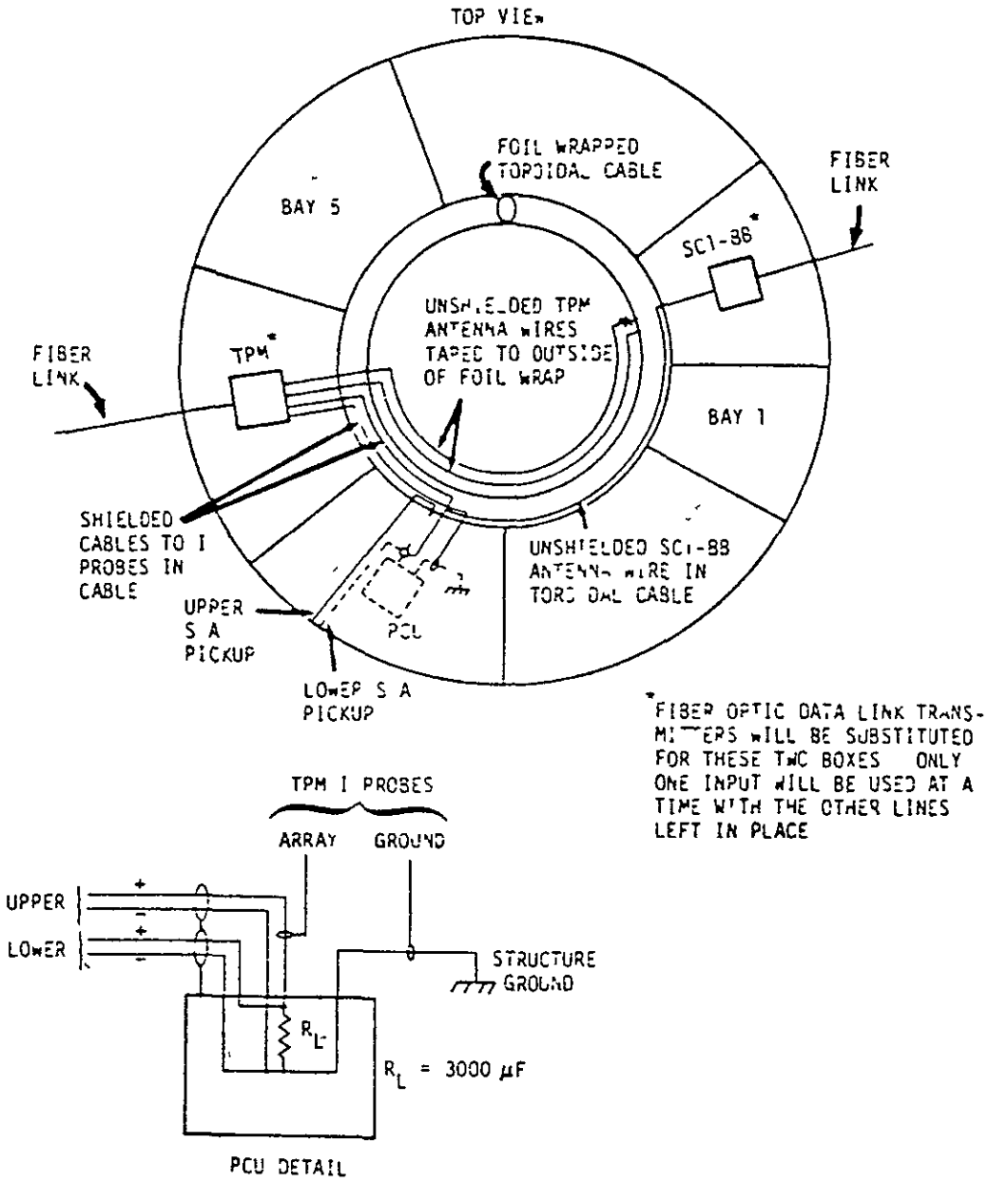

Figure 2-7. SCATHA and SCATSAT-Diagnostic Locations

Table 2-8. Test Points Monitored During SCATHA Arc Discharge Test

	Critical Test Point Name	Circuit Monitor Trip Level (+ Peak) (mV)
1.	CEA mode control "clock"	800
2.	CEA mode control "enable"	400
3.	Decoder input "0"	133
4.	Decoder input "1"	133
5.	Decoder input "S"	133
6.	Decoder input "activate"	133
7.	TCDU relay select "clock"	250.
8.	TCDU relay select "enable"	250
9.	OFU power "enable"	5500
10.	OFU power "disable"	5500
11.	SC1-7 battery power	±85
12.	SC1-8A battery power	±85

dielectric surface is a good choice in that it is located in the dark where large negative differential potentials may be generated. Its large area is appropiate to the study of large area discharges which have been the subject of much concern. The boom configuration is appropriate in that a long coupling path exists between the arcing element and the cable which is routed along its entire length. Furthermore, arc discharges at the end of the boom have a "good view" of space to which blowoff currents must flow if they do flow in that manner.

2.2 TASK 1.2. COUPLING MODEL ANALYSIS OF ARC DISCHARGES

In order to perform an electromagnetic coupling analysis of arc discharges into potential victim electronic subsystems using a computerized electromagnetic compatibility (EMC) code such as SEMCAP, it is necessary to incorporate ESD sources as voltage or current generators or as E or B fields in defined locations. It is our view that once the proper modeling of the arc discharge sources is accomplished, the EMC analysis using SEMCAP

is the most cost effective approach to evaluating the response of the spacecraft electrical subsystems and the resulting hazard to those subsystems. The rationale for this approach is that the SEMCAP code for a particular spacecraft system already contains all of the information relative to the nature and routing of all of the cabling as well as the response characteristics of every harness wire terminal at each box. For EMC purposes the EMI noise from each terminal is considered as a source and the signal coupled to every other terminal is computed. Magnetic, electrostatic, electromagnetic and common resistance coupling modes are taken into account. For arc discharges, then, the crux of the problem is the proper modeling of ESDs as sources for SEMCAP. The shortcomings of prior determinations of arc discharge characteristics have been discussed in our "Effects of Arcing" study. In this subtask another attempt is made to improve the characterization from an analytical point of view. A parallel experimental study is reported on in the following task, Task 2.

2.2.1 Arc Discharge Model Overview

The characterization of arc discharges resulting from differential charge buildup on spacecraft in an energetic plasma is essential in assessing the implications of arcing on the EMI margins of immunity of onboard equipment. During the past several years, a large effort has been expended in determining experimentally the waveform and amplitude of arc discharges of potential arcing elements on various spacecraft configurations. Many of the features of arc discharges observed were unexpected because of the absence of a valid theoretical model. The large area discharge of charged dielectric surfaces, and the partial (~15 to 60 percent) discharge of the stored charge are examples of surprises that were found after the experiments were performed. The implications of other features of arc discharges such as the blowout of surface charged particles versus flashover were not considered adequately, and appropriate test configurations and test diagnostics were not included in the tests.

A useful arc discharge model would be one which is consistent with the existing experimental data, but which also correctly predicts the arc characteristics of configurations which cannot be tested in the laboratory because of size or other cost limitations. Since in-flight data, aside from SCATHA and a few other space experiments are not available, the validity of an arc discharge model must be checked by performing laboratory experiments designed specifically to test various feaures of the model.

The following is a scenario for the evolutionary processes involved in an arc discharge

a) Differential chargeup by environmental plasma

b) Edge breakdown

c) Surface breakdown

d) Plasma film generation

e) Propagation of surface breakdown "brushfire"

f) Blowout and flashover, G'

g) Limitations on propagation of brushfire wavefront

h) Definition of arc parameters for the analysis of electromagnetic coupling to spacecraft subsystems.

2.2.2 Differential Chargeup Effects on Arc Discharges

The question of how external dielectric surfaces charge up differentially with respect to the underlying vacuum deposited aluminum (VDA), grounded, or structural metal is a complex problem which is not addressed here. Generally, the most hazardous situation exists when a dielectric surface is charged negatively with respect to the underlying metals by an excess of impinging electrons over positive ions. This is because the reverse polarity, when metals are negative and the dielectric surface is more positive because of photoemission or secondary emission, a field emission/secondary electron avalanche process tends to limit the magnitude of the differential potential to 500 to 1000 volts. This effect was demonstrated in a solar array sample test in which UV was irradiated on the solar cell side while the backside was irradiated with an electron beam.[1]

For the purpose at hand of developing an arc discharge model, the chargeup process is important in that negative chargeup potentials of 5 to 25 kV have been measured experimentally. The other important feature of chargeup for our present purpose is that theory and experimental evidence[2] indicate that significant densities of electrons may be buried at depths of the order of one micron below the surface at the time of the discharge. This feature of buried electronic charge should also exist on dielectric surfaces which have no net surface charge because of photoemission or excess secondaries. In fact, the buried charge should be somewhat deeper and more dense since retarding potentials are not present. The effects of differential chargeup on arc discharge characteristics are summarized in Figure 2-8.

2.2.3 Edge Breakdown

Dielectric breakdown due to high differential voltage stresses generally occurs for electric fields in range of 10^5 to 10^6 V/cm at the edges of thin (~50 microns or 0.005 cm) insulating sheets. Punchthrough far from edges occurs with fields on the order of 10^7 V/cm. In laboratory experiments at TRW, we have found that 2 mil Kapton will not break down with a 20 kV electron beam if the edges are folded over so that the edges are not exposed.[3]

In practice, even punchthroughs probably occur at weak points when slight imperfections or irregularities exist in the material. Edges consist of exaggerated irregularities because they are created by slicing with a knife edge or by punching with stitching needles, and thus are subject to high field emission and avalanche breakdown in a manner similar to that which will be discussed for surface breakdown. The similarity to surface breakdowns probably goes even further in that this type of breakdown is associated with surface and off surface processes rather than those within the bulk of the material.

The net effect of an edge breakdown is that the potential of the surface near the edge goes to nearly zero volt, assuming that the thin dielectric is over a conducting plate which is at zero volts. Taking a singly ionized particle of atomic weight 16 (oxygen) as being typical, the velocity associated with a 10 kV voltage drop is $3.5 \cdot 10^5$ m/s. Starting at

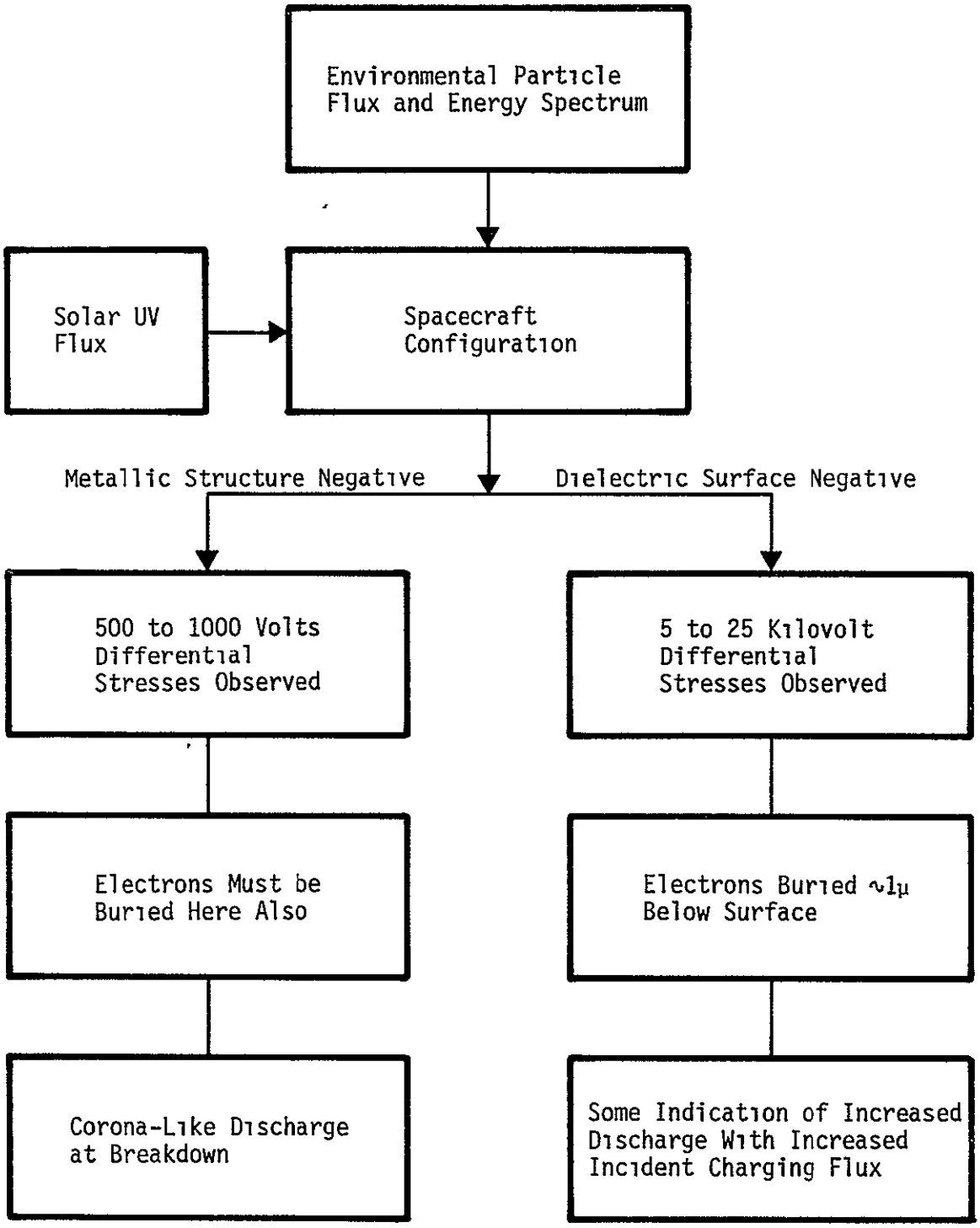

Figure 2-8. Differential Chargeup Effects on Arc Discharge Characteristics

zero velocity, the time for such an ion to traverse the 2 mils or 50 micron thickness of the dielectric is 0.3 ns. This order of magnitude time span, a fraction of an ns, is much shorter than the 10 to 1000 ns duration of vacuum dielectric surface arcs.

Assuming that a 2-mil-thick sheet of Kapton, ε_r=3, breaks down at 10 kV over a semicircular area with a radius equal to its thickness, the capacitance is 52 pf/cm^2 or $2 \cdot 10^{-3}$ pf, and the charge stored is $2 \cdot 10^{-11}$ Coulomb. Assuming that all of this charge is dissipated in 0.3 ns, the corresponding current would be 0.068 A. Thus the current, charge, time span, and energy ($\sim 10^{-7}$ J) involved in the initial edge breakdown are quite small and negligible compared to those in the events that follow. Its main effect is to create a plasma cloud and a surface electric field which initiates the surface discharge. The features of edge breakdown are summarized in Figure 2-9.

2.2.4 Surface Breakdown

Dielectric surface breakdown has been reported[4] to occur more readily, at 10^4 - 10^5 V/cm surface electric fields, than in the bulk of dielectric materials. At TRW we have found that arcs can develop over a 5 mm span of Kapton with bordering metal irradiated with a 10 kV electron beam.[5] This stress, less than 20 kV/cm, is in the lower portion of the above range of surface breakdown electric fields. The surface breakdown fields are expected to be highly dependent on surface conditions such as cleanliness, smoothness and adsorbed gases.

The reduction in the frequency of arcing with the number of arcs that have already occurred is a commonly reported observation on arc discharge experiments.

The dielectic surface breakdown process is most clearly discussed in terms of a configuration in which breakdown occurs between two metallic electrodes held at a fixed potential difference, V, by means of a power supply. It turns out that such a configuration is fairly well approximated by the solid teflon propellant fuel pulsed plasma thruster (PPT) in which a high voltage ($\sim$1 to 2 kV) discharge is initiated by means of a spark plug. With each discharge pulse, some of the teflon surface is ablated and ejected from the thruster at high velocity by the V x B and gas dynamic

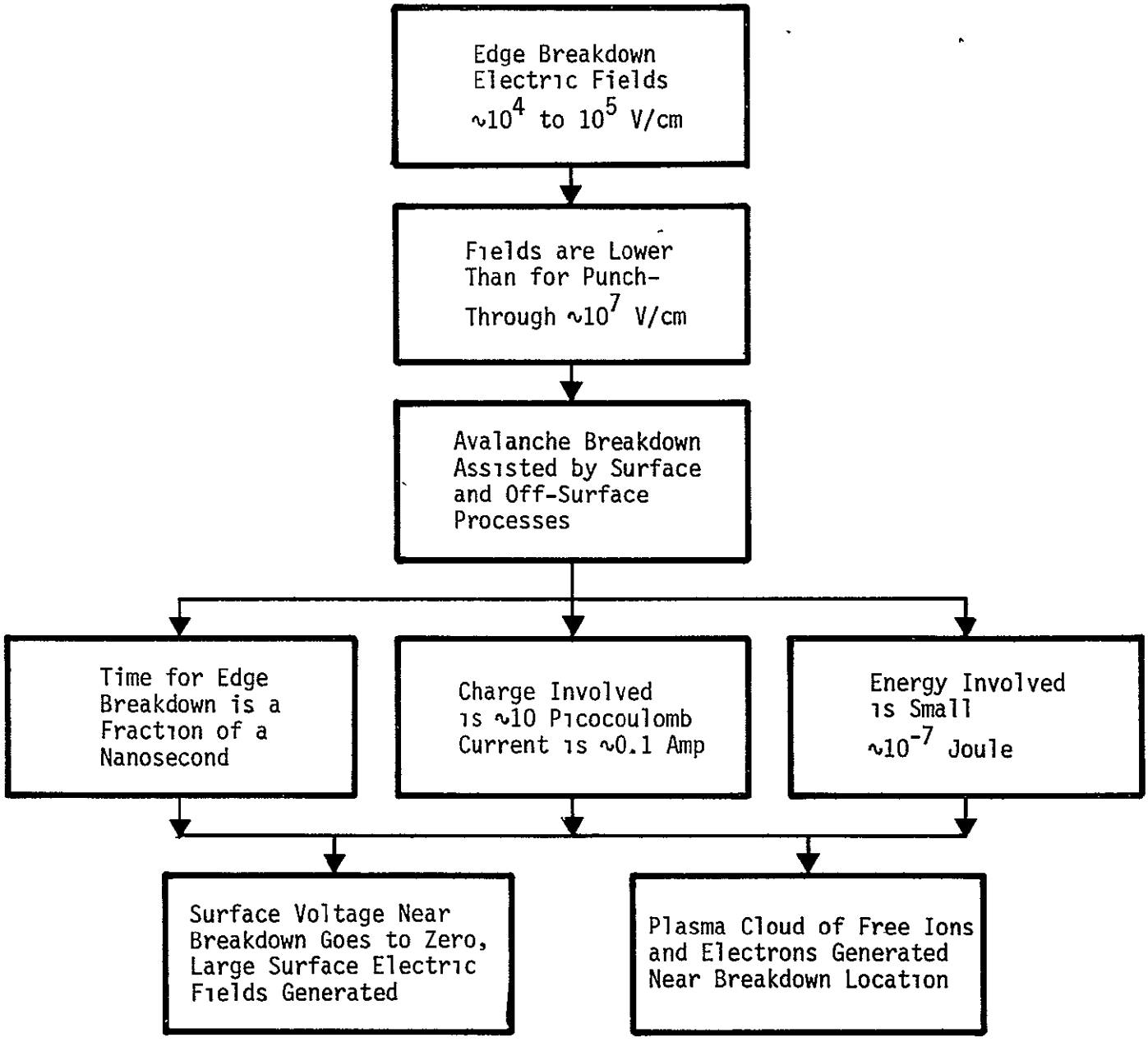

Figure 2-9. Edge Breakdown Features

forces which accompany the discharge. The PPT has a development and in-orbit performance history of more than 10 years, and some of the results of the associated research effort is applicable to the spacecraft charging problem. Pertinent information from the PPT technology is summarized in Appendix 1 and is referred to in the appropriate sections of this report.

The two main differences between the PPT configuration and that of the spacecraft charging problem are that:

- No metallic electrodes exist in our problem. This leads to the discharge propagation problem which is discussed in the following sections.
- The level of energy dissipation per unit dielectric surface area is much greater for the PPT. This leads to the question of appropriateness of extrapolation to lower levels (by ~3 orders of magnitude).

Of course, the emphasis of effort in the PPT is on the efficiency in generating mechanical thrust, which is not of major interest here. On the other hand, the results of the type of work performed in this study may be applicable to the PPT effort in the sense that the PPT may have a major impact on the EMI margins of immunity of the spacecraft into which it is incorporated.

Qualitatively, dielectric surface breakdown between metallic electrodes held at a fixed potential difference consists of the following sequence of events:

a) Acceleration of the spark plug plasma cloud positive ions towards negatively charged surface regions away from the breakdown region. The velocity of these ions would be $3.5 \cdot 10^7$ cm/s if they accelerate without collisions to regions where the potential is ~10 kV.

b) Collisions will knock free neutral surface atoms and adsorbed gas molecules as well as create more free ions and secondary electrons. Inside the material, bound electrons may be excited into conduction energy level bands.

c) Simultaneously with the movement of positive ions towards regions of buried or surface electrons, high field emission of electrons must be freeing electrons from "pointed" areas on the surface. Many surface irregularities with sharp points must exist on a sufficiently small microscopic scale.

d) These electrons, as well as secondary electrons due to positive ion bombardment, are accelerated by the surface field towards the initial edge breakdown location. These electrons, if they fall through the 10^4 volts potential without a collision, would have a velocity of $5.9 \cdot 10^9$ cm/s.

e) Collisions between these electrons and the surface material will create more secondary electrons as well as exciting bound electrons within the material up to conduction energy level bands. It should be noted, however, that surface electric fields tend to slant away from the surface so that this type of collision may be relatively scarce unless the microscopic irregularities are a prominent feature of the surface.

f) Collisions between the free and accelerating electrons and off-surface neutrals and ions can occur, resulting in more ions and more free electrons.

g) The net effect of these collisions of ions and electrons is the creation of a plasma film off of the surface with is initially very "hot" but very tenuous. The temperature corresponding to 10^4 eV is $1.2 \cdot 10^{8}$°. As the plasma builds up and becomes more dense, the collision frequency increases, and the temperature cools down. This happens in the first 10-100 ns, during which time the temperature cools down from 10^{8}° to 10^4°K, a few eV.

h) The initially hot plasma of 10 keV electrons and ions causes ablation of neutrals, ions and electrons off of the surface, creating a denser plasma. In the process, however, the frequency of collisions increases and the plasma temperature cools down to the 1 eV or 10^4°K range.

i) The plasma resistance, R_p, is initially zero (infinite conductance) if the released electrons are able to accelerate without any collisions. An expression for R_p (actually resistivity) given by Spitzer[6]:

$$R_p = \frac{m_e \nu}{n_e e^2}$$

Although not directly applicable to the situation being described here, it shows the proportionality of R_p with the collisional frequency, ν. In the initial phase, collisions are primarily between the released electrons and ablated molecules rather than between the ablated and ionized electron-ion pairs. The inverse proportionality of R_p with n_e, the plasma electron density, also corresponds to our expectation that the plasma

conductivity is proportional to m_e. As the plasma becomes fully ionized, n_e and ν change together proportionally and R_p depends only on the Maxwellian temperature, T, in what is termed an ideal Lorentz gas(6):

$$R = KT^{-3/2} \text{ (ohm-cm) where } K = 0.03 \text{ ohm-cm-eV}^{3/2}$$

This equation also predicts that R_p increases as the plasma cools down. Temperature, as described by the kinetic energy or velocity of the electrons, is lowered by collisions.

J) In the succeeding phase, the temperature rises as power is pumped into the plasma, and the plasma resistance decreases with time.

$$cM \frac{dT}{dt} = I^2 R_p = \frac{V^2}{R_p} = \frac{V^2 T^{3/2}}{K}$$

$$T = \left(\frac{2 V^2}{cMK} \right)^2 t^2$$

M is the mass of the plasma and c is the specific heat of the plasma. The plasma current, I, was assumed to be given by Ohm's law where the power source was a fixed voltage, V. Also, the energy loss processes in heating and ablating the dielectric surface material have been neglected in the above equations. These factors are considered further in the next section in which the propagation of the discharge over the dielectric surface is discussed. The surface breakdown process is summarized in Figure 2-10.

2.2.5 Brushfire Arc Discharge Model

The brushfire arc discharge model was presented at the third Spacecraft Charging Technology Conference at the Air Force Academy, Colorado Springs, Colorado on November 12, 1980. It is included in this final report as Appendix 4. The preceeding three appendices contain supplementary information for the brushfire arc discharge model.

- Appendix 1, Pulsed Plasma Thruster data
- Appendix 2, Dielectric Heating by a Surface Plasma
- Appendix 3, Effects of Magnetic Forces on G'

Appendix 1 presents a brief overview of the technical work that has been performed on solid propellant pulsed plasma thrusters. The result that 8.32 grams of surface material is ablated per joule of energy dissipated in the plasma at the surface of the propellant (teflon) is used.

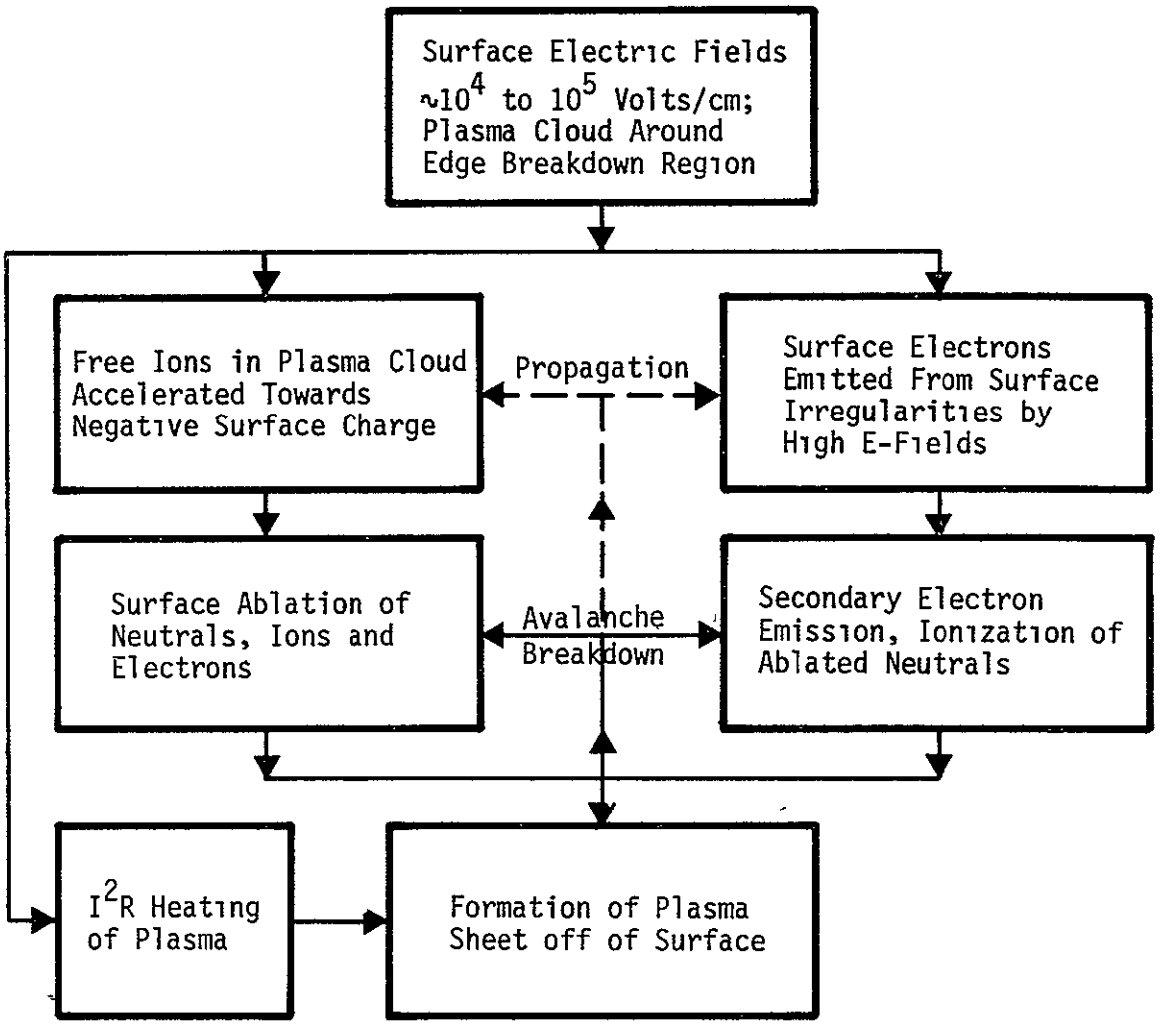

Figure 2-10. Surface Breakdown Features

This experimental result allows us to bypass a set of calculations involving the intricate physical processes of heating, ablation and ionization. Appendix 2 presents an analysis of the heat loss into a dielectric surface from a plasma at its surface. The main result of the analysis is that for the plasma temperature necessary for the brushfire propagation, a very large percentage of the energy dissipated in the propagation process is diverted into the dielectric. The third appendix is an analysis which shows that the magnetic deflection forces are negligible compared to the electric field forces.

The major subsection titles of the Brushfire Arc Discharge Model presented in Appendix 4 are listed below to indicate the scope of the paper.

Introduction

Arc Discharge Overview

Brushfire Propagation Model

Simplified Analysis

Blowout and Flashover Currents: G'

Effect of Spacecraft Potential on G'

Limiting Mechanisms on Brushfire Propagation

Summary and Conclusions from the Brushfire Arc Discharge Model Analysis.

Many of the results of the model analysis have guided the selection of tests to be performed in the experimental study, Task 2. The results of the experimental study are compared with the predictions of the brushfire model analysis in the Task 3 writeup.

REFERENCES

(1) G.T. Inouye and J.M. Sellen, Jr., "TDRSS Solar Array Arc Discharge Tests," Proceeding of the Spacecraft Charging Conference, NASA Conference Publication 2071 and AFGL-TR79-0082, 1978.

(2) K.G. Balmain, "Scaling Laws and Edge Effects for Polymer Surface Discharges," Proceedings of the Spacecraft Charging Technology Conference, NASA Conference Publication 2071 and AFGL-TR-79-0082, 1978.

(3) G.T. Inouye, N.L. Sanders, G.K. Komatsu, and J.R. Valles, "Thermal Blanket Metallic Film Groundstrap and Second Surface Mirror Vulnerability to Arc Discharges," Proceedings of the Spacecraft Charging Conference, NASA Conference Publication 2071 and AFGL-TR-79-0082, 1978.

(4) N.J. Stevens, C.K. Purvis and J.V. Staskus, "Insulator Edge Voltage Gradient Effects in Spacecraft Charging Phenomena," IEEE Transactions on Nuclear Science, Vol. NS-25 No. 6, December 1978.

(5) D.K. Hoffmaster and J.M. Sellen, Jr., "Measurements of Metal-to-Metal Arc Discharges Across Dielectric Surfaces in an Electron Swarm Tunnel," TRW Report No. 4351.3.74, November 18, 1974.

(6) L. Spitzer Jr., "Physics of Fully Ionized Gases," Interscience Publishers Inc., 1956, pages 82-83.

3. TASK 2: EXPERIMENTAL STUDY OF EMI IMMUNITY FACTORS

An experimental study of arcing configurations on the P78-2 spacecraft was performed in this task, Task 2, to study the factors which affect the EMI immunity of spacecraft to arc discharges. The principal objective of this experimental study was to determine the arc discharge parameters which can be used as source models to be incorporated into a SEMCAP model of the DSP spacecraft. In particular, the determination of the ratio of blowoff to flashover currents, G', was a prime objective because it has a large effect on the magnitude of coupled electromagnetic interference signal levels. Other characteristics of arc discharges such as the waveform, duration, magnitude and spatial extent are critical parameters that were studied. The angular distribution of blowout particles and their dependence on sample grounding resistance was determined. The brushfire propagation velocity and its dependence on sample configuration was determined since these parameters also affect the G' ratio.

As a result of the Task 1 study of the P78-2 configuration, two specific elements, one of the short booms and the bottom or aft closure dielectric surface, were selected as subjects for this experimental study as well as for the remaining analytical studies.

The rationale for using aluminized Kapton instead of the platinum rings/fiberglass of the booms and the white paint on the aft closure was that Kapton is a much more widely used material. Figure 3-1 shows the flow of subtasks for the experimental study.

3.1 TASK 2.1 DEVELOPMENT OF AN EXPERIMENTAL STUDY PLAN

A large number of arc discharge measurements have been made in the past by many different groups. The body of knowledge gained from these tests is impressive, and many features of arc discharges as related to spacecraft charging phenomena have been revealed which were not predicted on the basis of prior experience. On the other hand, many of the measurements that have been made have not reflected flight configurations and in-flight environments adequately. Thus many of the results were not directly applicable to spacecraft systems design and have to be "massaged" or "taken with a grain of salt." The performance of further laboratory tests is justified if the information gained is useful in providing further

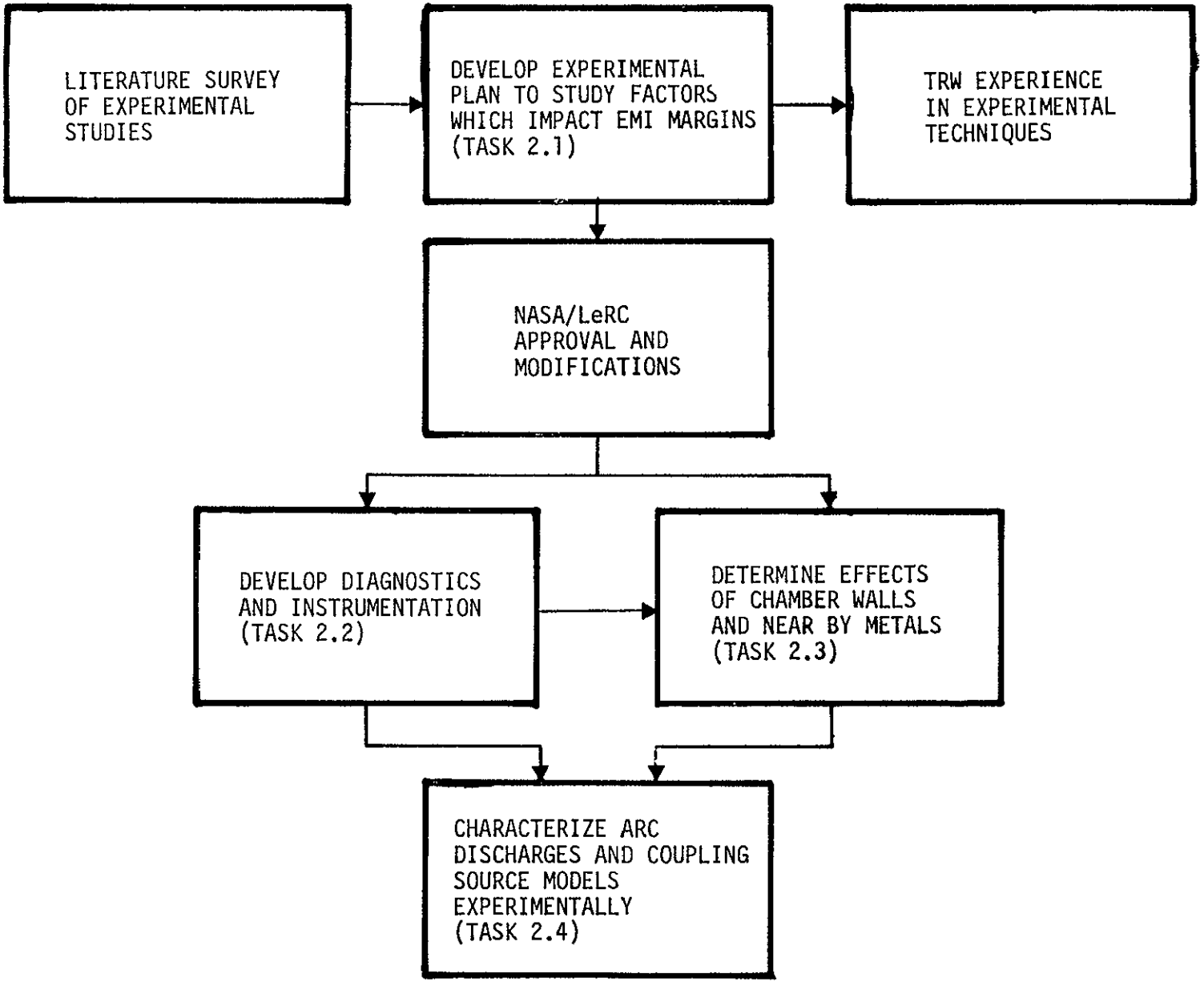

Figure 3-1. TASK 2 Experimental Study of EMI Immunity Factors

insight into the arc discharge process even though time and cost considerations limit the degree of "reality" incorporated into the tests. It is important, however, to have a knowledge of the limitations imposed by the actual test conditions on the applicability of the results to spacecraft design.

This experimental study focused on a number of features that had not been examined previously:

- Development of a reliable arc discharge trigger
  - permits propagation velocity measurements to be made easily
  - permits study of surface potential effects to be made easily
  - permits angular dependence of blowout particles to be made easily
- Velocity of arc discharge brushfire propagation
  - materials effects
  - configuration effects
- Angular distribution of blowout particles.

3.2 TASK 2.2: DEVELOPMENT OF DIAGNOSTICS AND INSTRUMENTATION

A principal factor affecting the EMI immunity is the ratio of arc discharge blowout currents to flashover currents, denoted as G'. In addition, however, are the many features of arc discharges such as the location, configuration, material, rise time, magnitude, duration and spatial extent which also affect the EMI-coupled-into-victim hardware. All of the foregoing arc discharge features have been considered in Task 1 as a part of the analytical modelling. A major feature of the model is that the arc discharge initiates at a weak point such as at an edge of a dielectric surface, and then propagates in a "brushfire" mode over a large fraction of the total surface area. An important part of this experimental study was the development of a reliable triggering technique so that arc discharges initiate at a predefined location and at a known instant of time. The analysis of Task 1 indicates that there should be an angular dependence of blowout electron currents favoring those angles which point closest to the initiation point of arc discharge. This angular dependence and the energy

and species dependence was determined as additional information relating to G'. Figure 3-2 shows an overall view of the 2 by 4 feet long diameter vacuum system used in this task.

3.2.1 Arc Discharge Trigger

Historically, experiments on spacecraft arc discharges have been performed by charging dielectric surfaces until breakdown occurred, and then measuring the currents and voltages that resulted. Because the breakdown voltage as well as the breakdown instant and location were unpredictable, such measurements were difficult to make and also gave a wide range of results. Other measurements, such as the propagation velocity of an arc discharge wavefront and the velocity of a brushfire over the dielectric surface, were nearly impossible to perform since the location and the "burning" directions were unpredictable.

In addition, the characteristics of the arc discharge itself, as distinguished from the breakdown initiation process, were not separately measurable. A reliable, predictable and reproducible arc discharge trigger also permits many measurements of arc discharge parameters to be made more easily in that discharge-to-discharge variations would be minimized. Propagation velocity measurements, for example, may be made with a single trace oscilloscope viewing a number of sensors on separate discharges.

Figure 3-3 shows the arc triggering circuit developed for this study. A 3μf capacitor is charged up from a 300 volt supply and is discharged by a SCR diode which is triggered manually from a pulse generator. The capacitor feeds the primary of a high voltage step-up transformer whose secondary is isolated from ground by a 100 kilohm resistor. The ignition electrodes are mounted below the sample and just peek out over the interface between the sample and the metallic side plate.

Nearly all of the data taken in the experimental study was obtained using the arc trigger system. In the sense that a lot of good data was obtained, the development of the triggering technique has been very successful. One of the unexplained aspects of the trigger was its inability to initiate arc discharges over a large range of chargeup differential potentials. One possible explanation of this effect is that the butt joint

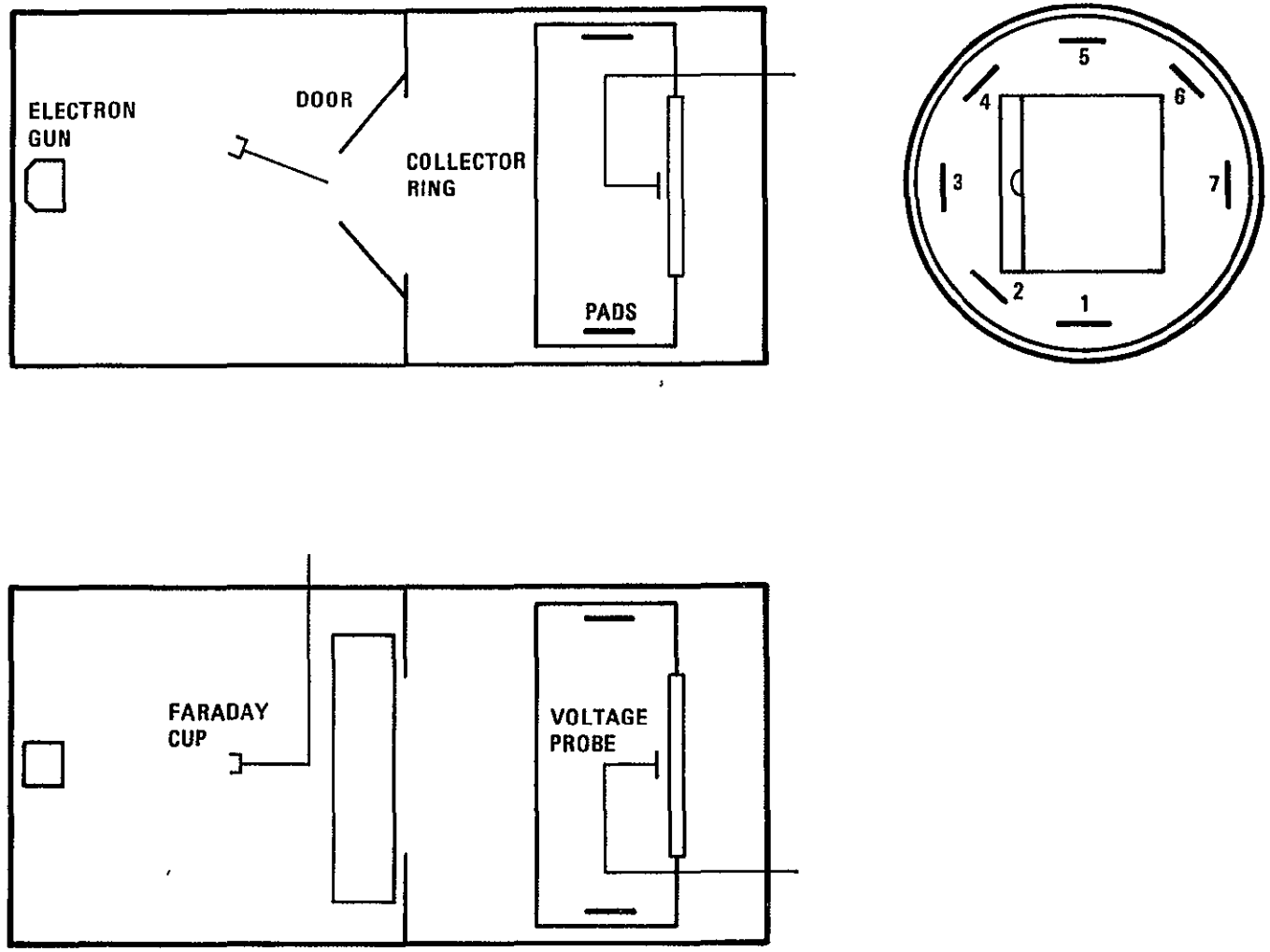

Figure 3-2. 2- by 4-Feet Vacuum System with Diagnostics

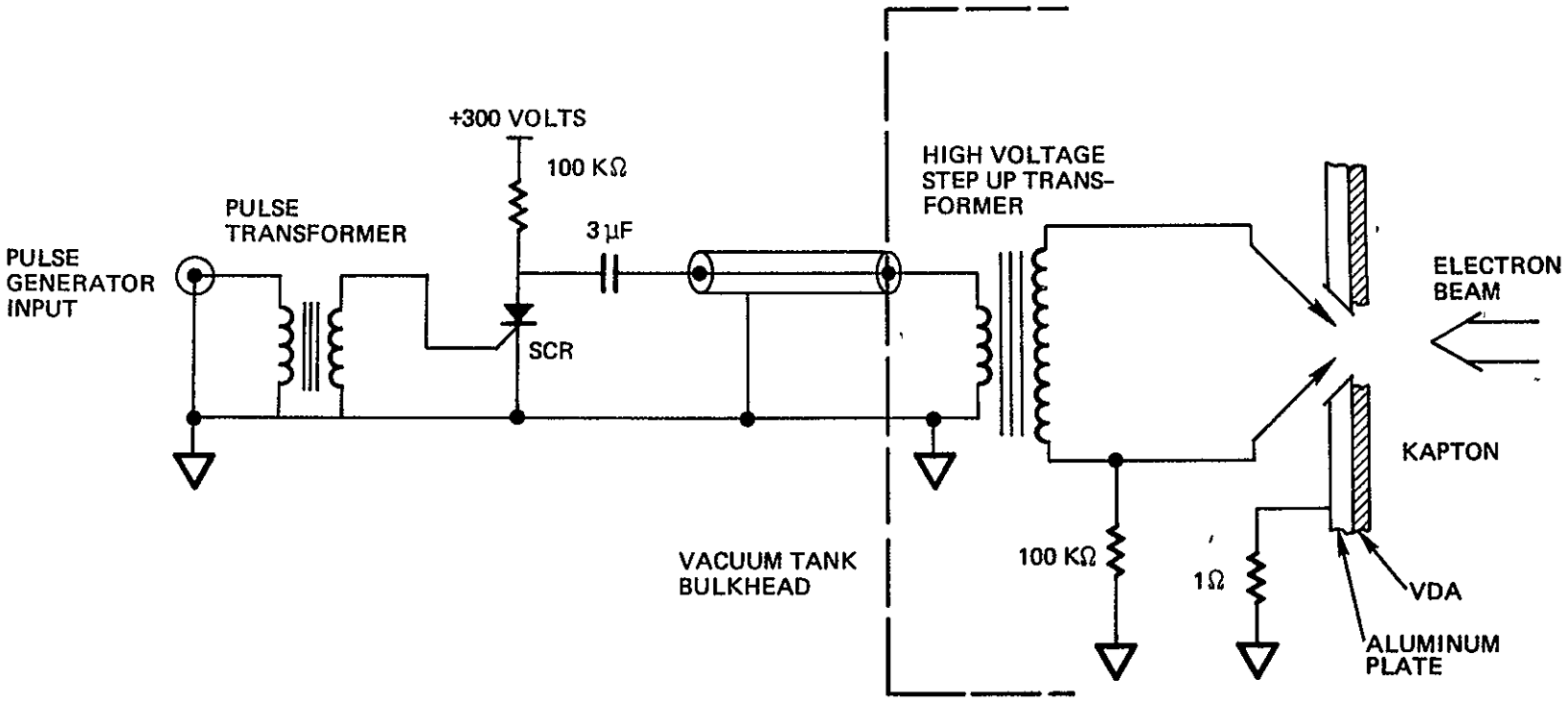

Figure 3-3. Arc Trigger Circuit

configuration of the folded-over Kapton against the metallic plate did not lead to an adequately high surface electric field to start a propagating wavefront.

3.2.2 Propagation Velocity Sensors

Two types of sensors were developed to determine the arc discharge propagation velocity. Both sensors were designed to detect the differential time-of-arrival of a signature at spatially separated locations on the test sample. The first consists of 1/2-inch diameter copper pads glued to the surface of the Kapton with wire leads brought out of the vacuum system. The voltage developed across a 1 ohm resistor was fed to the oscilloscope which was triggered from the manually operated pulse generator which also triggered the arc ignition system. Figure 3-4 shows the approximately 0.5 μs time delay between the close-in sensor and the distant sensor waveforms. For the 5-inch separation of the sensor, this leads to a velocity of $2.5 \cdot 10^7$ cm/s. The polarity of the signature (negative), is consistent with the collection of electrons as the wavefront passes by. The size of the signatures, 10 to 15 amperes at the close-in sensor and 2 to 5 amperes at the distant sensor, was unexpectedly large.

The second type of sensor used is shown in Figure 3-5. A 3/4-inch ring of the vacuum deposited aluminum on the backside of the Kapton was etched out leaving a 1/2-inch diameter disc to which a wire lead was epoxied. Outside the vacuum system, a 1 ohm termination resistor was used as before. The waveforms obtained are shown in Figure 3-6. The signature polarities (positive) are consistent with electrons leaving the Kapton surface. Again, the signal levels, >30 amperes close in to 15 amperes far out (7 inches) were unexpectedly large. On the average, these measurements lead to a propagation velocity of $2.1 \cdot 10^7$ cm/s and therefore an overall average of $2.3 \cdot 10^7$ cm/s for all of the measurements on 2 mil Kapton. By comparison, the value of $2.45 \cdot 10^7$ cm/s has been used throughout the analytical study of Task 1. That value was obtained as the velocity of an ion of gram molecular weight 16 accelerated from zero to a 5 keV energy. The coincidence is startling.

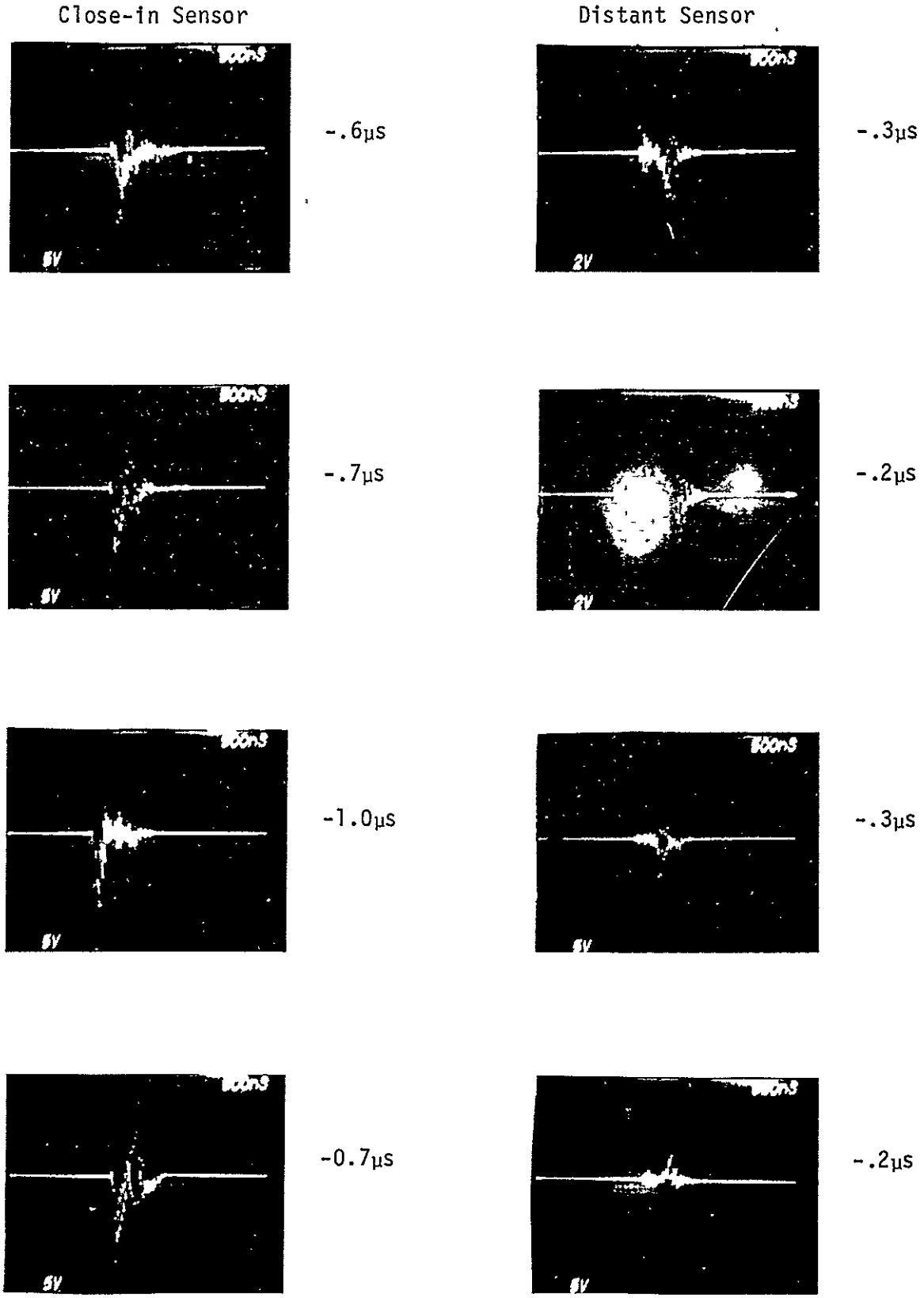

Figure 3-4. Metallic Sensor Pad Outputs (6- by 6-inch, 1 mil Kapton Sample) 0.5μs Propagation Time Delay, $v_b = 2.5 \cdot 10^7$ cm/s

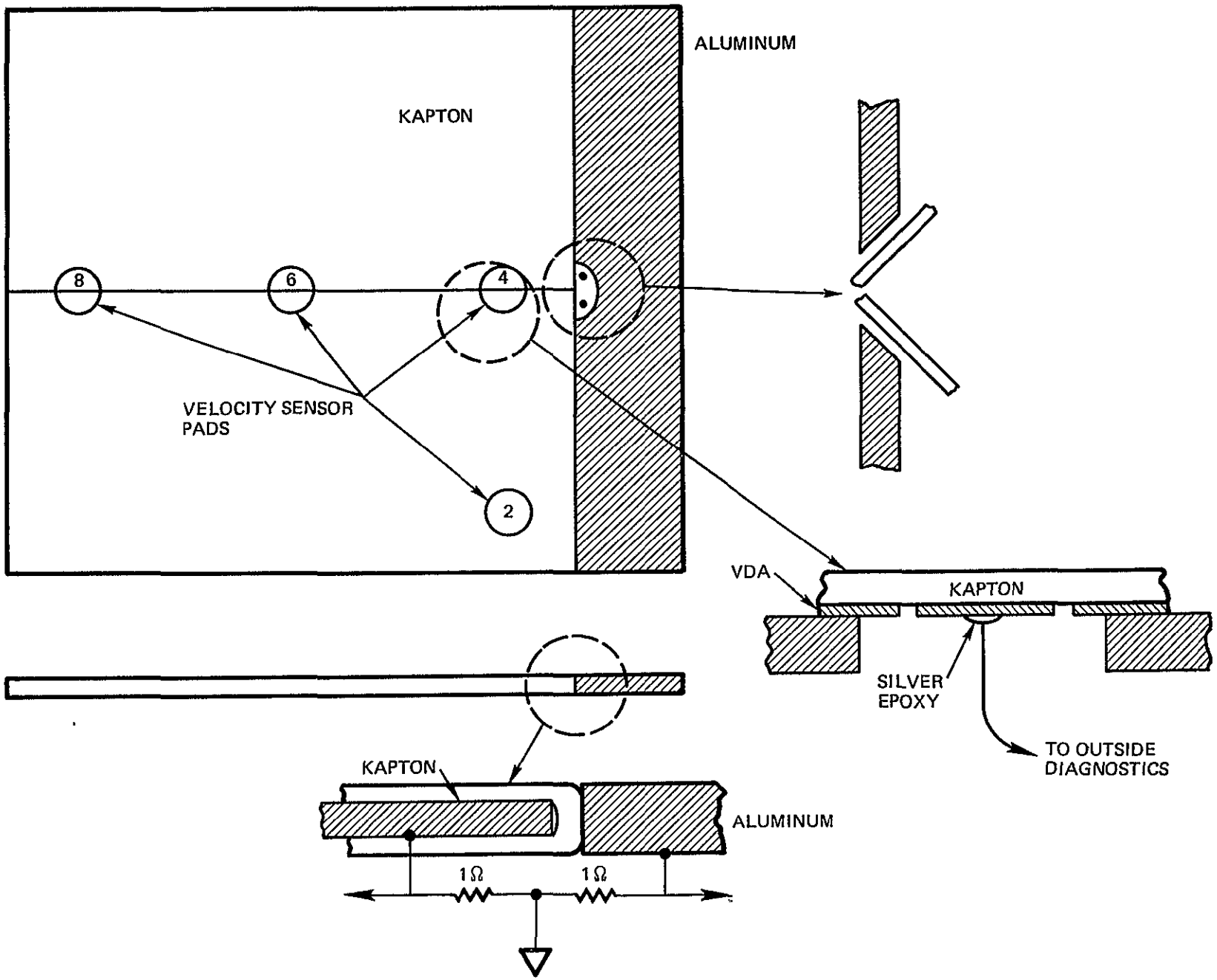

Figure 3-5. Sample Configuration Showing Capacitive Sensor Pads

Sensor #8 1 0μs delay

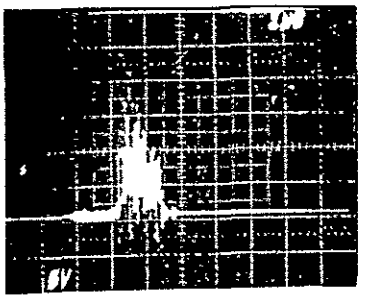

Sensor #6 0.5μs delay

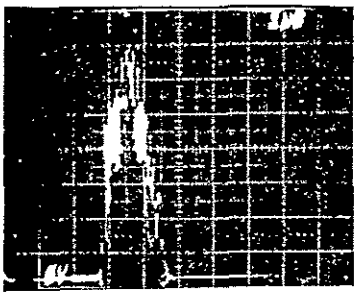

Sensor #4 0μs (reference)

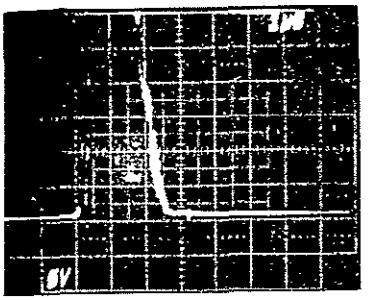

Sensor #2 0.3μs delay

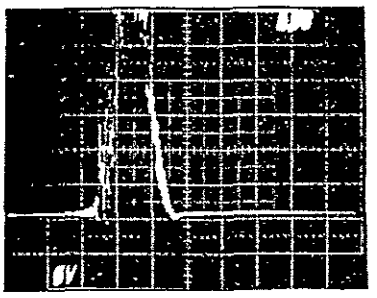

$v_b = 2.1 \cdot 10^7$ cm/sec.

Figure 3-6. Capacitive Sensor Pad Outputs Showing Propagation Time Delay (10- by 10-inch, 2 mil Kapton Sample)

One final comment on the velocity sensor outputs is the obvious decrease in signature level with distance from the ignition point by factors of about 5. Figure 3-7 shows typical surface potential scans before and after a discharge. There are no large gradients as might be expected from the velocity sensor outputs. No particular effort was made to scan the surface along the path joining the sensors, but rather, the scan was more or less along the sample diagonal. The results, particularly with the capacitive pads, seem to show an output related more to the charge flowing by rather than just the charge leaving that was originally on that pad.

3.2.3 Angular Distribution of Blowout Particles

The possible angular distribution of blowout currents was discussed as a result of the Task 1 analytical study. Seven 4- by 4-inch collector pads were located around the test sample as shown in Figure 3-2. Figure 3-8 shows voltage waveforms across a 1 ohm resister obtained from these pads. As expected, Pad No. 3 shows the largest current which is more than 10 times larger than that collected on Pad No. 7 which is in the opposite direction facing arc ignition location.

3.2.4 Other Diagnostics and Instrumentation

Figure 3-2 also shows the 10-inch cylindrical collector ring which is located under the pads discussed above. Having a much larger collecting area, it provides a much larger signal than the pads.

The connection to the side plate adjacent to the test sample was also brought out separately. It is most clearly shown in Figure 3-5. Because the sample itself is carefully folded over and covered, the side plate represents the only electrode to which "flashover" currents can flow. The waveforms of currents to the side plate show that the flashover current is small compared to the total replacement current.

Also under this category of diagnostic instrumentation is the "discovery" of the need to provide a high voltage feedthrough for the test sample grounding lead. Initial attempts to measure sample return currents and potentials with a high (>100 ohms) resistance led to incompatible results such as an apparent sample potential much greater than the 20 kV beam accelerating voltage. The breakdown of the feedthrough connector was

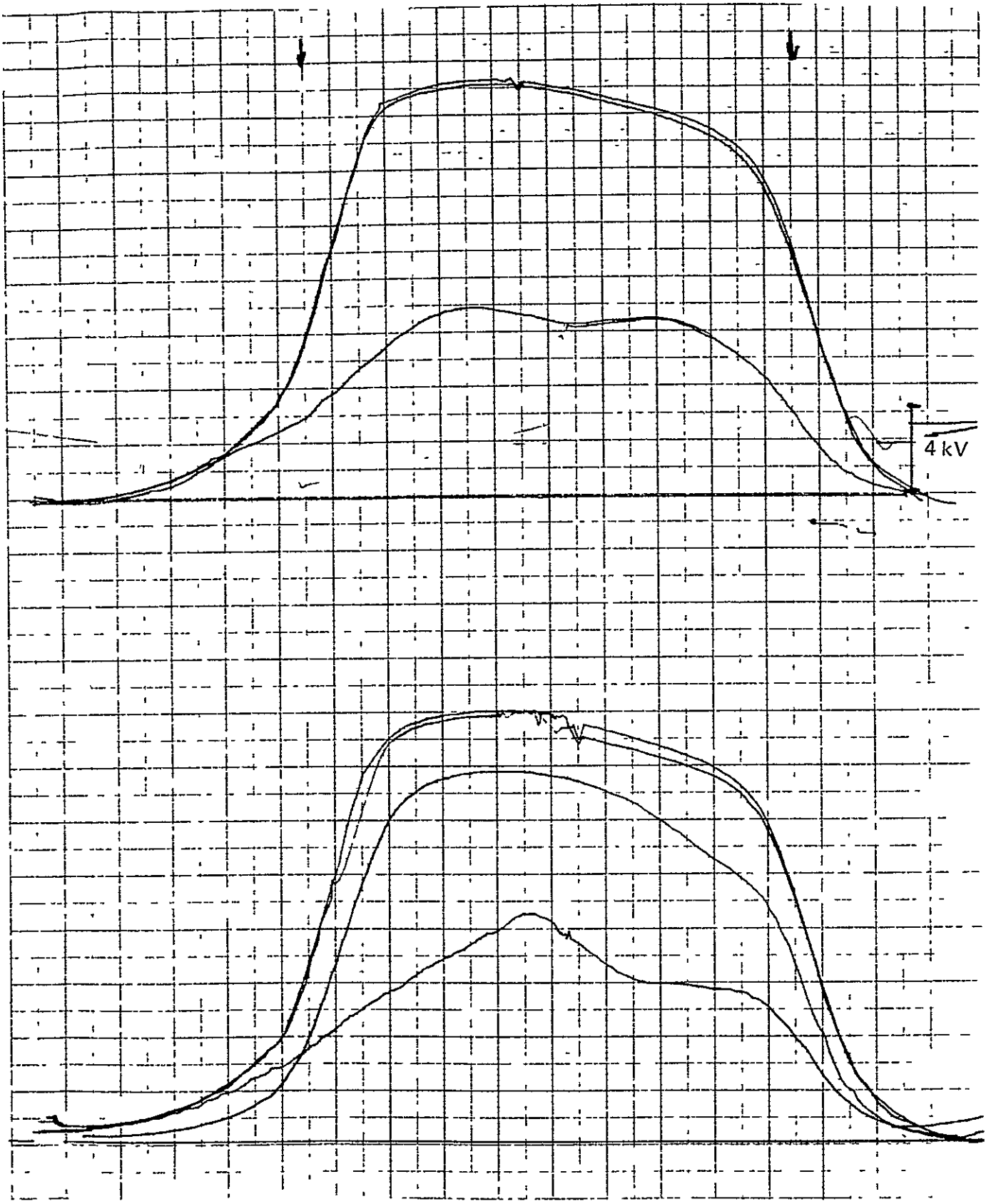

Figure 3-7. Surface Voltage Profiles Before and After Arc Discharge (8- by 8-inch, 2 mil Kapton Sample)

Pad #1 0.4 amps

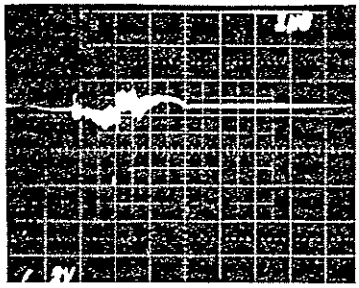

Pad #2 1.2 amps

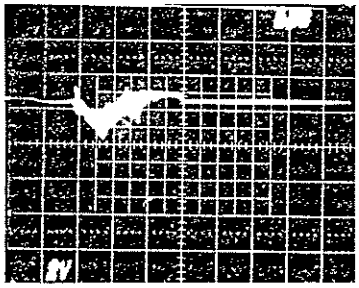

Pad #3 4.0 amps

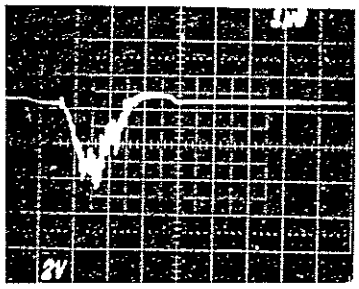

Pad #4 2.4 amps

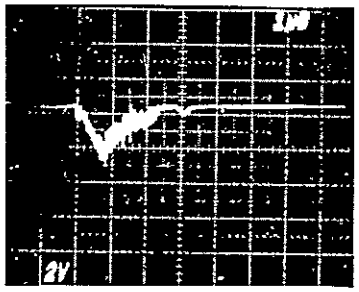

Pad #5 (shorted)

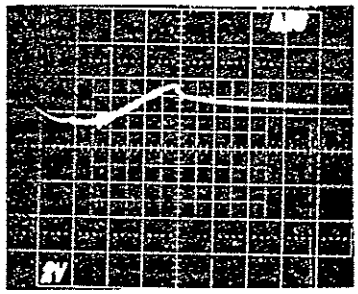

Pad #6 0.2 amps

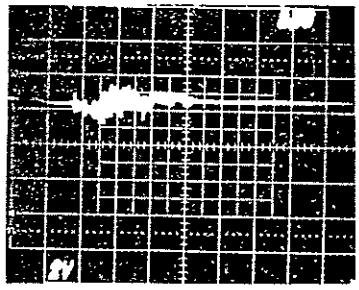

Pad #7 0.2 amps

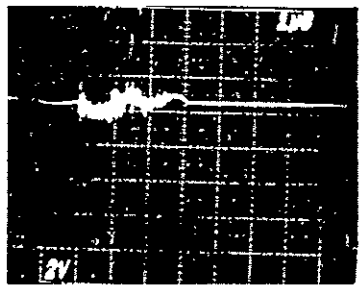

Figure 3-8. Pad Collector Currents Demonstrating Concentration of Blowoff Current in the Direction Towards Arcing Source (10- by 10-inch, 2 mil Kapton Sample)

the obvious conclusion, and replacement with a high voltage feedthrough solved the problem. Figure 3-9 shows the replacement currents and resulting sample potentials as a function of the grounding resistance.

The other instrumentation technique that should be noted here is that care in wiring to minimize cross-coupling of undesired signals is essential. It should also be recognized that the length of conductors and their inductance and capacitance to ground may affect the data obtained.

3.3 TASK 2.3: EFFECTS OF CHAMBER WALLS AND NEARBY METALS

The fact that the experimental study of arc discharges was performed in a vacuum chamber of limited dimensions as opposed to the real space environment undoubtedly affected the results in many ways. This environmental discrepancy is in addition to the fact that the real particle flux is multispecied, is usually omnidirectional, and has a distribution of energies. The rationale for not simulating the real environment more closely is the economic cost and that, hopefully, the characteristics of arc discharges are not significantly affected by the chargeup process.

In regards to the effects of the restricted volume of the test chamber, the obvious shortcoming is the zero potential boundary conditions imposed which tends to increase the magnitude of electric fields somewhat. The close-in fields near the surfaces of the test sample, however, should not be greatly influenced. The second obvious effect of the restricted volume is that the trajectories of blowoff particles are terminated at the chamber walls and thus the subsequent flow paths of the discharge particles are not properly simulated. The major effect of the blowoff particles is the generation of replacement currents flowing back to the arc source. The effect of the chamber walls is to provide a low impedance return path for the blowoff currents. The effective "impedance" of the complete "circuit," however, is determined to a major degree by the electric fields and the arc discharge processes in the vicinity of the discharging element. This is one of the conclusions of the arc discharge analysis of Task 1. The fact that experimental results on arc discharge characterization performed in vacuum systems varying in volume by several orders of magnitude give roughly the same results, is an indication that the analysis is correct in this respect. The relatively small fraction of the blowoff current going to the side plate, indicates that nearby grounded metals do not collect as

Ro=130kΩ
V_r=20 kV
I_r=.15A

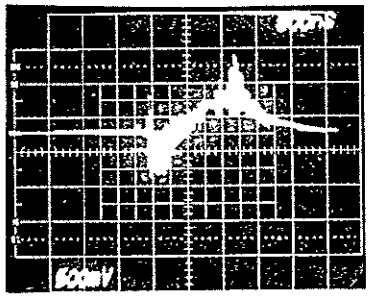

Ro=130 kΩ
I_c=.4A
V_c=.4v

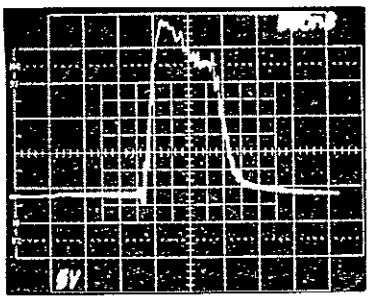

Ro=10 kΩ
V_r=20 kv
I_r=2.5A

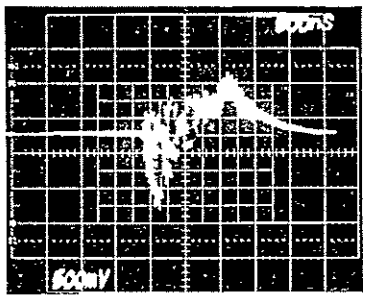

Ro=10 kΩ
I_c=.5A
V_c=.5v

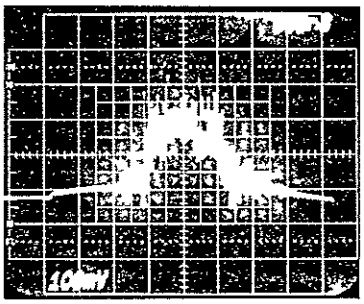

Ro=1 kΩ
V_r=20 kv
I_r=20A

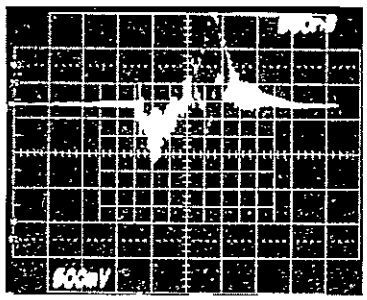

Ro=1 kΩ
I_c=.6A
V_c=.6v

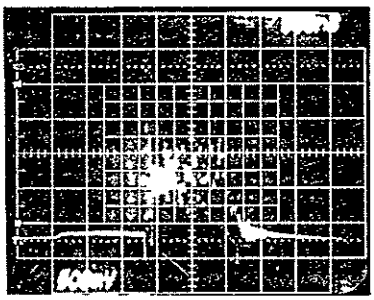

Ro=100Ω
V_r=10 kv
I_r=100A

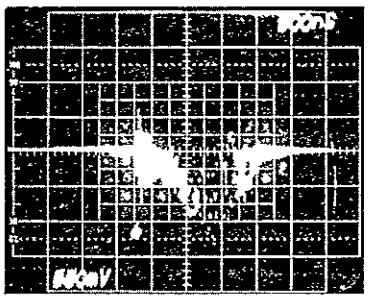

Ro=100Ω
I_c=8A
V_c=8v

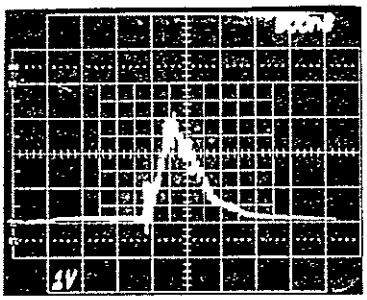

Ro=1Ω
V_r=250v
I_r=250A

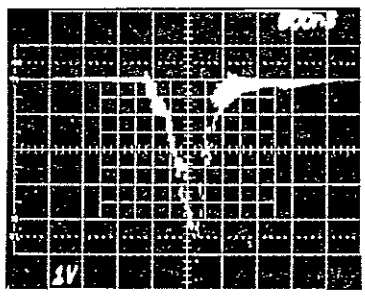

Ro=1Ω
I_c=40A
V_c=40v

Figure 3-9. Replacement and Collector Ring Waveforms as a Function of Sample Grounding Resistance (8- by 8-inch, 2 mil Kapton Sample)

much current as might be expected from predischarge electric fields. The analysis in Task 1 shows why this is the case. Figures 3-10 and 3-11 show the replacement currents and the side plate currents for a 10- by 10-inch sample and a 6- by 6-inch sample. The oscilloscope traces to the left show the replacement currents to the samples, and the traces on the right are the side plate currents. The side plate currents are less than 20 percent of the replacement currents.

3.4 TASK 2.4· EXPERIMENTAL CHARACTERIZATION OF ARC DISCHARGES AND COUPLING SOURCE MODELS

The objective of this task was to characterize arc discharges and electromagnetic interference coupling source models from the data obtained in the experimental study. A comparison of these results with those of the analytical study is presented in the writeup of the next task.

3.4.1 Arc Discharge Characterization with Low Impedance Grounding

The experimental data on arc discharges was presented in Figures 3-4 through 3-11. The propagation of a discharge wavefront in the "brushfire" mode is very real. The propagation velocity of about $2.3 \cdot 10^7$ cm/s is consistent with all of the data obtained. As a result of the finite propagation velocity, the rise time and width of the discharge currents are functions of the size of the arcing source. Figure 3-12 shows the peak replacement current as a function of the sample area for the three sample sizes tested. The peak replacement current, for the 1-ohm sample grounding resistance, varies nearly linearly with area.

$$I_{peak} \cong 0.65 \cdot \text{Area } (cm^2) \text{ amperes.}$$

Figure 3-13 shows the current pulsewidth plotted as a function of the length of the side of the square sample. The width, τ_p varies nearly linearly with this dimension.

$$\tau_p \cong 40 \cdot \ell \text{ (cm) ns.}$$

Replacement Current
(300-500 Amps)

Side Plate Current
(50-100 Amps)

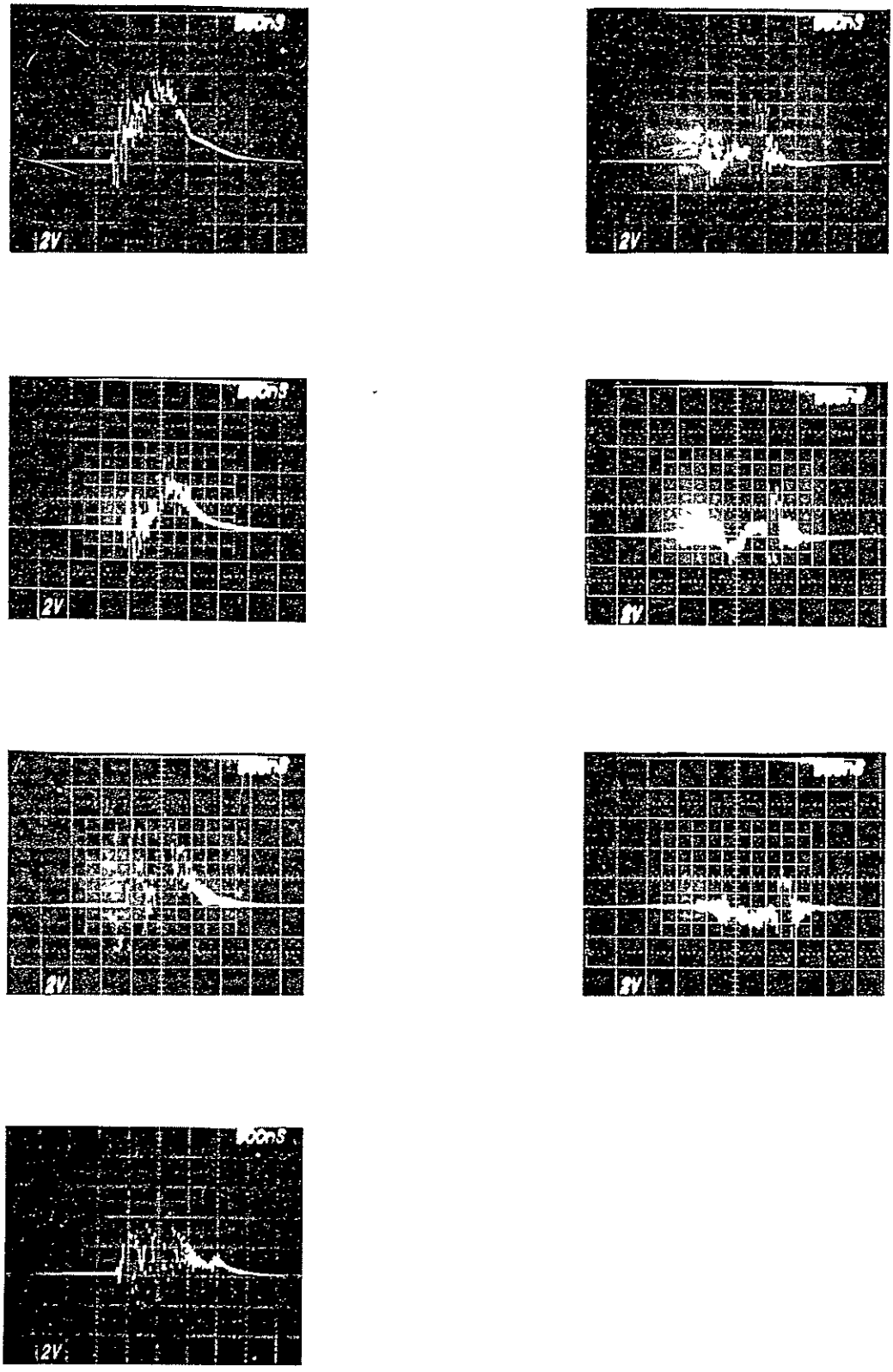

Figure 3-10. Replacement and Side Plate Currents (10- by 10-inch, 2 mil Kapton Sample)

Replacement Current
(100-200 Amps)

Side Plate Current
(< 20 Amps)

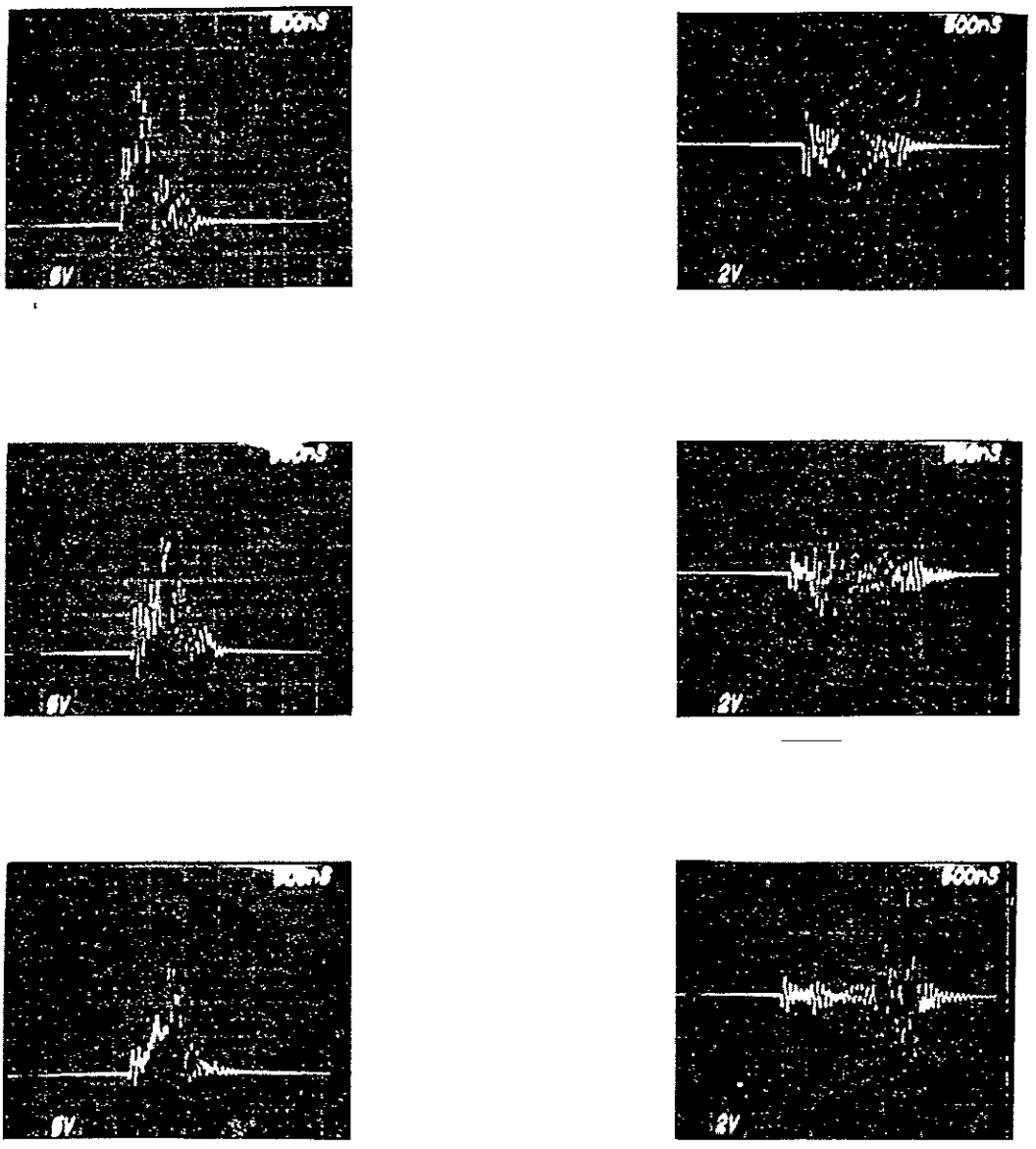

Figure 3-11. Replacement and Side Plate Currents
(6- by 6-inch, 2 mil Kapton Sample)

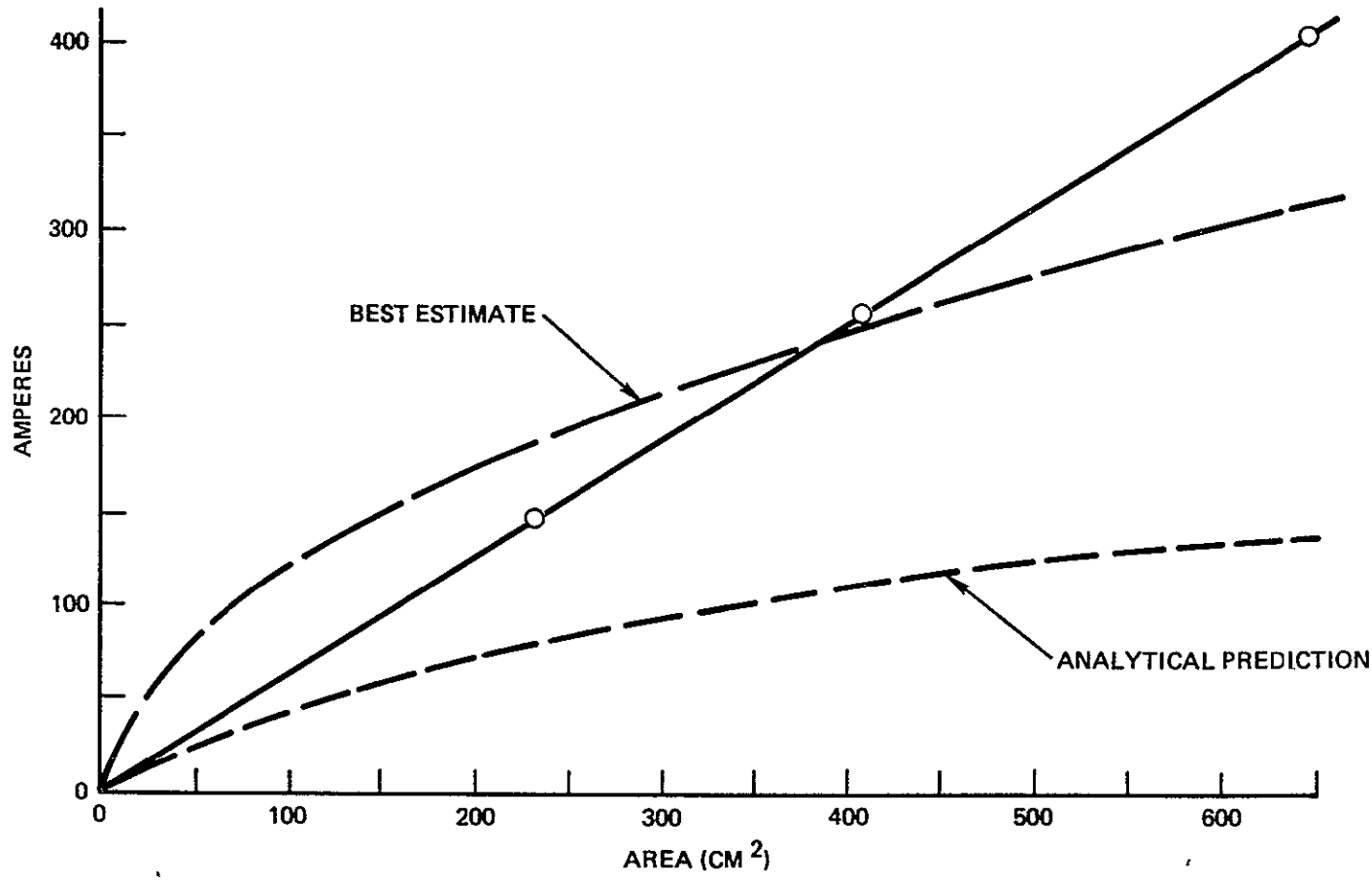

Figure 3-12. Peak Replacement Current versus Area (R_o = 1 ohm)

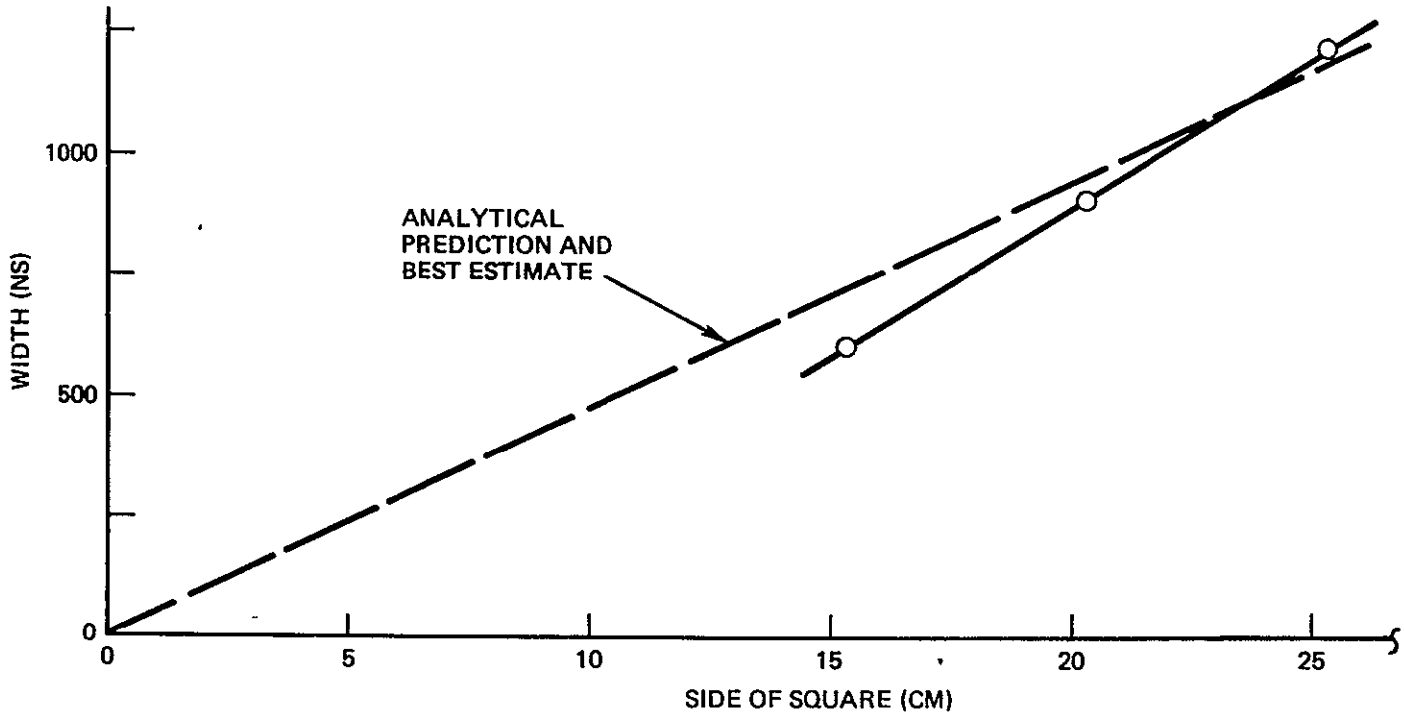

Figure 3-13. Replacement Current Pulsewidth versus Side of Square (R_o = 1 ohm)

This fit to the data has been made to force τ_p to equal zero for ℓ equal to zero, since it is consistent with our analytical expectations and because the quality and quantity of data is not inconsistent with this assumption. Since the current waveform is nearly triangular, the rise time of the pulse, τ_r, may be taken to equal to the pulsewidth

$$\tau_r = \tau_p = 40 \cdot \ell \text{ (cm) ns.}$$

3.4.2 Arc Discharge Characterization with High Impedance Grounding

Arc discharges as they exist on spacecraft in flight are more correctly characterized by the results of the tests performed with a high sample grounding resistance. The tests performed with a small (1-ohm) grounding resistance were important in that many facets of the brushfire analytical model were verified, and because many aspects of the high impedance tests are made more understandable in light of the low impedance test results. Furthermore many of the arc discharge processes such as the propagation have been observed to proceed independent of the value of the grounding resistance.

Figure 3-14 shows the peak sample replacement current and corresponding sample (spacecraft) potential as functions of the sample grounding resistance. These data are for the 8- by 8-inch sample with a 2 mil Kapton. It is seen that the "spacecraft" potential rises to about the 20 kV beam voltage (less the secondary emission crossover) for resistances as low as 1000 ohms. At 10 kilohms, the replacement current is down to 1 percent (2.5 amperes) of the 250 amperes obtained with a 1-ohm resistance.

In Figure 3-9 it is interesting to note that the waveforms of the collector ring currents on the right hand side are the positive ion currents obtained at late times when the sample potential is as high as ∿20 kV. The ions are "pushed" outward by the high potential and the arrival times are not inconsistent with the velocity computed for heavy ions. The negative triangular electron arrival current, observed with a 1-ohm sample grounding resistance, corresponds very closely to the sample replacement current waveform. As the sample potential rises with increasing grounding resistance, the electron blowout current is quickly cut off as is predicted by

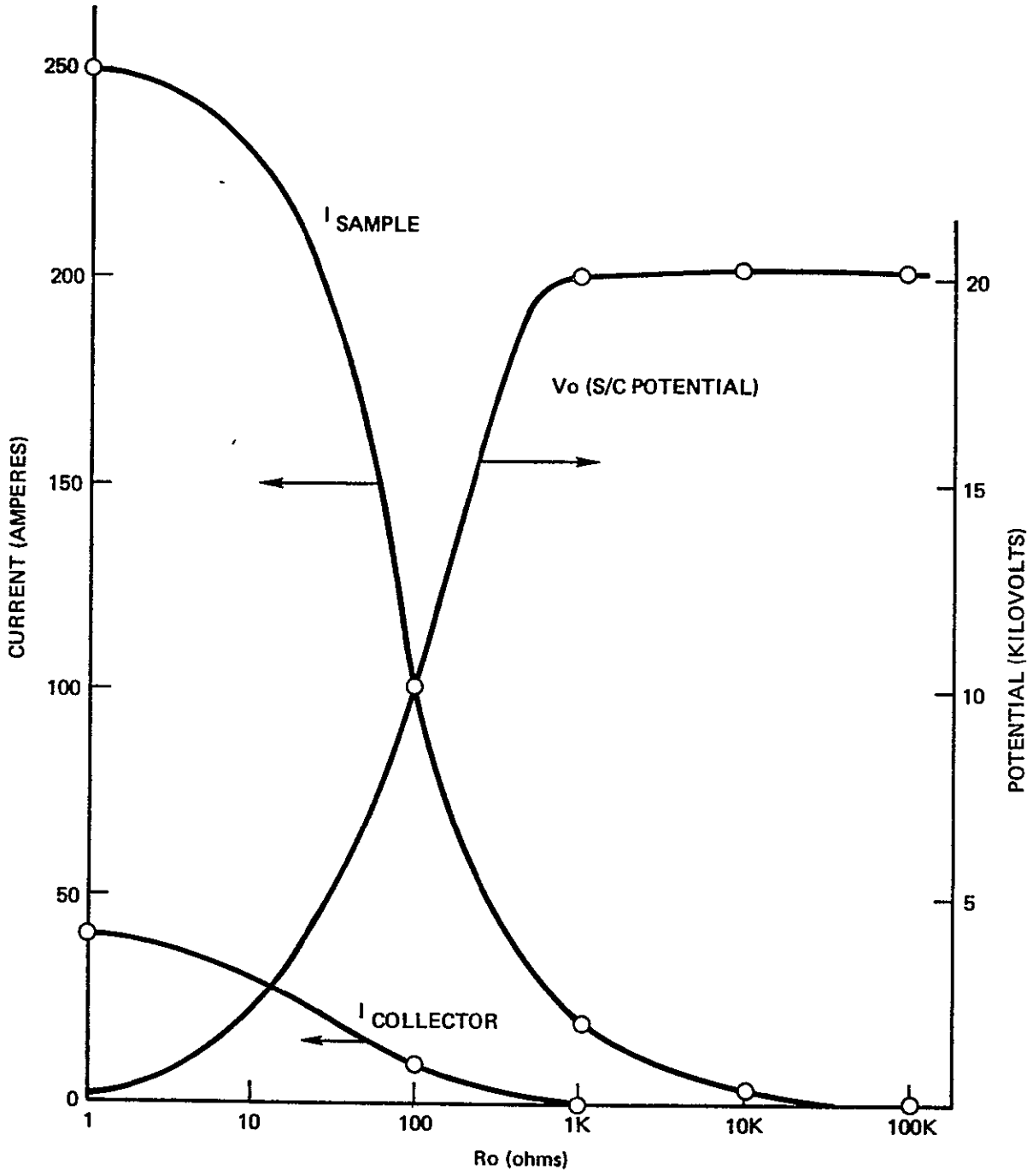

Figure 3-14. Potential and Currents as Functions of Grounding Resistance (8- by 8-inch, 2 mil Kapton Sample)

the analysis of Task 1. The similarity of the predicted variation of blowoff current and sample potential with grounding resistance of Figure 3-15 and the experimental data of Figure 3-14 is striking.

3.4.3 Characterization of High Frequency Transients

The characterization of arc discharges would be incomplete without acknowledging the existence of the "fine" details, the high frequency (>50 mHz, <10 ns) transients which appear to a greater or lesser degree in all of the waveforms recorded in the experimental study. Because the majority of the on-board circuits are not susceptible to these high frequency transients, because they may easily be shielded or filtered out, and finally, because they were not reproducible from discharge to discharge and from sample to sample, emphasis was not placed on them and no definite conclusions could be made in regards to them. It is clear that the appearance of these high frequency transients was highly dependent on the particular configuration of the test setup, the routing and shielding of diagnostic wiring, and the circuit inductance and capacitance associated with the diagnostics.

3.4.4 Additional Angular Blowout Current Distribution Data

Data on the angular distribution of blowout particles were discussed in Section 3.2.3 and presented in Figure 3-8. These data were obtained with collection pads located around the test sample in the plane of the sample, and showed that the largest concentration of blowout electrons was in the direction of the arc ignition source from the remainder of the sample.

Figure 3-15 shows the angular distribution of blowoff currents in a plane perpendicular to that of the test sample. The sample grounding resistance was 1 ohm as it was for Figure 3-8. The location of the six additional collection pads are shown at the bottom of Figure 3-15. The collector pad current waveforms are shown in approximately their correct relative positions. As might have been expected, Pads No. 2 and No. 3 show the largest peak currents with Pads No. 4, No. 5 and No. 6 showing the

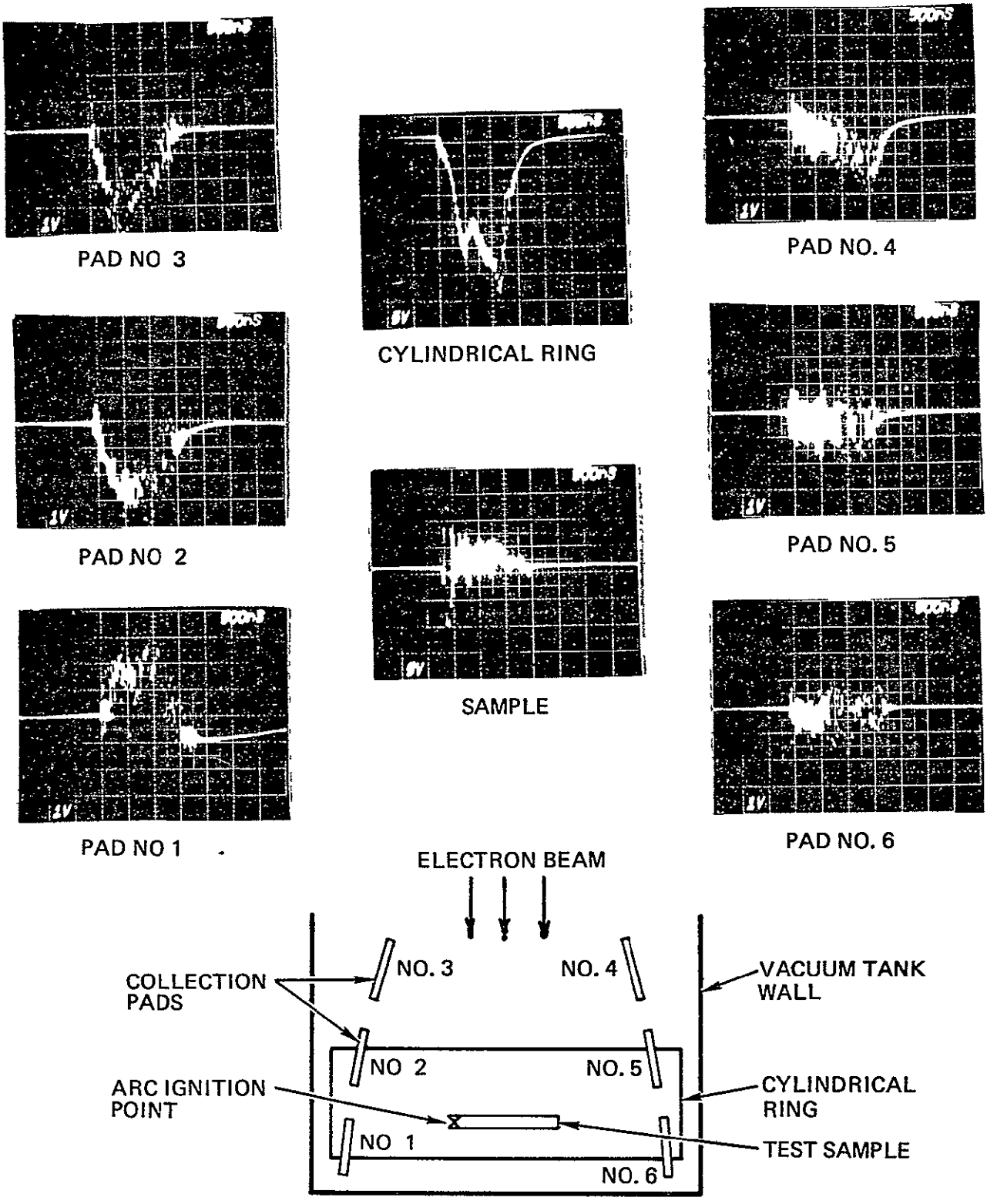

Figure 3-15. Polar Angle Blowoff Current Distribution 1 ohm Grounding Resistance (8- by 8-inch, 2 mil Kapton Sample)

lowest currents. The rationale for this expectation is that the brushfire wavefront propagation from the left side to the right results in the blowout of electrons from the right side towards the left side of the test setup as shown at the bottom of Figure 3-15. The sample replacement current is shown at the lower center and the cylindrical ring collector current at the upper center of Figure 3-15. A better waveform for the sample replacement current for the 1 ohm grounding resistance is shown at the bottom of Figure 3-9. It may be noted there that even with the 1 ohm grounding resistance, the peak sample voltage is +250 volts. This probably contributes to the fact that positive ion currents are collected on Pad No. 2. It may also be noted in Figure 3-15 that although Pads No. 4 and No. 5 show much smaller peak currents, the peaks also occur later in time than for Pads No. 2 and No. 3. This again is consistent with the brushfire propagation model.

Figure 3-16 shows the set of waveforms corresponding to Figure 3-15 but with a 10 kilohm sample grounding resistance. The blowout currents are much smaller than might have been expected. In accordance with the series of waveforms shown in Figure 3-9 in which the grounding resistance was varied from 1 ohm to 130 kilohm, positive ions are collected for the major fraction of the pulse duration. This is because the initial electron current is quickly cut off by the positive 20 kV potential of the sample and the ions are pushed out. Again, for some unknown reason, Pad No. 1 behaves anomalously and initially registers an ion current which then becomes an electron current.

The assistance of Dwight Anthony in this experimental study is gratefully acknowledged. He kept the laboratory work going with minimal supervision and was invaluable in assisting in the data taking process.

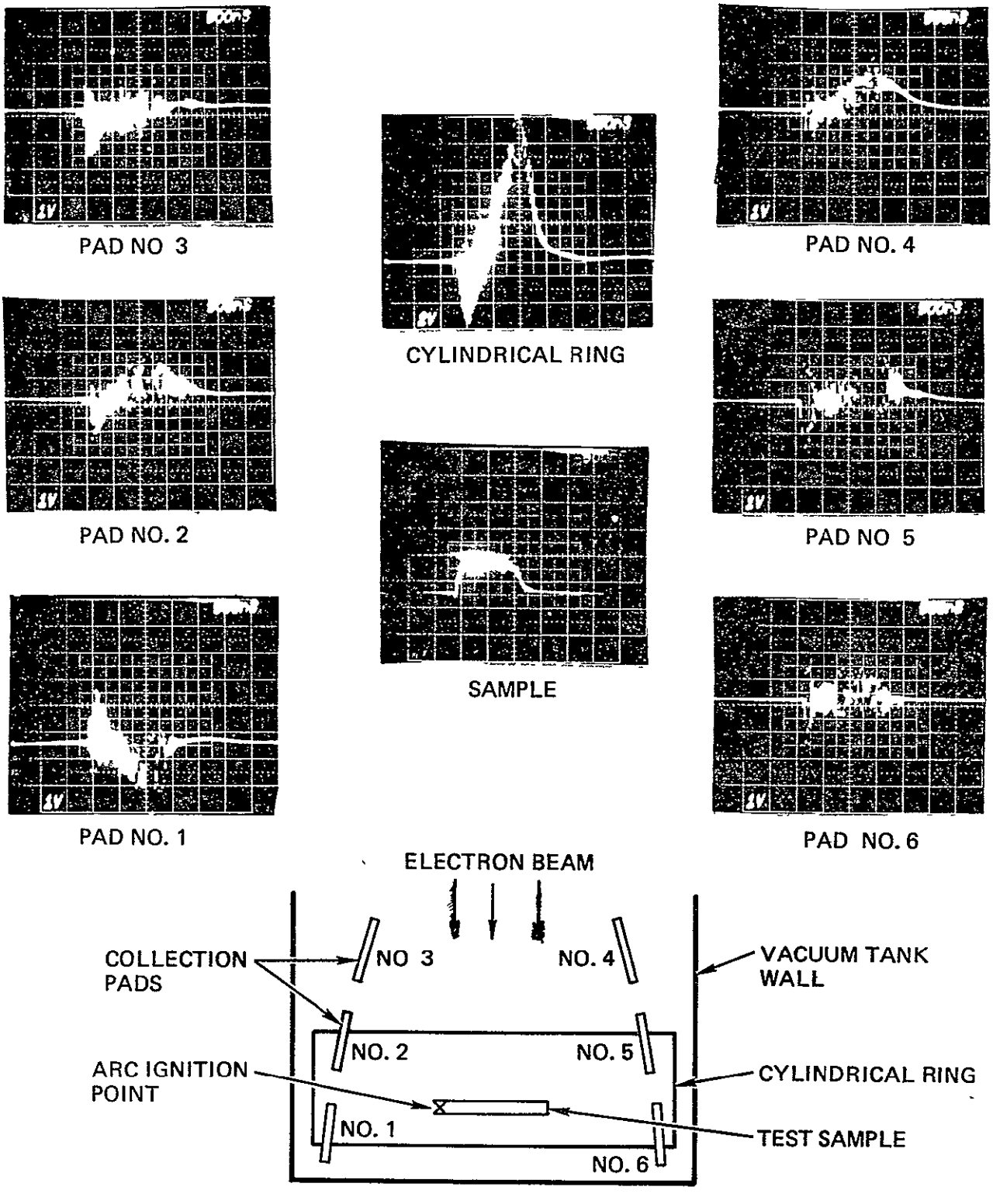

Figure 3-16. Polar Angle Blowoff Current Distribution 10 kilohms Grounding Resistance (8- by 8-inch, 2 mil Kapton Sample)

4. TASK 3. COMPARATIVE STUDY OF ANALYTICAL AND EXPERIMENTAL RESULTS

The objective of this task is to take the results of the analytical study, Task 1, and the experimental study, Task 2, of the characteristics of arc discharges and to come up with the best estimate arc discharge source models to be incorporated into a SEMCAP model. The actual running of the SEMCAP code and the analysis of its outputs constitutes the final task, Task 4. Figure 4-1 shows the logical flow diagram for Task 3.

The analytical and experimental approach each have their strong points and their weak points, or advantages and disadvantages. For example, the analytical approach is difficult to implement for complex configurations with multidimensional effects, but parametric effects such as area or sample size effects may be easily extrapolated if they are included in the analysis. The experimental approach permits "real" configurations to be tested, but the reality of the simulation of actual in-flight conditions must be evaluated carefully. In the past, many shortcomings of an analytical approach have been revealed by the experimental approach. An example is the large area wipeoff of charge built up over a dielectric surface. On the other hand, the many early tests on the measurement of discharge pulse amplitudes using small sample grounding resistances have tended to overestimate the threat. Some of the results obtained in the present work have not been available previously, but it is also recognized that a large body of knowledge about the phenomena associated with spacecraft charging has been built up in the past few years by the community of workers concerned with its effects. This data will also be used wherever it is appropriate.

4.1 TASK 3.1 COMPARISON OF ANALYTICAL AND EXPERIMENTAL STUDY RESULTS

A number of problems exist in "comparing" the results of the analytical and experimental studies performed in Task 1 and Task 2 of the present work. These are that the analytical characterization of arc discharges was basically a 1-dimensional analysis, whereas the experimental study was limited in the size of the test sample. A more appropriate view of this task is that the analytical and experimental approaches complement each other, and that each set of results must be interpreted in the light of the other.

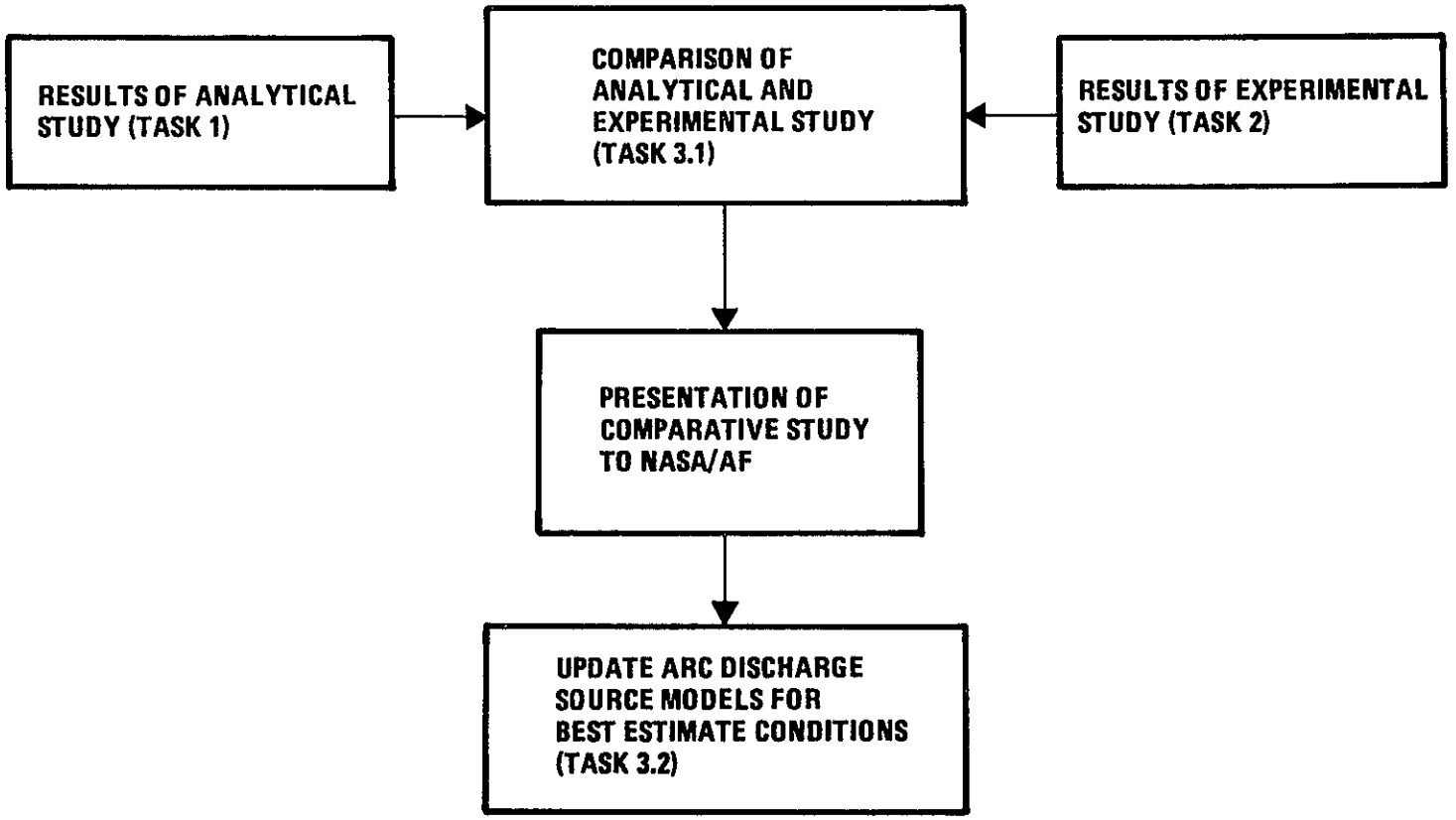

Figure 4-1. Task 3 Comparative Study of Analytical and Experimental Results

The primary parameters of interest in evaluating the implications of arc discharges on spacecraft EMI margins of immunity are the pulse amplitude and waveform (rise time and width). The location and configuration of the arcing source relative to the remainder of the spacecraft, e.g., the presence of nearby cabling and the presence of bulkheads for electromagnetic shielding, are important factors in determining the coupled EMI. These, however, are taken care of in the SEMCAP model and analysis. The physical parameters such as the size, shape, and thickness of the arcing source, must be incorporated into the amplitude and waveform characterization. Some physical parameters such as the size and shape enter into both the arc characterization and the coupling analysis.

4.1.1 Arc Discharge Amplitude and Waveform: Low Grounding Resistance

Only a limited range of sample areas was tested. Figures 3-12 and 3-13 summarize the data on the dependence of the amplitude and width of the sample replacement current pulse with sample size for a 1 ohm grounding resistance. Figure 3-12 shows a nearly linear increase of peak current with area. The consensus of the community, however, is that it should vary as the square root of the area. Figure 4-2 is taken from our earlier study of the "Effects of Arcing." The data from Task 2 of the present study are shown on Figure 4-2. On the log-log scales of that figure, the new data is not inconsistent with the prior data. Two additional data points obtained by JAYCOR workers are also shown on Figure 4-2.

The brushfire arc discharge propagation velocity of $2.45 \cdot 10^7$ cm/s will be used for the following analysis. Referring back to Figures 3-9, 3-10, and 3-11, it is seen that the replacement current waveform is approximately triangular in shape for a low (1 ohm) grounding resistance. This waveform is consistent with the brushfire propagation model as developed in Task 1 in that the periphery of the high gradient region expands nearly linearly with time. Figure 4-3 shows three additional replacement current waveforms. Also shown at the upper right is a representation of a square sample with circular arcs centered at the ignition point. At the lower right is shown the replacement current waveform (low grounding resistance) deduced by assuming that the amplitude varies directly as the length of the circular arcs. The nicks and changes in slope of the oscilloscope waveforms seem to correspond to those in the simplified analytical model.

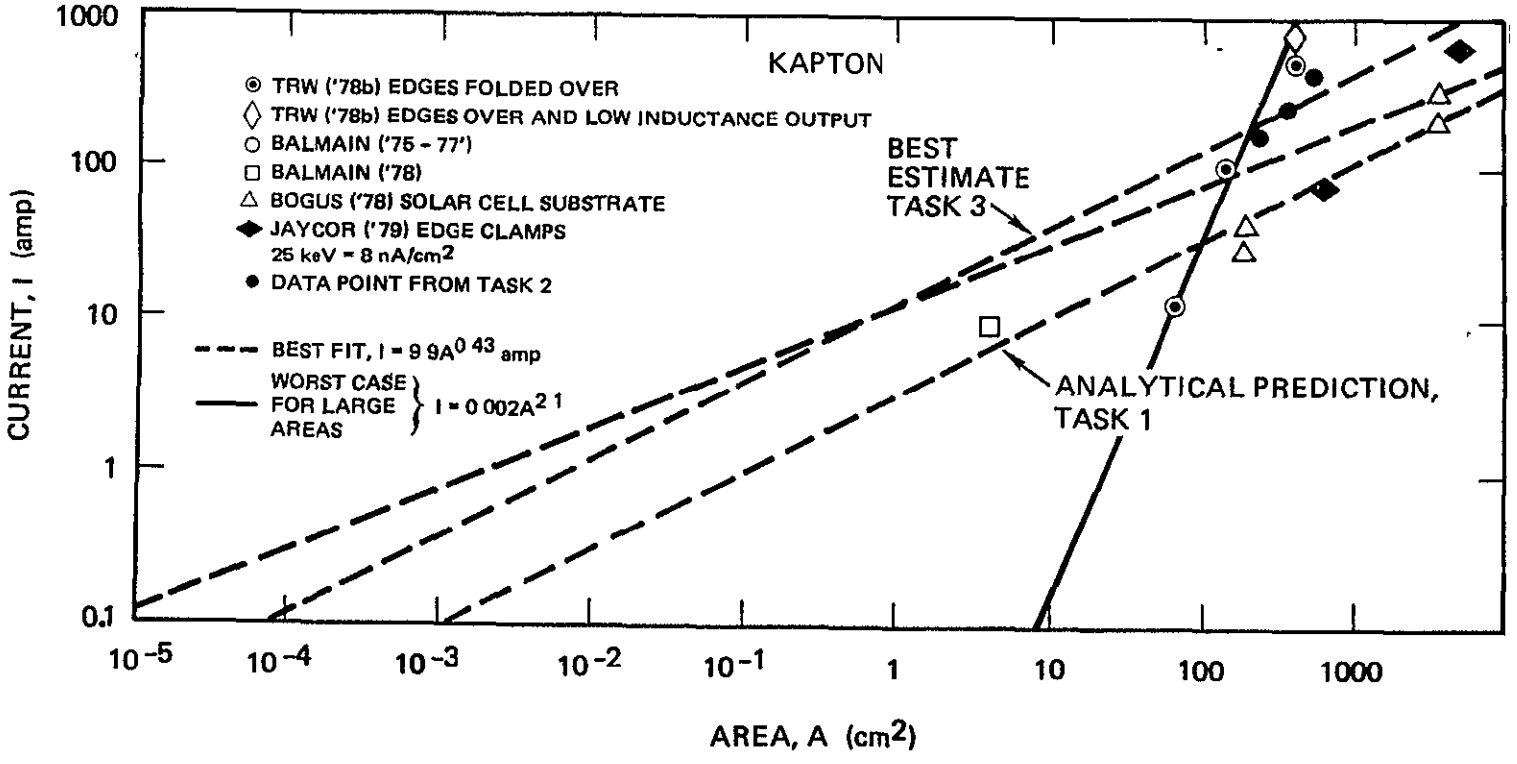

Figure 4-2. Discharge Peak Current versus Area for Kapton

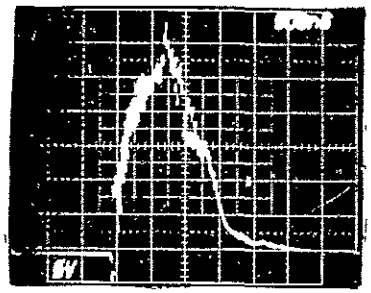

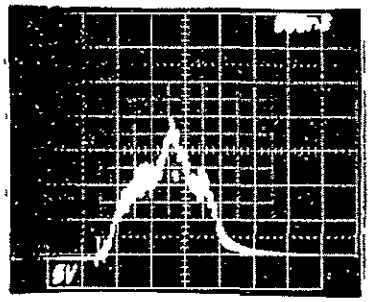

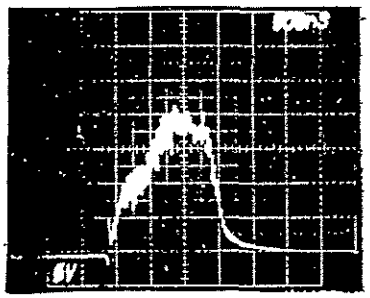

EXPERIMENTAL REPLACEMENT CURRENT WAVEFORMS

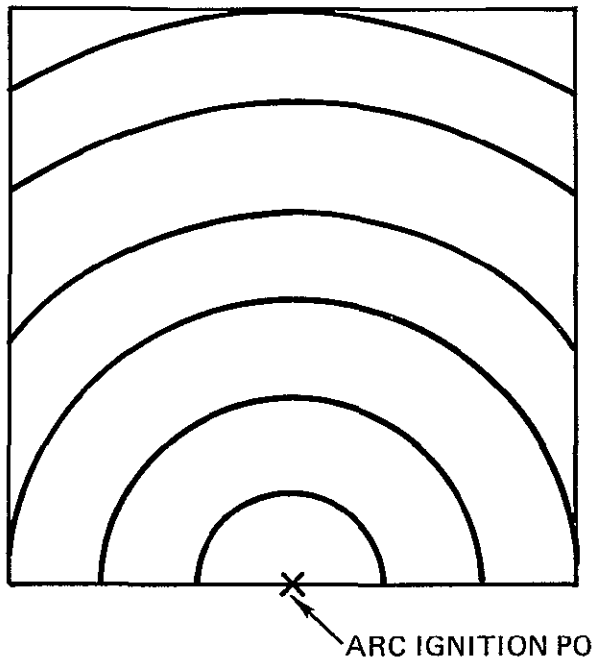

SQUARE SAMPLE SHOWING EXPANDING BRUSHFIRE WAVEFRONT

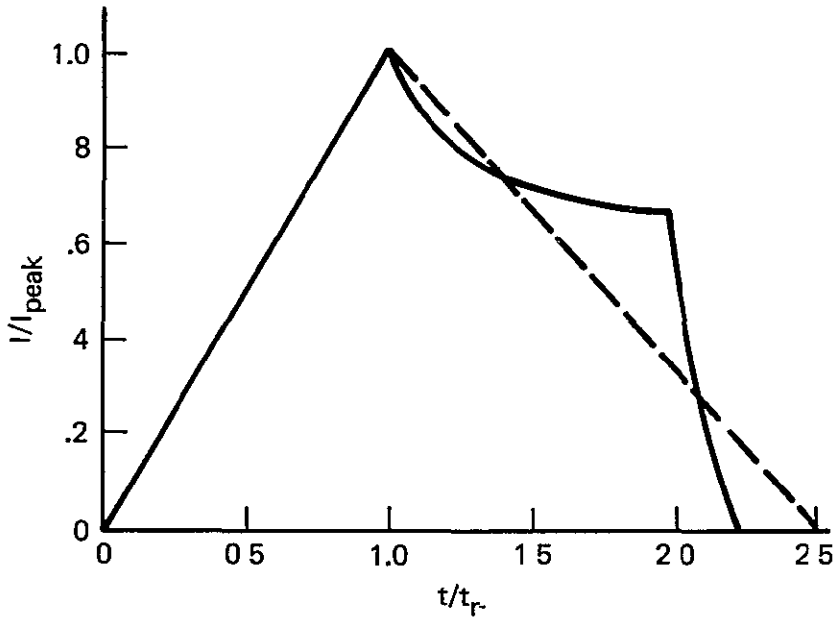

ARC DISCHARGE WAVEFORM DEDUCED FROM WAVEFRONT DIMENSION

Figure 4-3. Comparison of Experimental and Analytically Deduced Replacement Current Waveforms for a Square Sample

For the purposes of the arc characterization, a triangular waveform with the fall time 50 percent greater than the risetime, t_r, will be assumed. A dashed line in the "deduced" waveform of Figure 4-3 shows the assumed current falloff.

The amplitude of the triangular current pulse may be determined as follows. The stored charge, Q_s, is given by

$$Q_s = C\ V_b\ A = C\ V_b\ s^2 = 2.6 \cdot 10^{-7} s^2 \text{ coulomb}$$

where C is the capacitance per unit area, or 52 pf/cm^2 for 2 mil thick Kapton. V_b, the breakdown voltage, is estimated by assuming a breakdown electric field of 10^6 V/cm. With the 2-mil thickness, V_b is 5000 volts. A is the area in square centimeters. Assuming only half of Q_s is used up in an arc discharge, the charge in the arc, Q_a, is

$$Q_a = 1.3 \cdot 10^{-7} s^2 \text{ coulomb.}$$

From the assumed waveshape shown in Figure 4-3, the charge is given by

$$Q_a = I_{peak} \cdot (t_r \cdot 2.5)/2$$

Equating these two expressions for Q_a will give a value for I_{peak}. First, however, the risetime, t_r, must be obtained in terms of the propagation velocity, v_b, and the side of the square, s, as:

$$t_r = \frac{s}{2v_b} = 2.04 \cdot 10^{-8} \cdot s(\text{cm}) \text{ seconds.}$$

Now, equating the two Q_a's gives.

$$I_{peak} = 4.992 \cdot s(\text{cm}) \text{ amperes.}$$

This linear relation is plotted on Figure 4-2 with all of the data on current amplitudes versus area. The fit is not bad considering the variety of organizations contributing data points to the figure.

A second method of obtaining a comparison of analytical and experimental data is by using the 3.18 A/cm surface current density, J_s, obtained in the analysis of Task 1. The dimension required to convert J_s to I_{peak} is the largest circular arc or $\pi s/2$. With this

$$I_{peak} = J_s \cdot \pi s/2 = 4.99 \cdot s(cm) \text{ amperes.}$$

It is not surprising that the two analytical results are identical since the same basic assumptions were made of the charge in the arc, Q_a, and the brushfire propagation velocity, v_b.

For a long narrow arcing source such a boom, the waveform should not be triangular but more nearly rectangular. Figure 4-4 shows sample replacement currents and collector ring current waveforms for a 2- by 10-inch, 2 mil Kapton sample with a 1 ohm grounding resistance. Compared to those for the 10- by 10-inch square sample of Figure 4-3, the waveforms are more nearly rectangular. Assuming that the boom diameter, d, is 5 cm and its length, L, is 2 meters, the pulse rise time, t_r, and the pulse duration, t_p, would be

$$t_r = \frac{d \cdot \pi}{2v_b} = 374 \text{ ns}, \quad t_p = \frac{L}{v_b} = 9.52 \text{ } \mu s$$

The peak amplitude would be

$$I_{peak} = \pi^2 \, dJ_s/2 = 78.5 \text{ amperes.}$$

The experimental measurements of peak current amplitude are two to three times larger than the analytical predictions. Taking the average, 2.5 times, the best estimate peak pulse current for the square sample is

$$I_{peak} = 12.5 \text{ s(cm) amperes.}$$

We assume that this expression applies to circular or any other shape in which the dimensions of the arcing source are approximately equal in two orthogonal directions. The analytical and best estimate predictions of

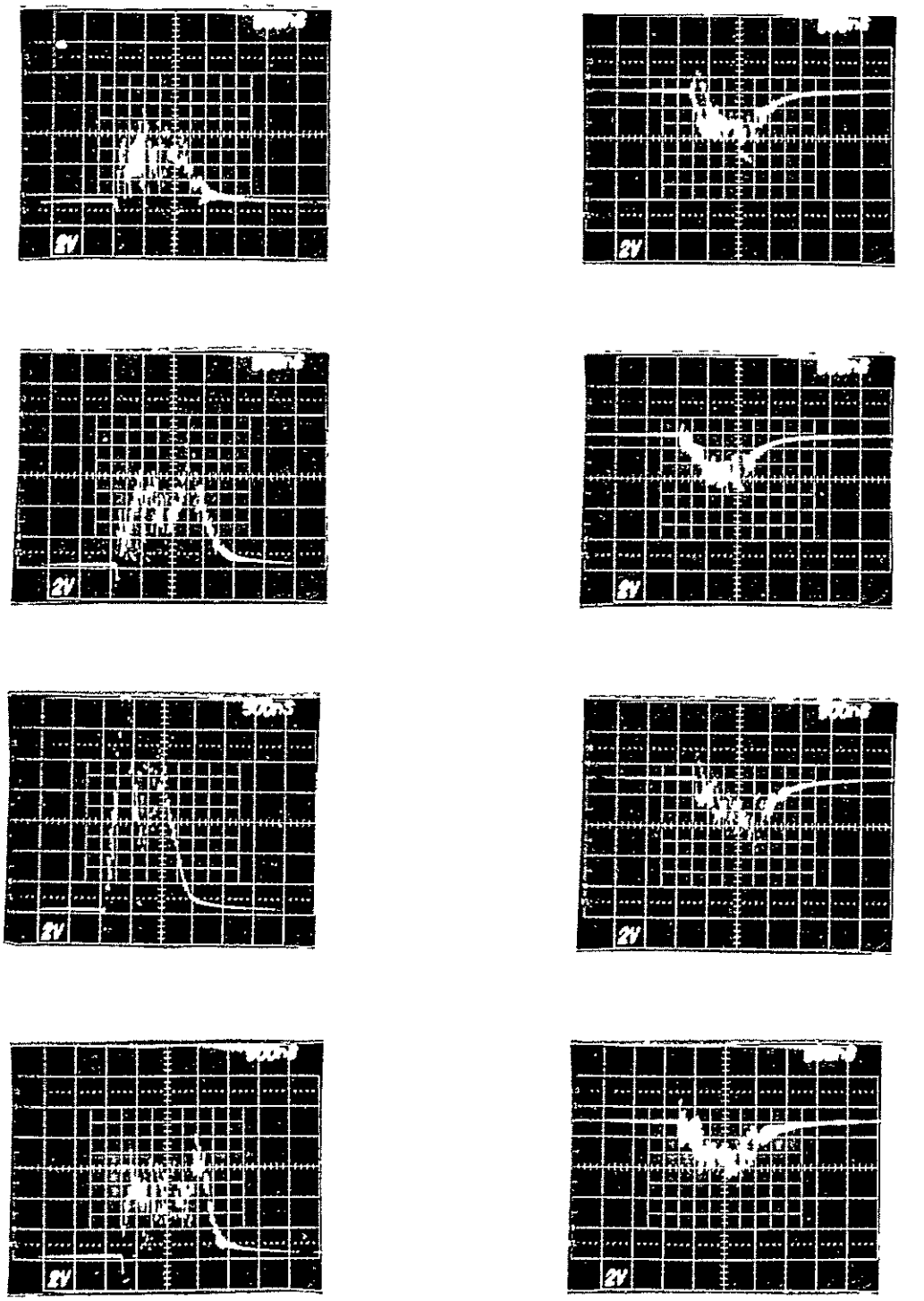

SAMPLE REPLACEMENT CURRENT

CYLINDRICAL RING CURRENT

Figure 4-4. Arc Discharge Waveforms for a "Long" Sample Ignited at One End (2- by 10-inch of 2 mil Kapton, 1 ohm Sample Grounding Resistance)

peak amplitude currents are shown on Figures 3-12 and 4-2. The fit of either prediction to the data points in Figure 4-2 is not bad considering the variety of organizations contributing information to that figure. The best estimate seems to be a reasonable worst-case prediction.

For the best estimate pulsewidth, t_p, we have assumed it to be 80 percent of the width at the base. This is equal to twice the rise time since the fall time was assumed to be 50 percent greater than the rise time:

$$t_p = 2t_r = 4.08 \cdot 10^{-8} s(cm) \text{ seconds.}$$

This prediction, which is both the analytical and best estimate prediction, is shown on Figure 3-13 and also on 4-5. Figure 4-5 is taken from our "Effects of Arcing" report and shows data from other workers as well as prior TRW data.

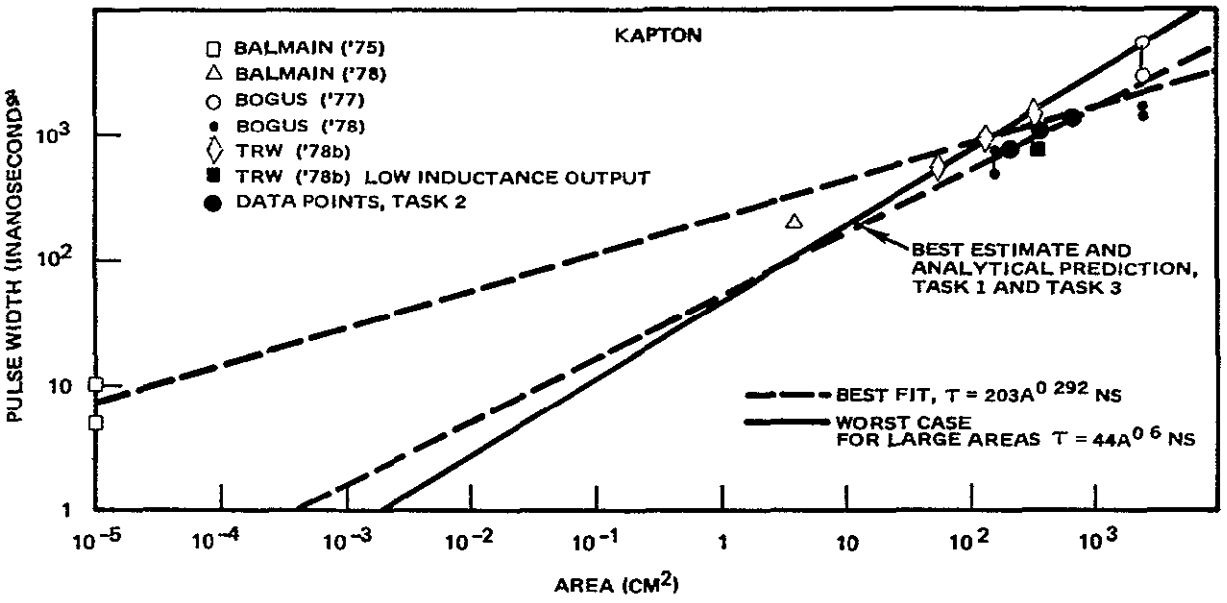

Figure 4-5. Area Dependence of Discharge Pulsewidth

The low sample grounding impedance arc discharge parameters obtained here pertain to the replacement current observed in the grounding resistor, i.e., its voltage divided by its resistance. The replacement current is what we have been referring to as the blowout current. The flashover current is not manifested in the grounding resistor voltage since it does not flow through the resistor. The only exceptions to this situation are

those such as in our test configuration in which the side plate return was monitored separately, and in which the sample substrate was completely covered with insulation so that return currents to it only flowed via the sample grounding wire. The distinction between flashover and blowout currents is more clearly evident in the discussion of the next section on the high sample grounding impedance arc discharge parameters.

One further point should be made in regards to arc characterization for the in-flight configuration. This has to do with the importance of particle trajectories as they are released or blown off by the arcing source. Our point of view is that the concentration of structural replacement currents is greatest at the arcing source and its grounding strap. Therefore this is the location of the greatest hazard to the spacecraft. The determination of blowoff electron and ion trajectories is interesting but the magnitude of currents collected at remote surfaces is generally insufficient to be of concern. What is of crucial importance is the ability or inability of the total spacecraft surface to collect sufficient charge to replace the charge blown off at the arcing source. This determines, as was shown in the analysis of Task 1, the potential to which the entire spacecraft rises during the discharge which in turn determines the amount of charge that is blown off. Because of this consideration, the waveforms and data presented on the left half of Figure 3-9 for the sample replacement current are more important than those on the right side of the figure which shows the collector ring currents.

4.1.2 Arc Discharge Amplitude and Waveform: High Grounding Impedance

The evaluation of the implication of arc discharges on spacecraft EMI margins of immunity requires that the discharge parameters be applicable to the in-flight situation. Specifically, the arc discharge characterization obtained with a low sample grounding impedance as discussed in the previous section are not directly applicable. This is because of the change in spacecraft potential and the resulting cutoff of the blowout currents that would have existed if the potential had not changed. This cutoff process was discussed analytically in Task 1 (Appendix 4) and verified experimentally in Task 2 (Section 3.4.2).

With the quantification of the arc discharge parameters for the low impedance case into best estimate values in the preceeding section, we are now in a position to extend these to the in-flight or high impedance situation using both the analytical and experimental results. Since the discussion in the last section relied on experimental data to correct the anlaytically derived parameters, the conclusions apply to the blowout currents rather than the flashover currents. The correction factor, applying to the analytically derived low-impedance blowout surface current density, J_{sz}, of 1.86 A/cm is

$$\text{Correction factor} = 2.5$$

The corrected value of J_{sz} is, therefore, 4.65 A/cm, and this gives the best estimate peak blowout current as

$$I_{peak} = J_{sz} \cdot (\pi s/2) = 7.30 \cdot s(cm) \text{ amperes.}$$

Assuming that the experimentally obtained brushfire propagation velocity of 2.3 10^7 cm/s is correct and, for worst case purposes, that three/fourths of the stored charge is dissipated rather than one-half, the largest flashover surface current density, J_s, possible is

$$J_s = CV_b v_b = 4.49 \text{ A/cm.}$$

We have assumed the capacitance per unit area, C, to be 52 pf/cm^2 corresponding to a dielectric constant of 3 and a thickness of 2 mils. The breakdown voltage, V_b, of 5000 volts corresponds to an electric field of 10^6 V/cm. With these values for J_{sz} and J_s, the corresponding G' factor is

$$G' = J_{sz}/J_s = 1.04.$$

This is 1.77 times larger than our analytically obtained value for G' of 58.5 percent, and in fact violates our initial notions which gave rise to the G' concept. Originally, the view was that the stored charge was dissipated in two ways, a flashover current and a blowout current. Thus there was no way in which either integrated component could be greater than the stored charge, and therefore, G' could not be greater than 100 percent. The brushfire analysis, however, showed that because of the ablation and ionization processes, there was a reservoir of free electrons (and ions) generated which could greatly exceed the originally stored charge which led to the breakdown voltage. The only reason that G' happened to be 58.5 percent was that only that amount of electrons could be ejected before Debye shielding of the external electric field stopped the blowout process. Therefore a G' value of 1.25 is not impossible, because the initial conceptions about G' have changed as a result of this study. An equally valid computation for G' is to assume that the 3.18 A/cm value of J_s obtained analytically is correct giving

$$G' = 4.65/3.18 = 1.46.$$

With the assumed linear rise of blowout current with time, the time dependent current, I(t), may be written as

$$I(t) = I_{peak} \cdot (t/t_r) = J_{sz} \cdot (\pi s/2) \cdot (2v_b t/s)$$

$$= (\pi v_b J_{sz}) \cdot t = 3.58 \cdot 10^8 t \text{ (sec) amperes.}$$

In terms of J_s and G', I(t) is given by

$$I(t) = (\pi v_b G' J_s) \cdot t,$$

in which G' is 1.46 and J_s is 3.18 A/cm. The current, for the rising amplitude portion, is independent of the size, s, of the arcing source. The cutoff of current by the rising spacecraft potential, V_o, may be

derived by assuming that the replacement current is entirely comprised of displacement current which charges the spacecraft capacitance to space, C_o:

$$C_o = 4\pi\varepsilon_o R = 150 \text{ pf for } R = 1.5 \text{ meters.}$$

The equations to be solved, the solutions and the curves for $I(t)/I_o$ and $V_o(t)/V_r$ are shown in Figure 4-6.

The value for the remaining voltage, V_r, to be used in the equations shown on Figure 4-6 is the full bulk breakdown voltage, 5 kilovolts, and not the 2.5 kilovolts remaining after the discharge. This is because, as was shown in the blowout analysis, the blown out charges are emitted only at the head of the brushfire wavefront where the potential has not yet dropped appreciably. The square root dependence of the blowout current, I(t), on the surface potential, V_s, stems from the velocity which is derived from the energy equation·

$$1/2\ mv^2 = eV_s.$$

The time constant, τ, for the 1.5-meter radius spacecraft (DSP) is 91.5 nanoseconds. This is the time in which the spacecraft reaches its maximum potential of 5 kilovolts , and also the time in which the electron charging current goes back to zero, i.e., is cut off. I_o is a current, 32.8 amperes, defined by C_o, V_r, and the rate of increase, $3.80 \cdot 10^8$ A/sec, of the current with the spacecraft potential remaining at zero. The maximum replacement current is

$$I(t)_{max} = \frac{2}{3\sqrt{3}} I_o = 12.61 \text{ amperes.}$$

This maximum current, with the waveform shown, is independent of the size of the arcing source as long as its dimension is greater than that defined by the 51.1-nanoseconds time constant, τ:

$$I(t) = (\pi v_b J_{sz}) \cdot t = 3.85 \cdot 10^8 t$$

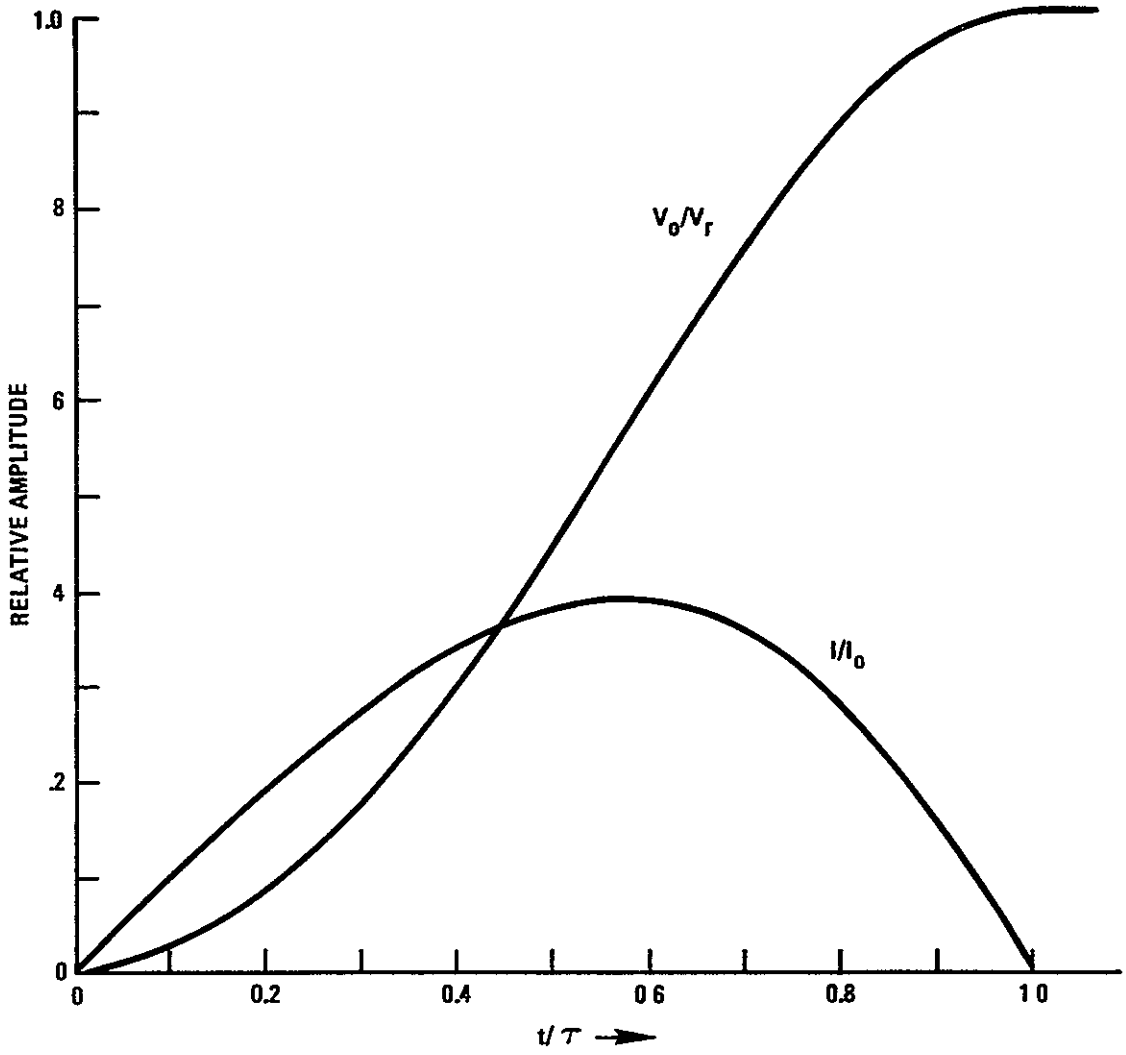

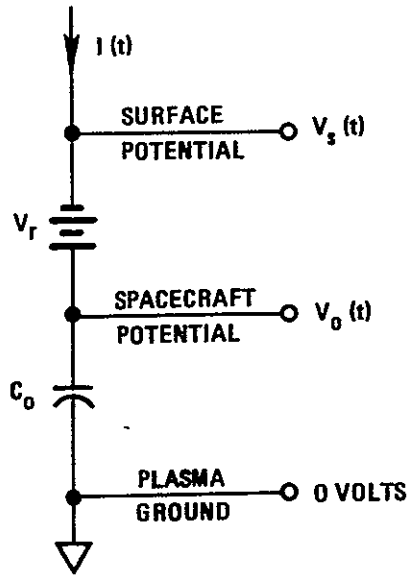

$$I(t) = \sqrt{-V_s/V_r} \cdot 3.58 \cdot 10^8 t$$

$$V_s = V_0 - V_r; \quad \frac{dV_0}{dt} = \frac{1}{C_0} I$$

$$I(t)/I_0 = (t/\tau)\,[1-(t/\tau)^2]$$

$$V_0(t)/V_r = 2(t/\tau)^2\,[1-t^2/(2\tau^2)]$$

where $\tau = [4C_0V_r/3.58 \cdot 10^8]^{0.5}$

$$I_0 = 4C_0V_r/\tau$$

Figure 4-6. Solutions for the Blowout Current and Spacecraft Potential for Large Area Arc Discharge Source

Again, the current during the linear rise is independent of the boom diameter. In the case of a 5 cm diameter boom, its circumference, 7.85 centimeters, is greater than the 4.35-centimeter threshold at which cutoff occurs. Thus the current is cut off at t equal to or 91.5 nanoseconds, and the spacecraft potential at this time has reached 5 kilovolts. The replacement current pulse is identical to that for the square or circular arcing source.

4.2 TASK 3.2 BEST ESTIMATE ARC DISCHARGE PARAMETERS

As discussed in the previous section on the arc discharge parameters obtained with a high sample grounding impedance, it is these that apply to the in-flight situation rather than the parameters obtained with a low impedance. Both low and high impedance arc discharge parameters are summarized in Table 4-1. Table 4-1 includes transient flashover and blowout current pulses which are assumed to last for 10 nanoseconds.

The actual models of the arc discharge sources used in the SEMCAP study of the EMI coupled to the electrical subsystems of a typical spacecraft are included as a part of the discussion for the final task, Task 4.

Table 4-1. Best Estimate Arc Discharge Parameters

Parameter	Value	Dependence	Definitions and Assumptions
Brushfire Propagation Velocity $v_b = (2eV_b/m_1)^{0.5}$	2.45 cm/sec	$E_b^{0.5} d^{0.5}$	E_b = breakdown electric field V_b = breakdown voltage
Flashover Surface Current Density $J_{sx} = Cv_bV_bF$	3.18 A/cm	$E_b^{1.5} d^{0.5} F$	$E_b = 10^6$ V/cm, V_b = 5000 V
Blowout Surface Current Density $J_{sz} = Nev_z$	1.86 A/cm	$gE_b^{2.5} d^{1.5} F^2$	d = dielectric thickness = 2 mils = 0.005 cm
Flashover Current Pulse* $I_{peak} = 2.5\ (\pi s/2)\ J_{sx}$	12.5(s) A	$E_b^{1.5} d^{0.5} F$	C = capacitance/area = 52 pf/cm^2
$t_p = 2t_r = s/v_b$	40.8(s) ns	$E_b^{-0.5} d^{-0.5}$	for d = 2 mils, $\varepsilon_r = 3$
Blowout Current Pulse $I_{peak} = (2k/3^{1.5})\ t_p$	12.61 A	$(Rg)^{0.5} E_b^{\ 2} (dF)^{1.5}$	F = fraction of stored charge dissipated in discharge = 0.5
$t_p = 2t_r = (4C_oV_b/k)^{0.5}$	91.5 ns	$R^{0.5}\ (gE_b^{\ 2} dF)^{-0.5}$	

*Applies to approximately square or circular sources. See text for long narrow sources.

(Continued on Page 4-17)

Table 4-1. Best Estimate Arc Discharge Parameters (Continued)

Parameter	Value	Dependence	Definitions and Assumptions
Transient Flashover Pulse			g = ablation factor
$I_{peak} = 2.5\ \pi v_b\ t_p\ J_{sx}$	6.12 A	$E_b{}^2 dF$	$= 8.32 \cdot 10^{-6}$ g/J
$t_p = 2t_r$	10 ns	-	$k = 3.58 \cdot 10^8$ A/cm
			s = square root of area (cm)
Transient Blowout Pulse			R = spacecraft radius = 1.5 m
$I_{peak} = 2.5\ \pi v_b\ \tau_p\ J_{sz}$	1.43 A	$gE_b{}^3 d^2 F$	t_p = pulse width = $2t_r$
$t_p = 2t_r$	10 ns	-	t_r = pulse risetime

5. TASK 4: SEMCAP STUDY AND P78-2 RESULTS COMPARISON

The overall objective of the present study was to investigate the implications of arcing due to spacecraft charging or spacecraft EMI margins of immunity. To achieve this objective, the analytical and experimental portions, Task 1 and Task 2, were performed and a best estimate characterization of arc discharges was obtained in Task 3 by comparing the results of Task 1 and Task 2.

This task, Task 4, takes the results of Task 3 and examines the EMI immunity response of a specific spacecraft configuration, the DSP, to two elements of the P78-2 spacecraft. The rationale for this procedure was that an excessive cost would have been involved in modeling the entire P78-2 spacecraft into the SEMCAP code. The results, then, apply neither to DSP or P78-2. Instead, the results should be interpreted as the response of a typical spacecraft.

5.1 SEMCAP OVERVIEW

An overview of SEMCAP is shown in Figure 5-1. Basically, SEMCAP resorts to a computerized analysis because of the huge number of terminal-to-terminal cable connections involved in any spacecraft system. After all of the system descriptions, such as the source and receptor characteristics and the wiring layout, are put into the computer, the coupling is computed via four types of coupling matrices. Fortunately, since many of the wires run in common bundles or cable harnesses, the size of the matrices is not comparable to the number of terminals. The output of SEMCAP includes:

- Voltages at each receptor terminal
- Margins of immunity in dB
- Alphabetical indicators of negative immunity margins.

The modifications to SEMCAP to incorporate arc discharges are minimal in comparison with the effort required to implement it originally. What is required is to characterize each arc discharge location with a voltage and current, or as an E- or B-field source. This is indicated in Figure 5-1 in dotted lines.

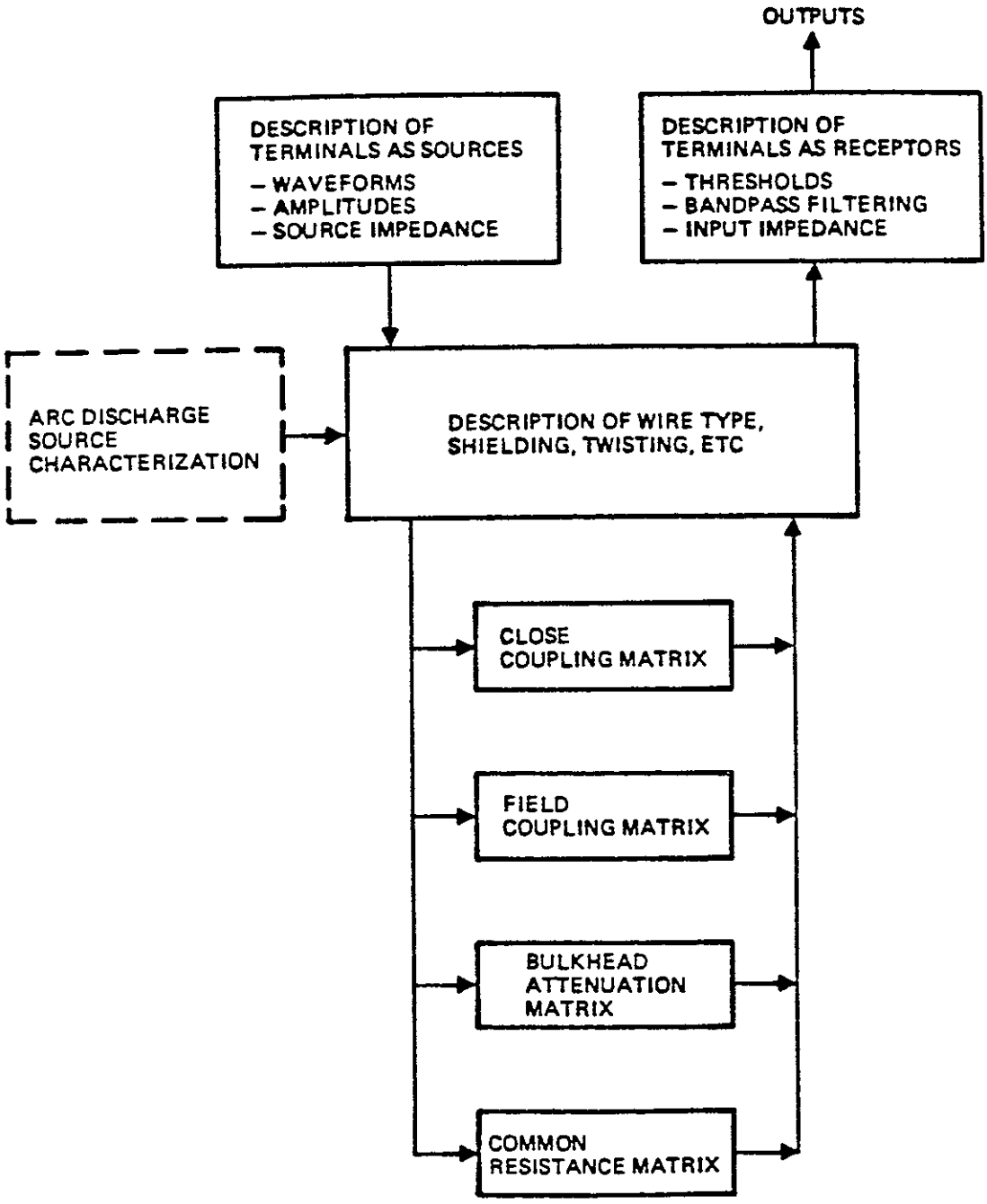

Figure 5-1. SEMCAP Overview

5.2 BEST ESTIMATE ARC DISCHARGE SOURCE MODELS

Best estimate arc discharge parameters have been developed in the previous section on arc discharge amplitudes and waveforms for the high grounding impedance situation. The remaining task here is to define the source models as they are incorporated into the EMI coupling analysis which was performed using the SEMCAP code.

The two elements of the P78-2 spacecraft selected to be modeled were the large flat doughnut-shaped dielectric area at the aft end, and one of the short booms. We assumed that the aft dielectric was 0.87 m^2 of 2-mil Kapton and that the boom was to 5 cm in diameter and 2 meters long, also covered with 2-mil Kapton. Both dielectrics are assumed to be coated with vacuum deposited aluminum (VDA) which is electrically grounded to structure. The breakdown voltage was assumed to be 5000 volts corresponding to an electric field of 10^6 V/cm (as was assumed in the analysis).

5.2.1 Summary of Arc Discharge Source Models

The large dielectric surface area was modeled as six separate sources

1) Equivalent fat wire for localized inductive and capacitive coupling
2) Arc to cable shield
3) Conductive (blowout) replacement current
4) Capacitive replacement current
5) H-Fields due to blowout current
6) Transient (<10 ns) currents and voltages.

The sixth source, the transients, comprise a subset of sources for each of the preceding five sources. The parameters are listed in Table 5-1 for both the large area arcing source and the boom. Since the boom is already in a wire-like configuration an equivalent fat wire description was not necessary for modeling localized coupling effects. The equivalent fat wire and boom configuration are shown in Figure 5-2 and Figure 5-3. Each of the source models are discussed in the following sections.

Table 5-1. Arc Discharge Source Models for SEMCAP

Large Area Discharge Models	Peak Voltage (volts)	Peak Current (amperes)	Pulse Risetime (ns)	Pulse Width (ns)
Equivalent Fat Wire	2500	466	2220	4440
Transients	2500	4.20	5	10
Arc-to-Cable Shield	37.2	20.9	2220	4440
Transients	168	0.80	5	10
Conductive Replacement Current	-	11.3	20	40
Transients	-	10.5	5	10
Capacitive Replacement Current	-	0.33	2220	4440
Transients	-	0.058	5	10
Blowout Current H-Fields*	1.80 amp/m at 1 meter		20	40
Transients*	1.67 amp/m at 1 meter		5	10
Boom Discharge Models				
Localized Coupling	2500	78.5	374	9520
Transients	2500	4.20	5	10
Arc-to-Cable Shield	0.48	3.39	374	9520
Transients	168	0.80	5	10
Conductive Replacement Current	-	11.3	20	40
Transients	-	10.5	5	10
Capacitive Replacement Current	-	0.12	374	9520
Transients	-	0.058	5	10
Blowout Current H-Fields*	1.80 amp/m at 1 meter		20	40
Transients*	1.67 amp/m at 1 meter		5	10

*H-Field drops off as 1/r

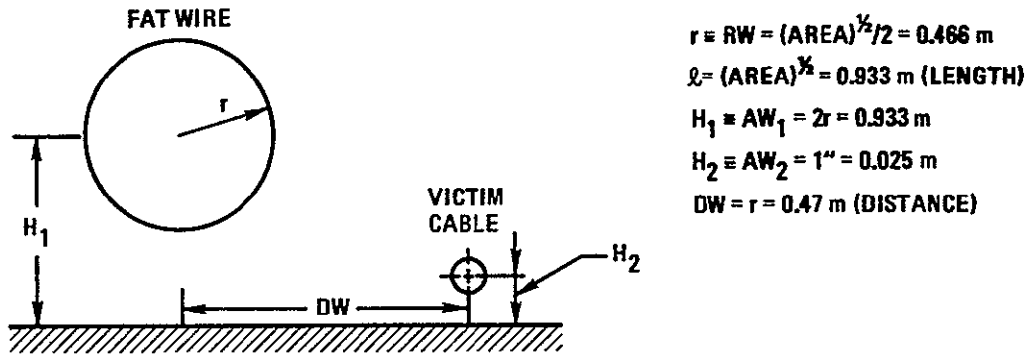

Figure 5-2. Equivalent Fat Wire Geometry for Localized Effects

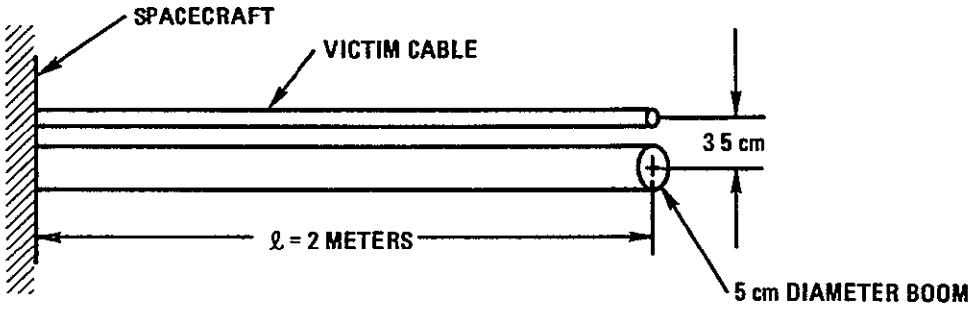

Figure 5-3. Boom Geometry

5.2.2 Equivalent Fat Wire Model

For nearby or localized capacitive and inductive effects the large area source was modeled as an equivalent fat wire as shown in Figure 5-2. The radius of the wire, r is taken as:

$$r \equiv RW_1 = (\text{Area})^{1/2}/2 = 0.466 \text{ meter},$$

and its length, ℓ, as:

$$\ell = (\text{Area})^{1/2} = 0.933 \text{ meter}.$$

The height, h, of this fat wire above the ground plane is twice its radius.

$$h \equiv AW = 0.933 \text{ meter}$$

A victim wire is assumed running parallel to the fat wire at a height, AW_2, of 1 inch or 0.025 meter at a distance, DW, equal to r or 0.466 meter.

For localized capacitive coupling purposes, the voltage-time history must be specified:

$$\text{peak voltage} = 2500 \text{ volts} = V_p$$

$$\text{rise time} = s/(2\ v_b) = 2.22 \cdot 10^{-6} \text{ second} = t_r$$

$$\text{pulsewidth} = 2\ t_r = 4.44 \cdot 10^{-6} \text{ second}.$$

Since one-half of the initial stored charge remains after the discharge, V_p was taken to be one-half of the 5000 volts breakdown voltage. The risetime, t_r, and pulsewidth, t_p, are computed from the brushfire propagation velocity, v_b, of $2.1 \cdot 10^7$ cm/s. Side, s, is taken to be the square root of the area or 93.3 cm. For localized inductive coupling purposes, the peak current, I_p, must be specified.

$$I_p = (\pi/2)\ s \cdot J_s = 466 \text{ amperes}.$$

I_p is the flashover surface current density, J_s, of 3.18 amp/cm multiplied by the equivalent arcuate length, $(\pi/2) \cdot s$.

5.2.3 Arc-to-Shield Model

The second arc discharge model, the arc-to-shield, is the most likely source of hazardous EMI levels. We assume that the entire flashover discharge current flows to the shield of a cable. In order to characterize this type of discharge, it is first necessary to determine where on the cable the greatest coupling would occur. An arc striking at the middle, because of the even split of currents going both ways to the shield grounds at either end, causes no net induced voltage. For a finite shield terminating impedance, Figure 5-4 shows that the unwanted induced voltage increases linearly from zero at the center to a maximum at either end. For our analysis we have assumed the shield terminating impedance, Z_o, to have a resistance of 2.5 milliohms and an inductance of 0.1 microhenry.

To model the discharge to the cable shield, for SEMCAP, it is first necessary to compute the shield current and voltage. In order to do this, an equivalent arc resistance, R_a, and inductance, L_a, must be characterized from the available data which applies only to the flashover arc current. After R_a and L_a are defined, then the shield current, I_s, must be computed for the actual configuration. The arc-to-shield configuration and the two circuits that must be solved are shown in Figure 5-5.

The analysis is simplified by assuming that the arc discharge current is the sum of two exponentials:

$$I(t) = I_o \left(e^{-t/t_p} - e^{-t/t_r}\right)$$

where t_p and t_r are the current pulse width and resistance respectively. The maximum or peak current for the waveform defined by this equation is:

$$I_{peak} = I_o \cdot (1-\gamma) \cdot \gamma^{\gamma/(1-\gamma)} \text{ where } \gamma \equiv t_r/t_p.$$

For t_r equal to one-half t_p, γ is 0.5 and I_{peak} is one-fourth of I_o. The equivalent arc resistance, R_a, and inductance, L_a, obtained by solving the circuit of Figure 5-5B are

$$R_a = \frac{1+\gamma}{C} t_p = 14.72 \text{ ohms}, \quad L_a = \frac{\gamma}{C} t_p^2 = 21.8 \text{ } \mu\text{h}$$

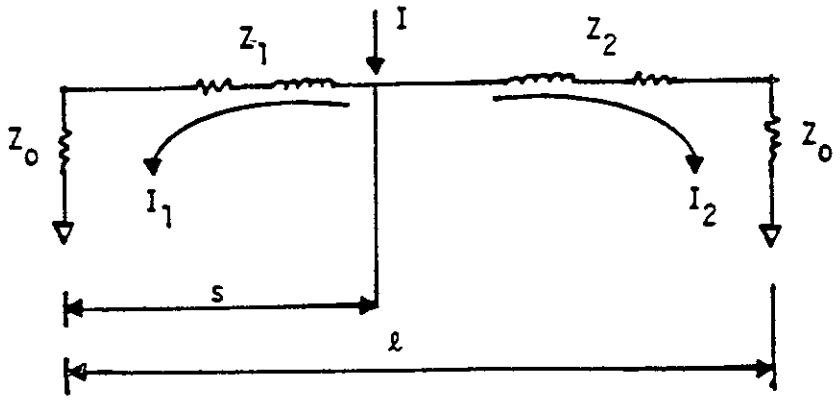

$$I = I_1 + I_2, \qquad I_2/I_1 = (Z_1 + Z_o)/(Z_2 + Z_o)$$

$$Z = Z_1 + Z_2, \qquad Z_2/Z_1 = (\ell - s)/s.$$

$$U(s) = \text{UNWANTED SIGNAL} = I_2(\ell - s) - I_1 s$$

$$= I\left(\frac{Z_o}{2Z_o + Z}\right)(\ell - 2s);$$

$\therefore$ U(s) is maximum for s = 0 and s = ℓ, and U(s) = 0 for s = ℓ/2. Also, I is maximum at s = 0 or s = ℓ.

Figure 5-4. Demonstration that Unwanted Induced Signals are Maximum for an Arc Striking at the Ends of a Cable Shield

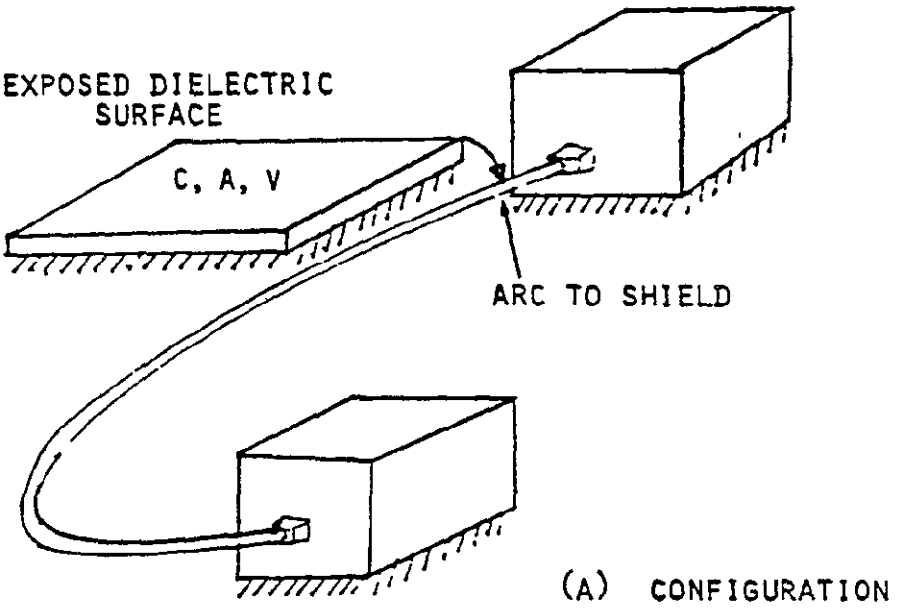

(A) CONFIGURATION

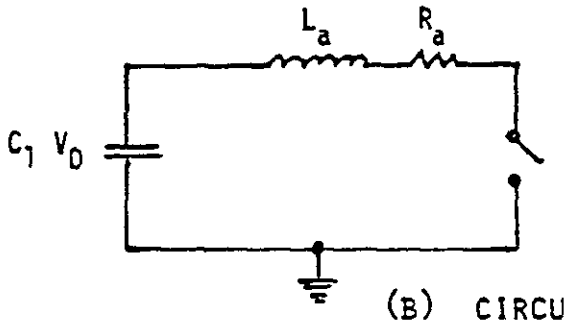

(B) CIRCUIT TO SOLVE FOR R_a AND L_a

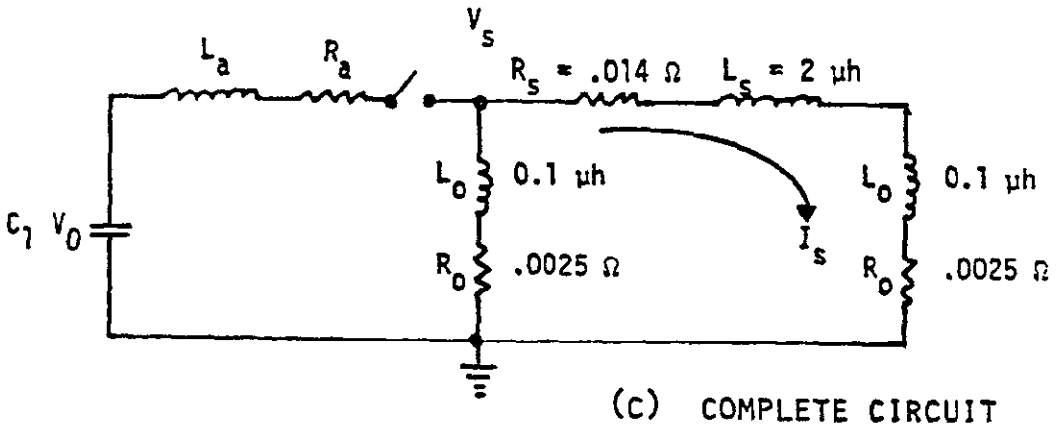

(C) COMPLETE CIRCUIT

Figure 5-5. Configuration Circuits to be Solved to Determine Arc-to-Shield Currents and Voltages

The numerical values for R_a and L_a were obtained using the large area arcing source parameters. The point here is that the arc impedance is much greater than the cable shield termination impedance shown in Figure 5-5C.

The solution of the complete circuit of Figure 5-5C is a considerably more time consuming task involving a third degree equation. By assuming that the voltage across the shield terminating impedance is due to the entire discharge current flowing through it, and then applying Thevenin's theorem, the current through the cable shield, I_s, may be computed in a fairly straightforward manner. Table 5-2 compares the results of the approximate calculation and the complete solution and shows that the former is within 10 percent of the latter.

Table 5-2. Comparison of Complete Solution Versus Approximate Solution for Arc-to-Cable SEMCAP Parameters

Common Parameters

$V = 2200$ volts

$C = 1.6 \cdot 10^{-8}$ farads,

$t_p = 270$ ns,

$t_r = 27$ ns

$L_a = 0.446$ µh,

$R_a = 18.56$ ohms,

$I_{arc} = 100.94$ amperes

	Complete Solution	Approximate Solution	Difference
Peak Shield Current, I_s	4.323 amperes	4.694 amperes	+8.6%
Peak Shield Voltage, V_s	390.3 volts	396.0 volts	+1.5%
Pulse Width	266.2 ns	263.3 ns	-1.1%
Pulse Risetime	30.86 ns	33.77 ns	-9.4%

5.2.4 Conductive Replacement Current Model

This source models the replacement currents which flow as a result of the electron blowout process. As derived in the analysis of the high grounding impedance configuration, the electron current is limited to 11.3 amperes and is cutoff in 51.1 ns by the rise in spacecraft potential. These values are determined by the size of the spacecraft, the DSP. The values of the pulse width and risetime, 40 ns and 20 ns, were taken as 80 percent and 40 percent, respectively, of the cutoff time. Since blowout occurs only at the beginning of the discharge, the parameters are the same for the large area and boom discharge models.

5.2.5 Capacitive Replacement Current Model

This model accounts for the replacement currents due to the displacement or $C_s(dV/dt)$ currents that flow due to the change of surface potential of the arcing source. The original concepts of the G' factor arose from this model, and the fact that it did not account for the electron blowout currents seemed to be a deficiency in the model. As may be noted in Table 5-1, the conductive replacement current sources, while larger than the displacement current sources, are not in the range of hundreds of amperes, as was initially feared. Instead, they are in the order of 10 amperes, independent of the size of the source, and are over in less than 100 ns.

The displacement currents are calculated on the basis of the capacitance to space, C_s, of the source and the rise time, t_r, of the voltage change. C_s is estimated by calculating the radius, R, of an equivalent sphere having the same area as the source, and then assuming that C_s is that of the sphere

$$R = [A/4\pi]^{0.5}, \quad C = 4\pi\varepsilon_o R.$$

Although we now know that the entire surface does not change its poential in unison, but rather in a brushfire mode, t_r was used as the time in which the voltage change occurred in order to give a reasonable average time.

5.2.6 H-Field Model of Blowout Current

This model accounts for the H-fields generated by the blowout electron current. The Biot-Savart relation,

$$H = I/(2\pi r),$$

was used, implying that the current flows in an infinitely long wire. This field drops off inversely as the distance from the source. As noted for the conductive replacement current model, the blowout current is 11.3 amperes independent of the size of the source. Its waveform, defined by t_r and t_p, is also independent of the size of the source.

5.2.7 Transient Model

The transient arc discharge models account for the short duration (<10 ns) spikes that were observed in many of the experimental study tests. These have been included as an additional source to each of the five types of sources discussed above. The pulse width was assumed to be 10 ns and the rise time, 5 ns. The voltage was assumed to be that of the maximum change, 2500 volts. The current was calculated on the basis of the 10 ns duration and the brushfire propagation velocity, $2.3 \cdot 10^7$ cm/sec, which gives the radius of discharged circular area of 0.23 cm. The circumference of this circle times the surface current density, J_s, of 3.18 amp/cm gives a flashover current, I, of

$$I = 2\pi r \cdot J_s = 4.2 \text{ amperes.}$$

The transient arc-to-shield models were computed using the same double exponential approximation as before. Because of the short duration, the currents are small but the inductive voltages are larger than for the longer pulses. The transient blowout current, since it is not limited by spacecraft potential, was calculated by multiplying the flashover current by the experimentally determined G' factor of 2.5 to give

$$I_{blowout} = G' \cdot I_s = 10.5 \text{ amperes.}$$

This current also applies to the transient H-field model.

5.2.8 Boom Arc Discharge Source Models

The boom arc discharge source models were computed in a manner similar to that for the large area sources. As stated previously, the equivalent fat wire model for computing localized capacitive and inductive coupling effects was not necessary because its configuration was already that of a fat wire. As shown in Figure 5-3, the victim cable was taken to be 1 cm off of its surface or 3.5 cm between centers. The boom was assumed to be 5 cm in diameter, d, and 2 meters, in length, L.

The principal difference from the large area source was in the rise time and pulsewidth:

$$t_r = \pi d/(2v_b) = 374 \text{ ns}, \quad t_p = L/v_b = 9.52 \ \mu s.$$

Their ratio, γ, of 0.0393 is considerably smaller than the value of 0.5 for the large area source.

5.3 SEMCAP RESULTS

Table 5-3 summarizes the results of the SEMCAP analysis. The dB margins of immunity are given in two columns, one for the circuits and a separate column for the housekeeping telemetry lines. The results show that the DSP satellite circuits have safety margins ranging from +5 dB to +139 dB. The housekeeping telemetry lines, which show margins of -44 dB to +58 dB, have a number of receptors which have negative margins of immunity. The housekeeping telemetry lines tend to show smaller margins of immunity on DSP because they are generally unshielded in order to save weight. On the other hand, the probability that voltage spikes would be detected on these lines is extremely low because of the low-duty cycle at which they are telemetered. Housekeeping telemetry lines have either 5-volt analog or bilevel signals. Even if they were detected, a single anomalous reading would be ignored.

The main concern would be that a sufficiently large spike could damage an interface circuit. The telemetry line with the highest negative margin of immunity, -44 dB happens to be a temperature line with a threshold of 0.1 volt. The -44 dB implies a voltage of 15.7 for (10 ns) which would not damage the telemetry interface. In general, SEMCAP has a $\pm$9 dB

Table 5-3. The Lowest Safety Margin (dB) of the Satellite versus Different Types of Arc Sources and Transients (at Large Area)

Source	Circuits	Telemetry Lines
Localized Field Coupling	20	0
Transient	23	-31
Arc to Cable Shields	5	-2
Transient	21	-21
Conductive Replacement Current	41	-18
Transient	42	-22
Capacitive Replacement Current	72	43
Transient	87	23
Blowout Current H-Fields	44	12
Transient	62	11

The Lowest Safety Margin (dB) of the Satellite Versus Different Types of Arc Sources and Transients (at Boom)

Source	Circuits	Telemetry Lines
Localized Field Coupling	19	-13
Transient	22	-25
Arc to Cable Shields	14	-13
Transient	19	-44
Conductive Replacement Current	40	-18
Transient	43	-22
Capacitive Replacement Current	80	38
Transient	87	23
Blowout Current H-Fields	51	8
Transient	59	9

statistically predicted error, and tests have shown that SEMCAP usually underpredicts the safety margin, i.e., a predicted safety margin of +40 dB is more likely to be 49 dB.

The lowest margins of immunity, aside from the housekeeping telemetry lines, were due to the arc-to-cable shield and the localized field coupling sources. The localized field coupling sources were assumed to fall off in

intensity as r^{-2} for worst-case purposes. For near-field purposes, an inverse cube falloff would have been more appropriate. A 10 dB bulkhead attenuation was assumed for the shielding of the victim circuits by the structural aluminum sheets. This was probably too pessimistic, and 20 dB would be a better estimate. The low margins of immunity to the arc-to-shield sources is not surprising because of the large currents delivered directly to the shield. The lesson to be learned here is that cabling should be routed away from dielectric surfaces which are likely to arc. If this is unavoidable, then the lines should be filtered heavily to withstand the pulses that are likely to occur.

The margins of immunity to the replacement current sources for blow-out, about 40 dB, are certainly in the nonhazardous regions. As noted earlier, this is due to the early cut off of the blowout process by the positive spacecraft potential, which limited the amplitude as well as the duration. As expected, the capacitive replacement current sources had a smaller effect — by a factor of about 40 dB. The transient sources in general had an average of 7 dB greater immunity, mainly because of their shorter duration.[1]

5.4 COMPARISON OF SEMCAP STUDY AND P78-2 IN-FLIGHT RESULTS

As noted previously the results of the SEMCAP study performed here are not directly applicable to the P78-2 spacecraft and its performance in orbit. For the purpose of this task the following in-flight operational data are pertinent:

- The failure of the SC2-1 and SC2-2 plasma potential sensors occurred during electron gun operations on March 30, 1979.
- Only a handful of transient arc discharge waveforms have been identified and recorded. There is no apparent consistency between the few waveforms available.
- A large number of transient pulse monitor (TPM) pulses have been recorded.
- No indication of the location of the arc discharges is available.

The failure of the SC2 plasma voltage probes has been ascribed to arc discharges occurring on the booms on which they were mounted. The initial analysis presented became hung up in an inconsistency which required that

any arc discharge pulse have a time constant longer than 10 μs, i.e., the presence of a 10 kΩ, 0.001 μf RC filter. The 9.52 μs pulse duration estimated for the boom discharge propagation time approaches the required duration. However, a much simpler explanation is that the 10 kΩ resistor, a 1/4-watt unit, probably broke down with the several kV associated with the discharge. This allowed instant access for the discharge into the probe circuitry.

The small number of arc discharge transients recorded on the P78-2 spacecraft is consistent with the observations made in the Task 1 analysis:

- The Faraday cage design should shield the interior portions of the spacecraft from the effects of arc discharges.
- No large area arcing should occur because of the extensive use of conducting surfaces. The large area painted surface should not arc because of its low resistivity.
- The small areas of dielectric samples should not arc easily because of the careful design to minimize rough edges.

In spite of the few transient waveforms recorded, the TPM did record a large number of pulses, which, according to the experimenter, were related to environmentally induced arc discharges. The problem seems to be to implement an automated data analysis system which eliminates pulses from known onboard sources such as mode changes and equipment turn-on and turn-offs. The TPM sensitivity is such that these internal events are easily detected. The inability to identify the location of the discharges makes a quantitative evaluation of the data impossible. The comparison with the present SEMCAP study results is also difficult except to state that both the predictions and the in-flight results agree in that no serious operational problems have arisen except for the failure of the two SC2 probes.

The implementation of the SEMCAP analysis reported here was performed by David Ying. His understanding of and familiarity with the SEMCAP code permitted the work to be done efficiently with a minimal number of false starts.

APPENDIX 1 - PULSED PLASMA THRUSTER DATA

The solid propellant pulsed plasma thruster (PPT), which uses teflon as the fuel, has a history of development and orbital experience of more than 10 years.* During this period an extensive body of information regarding the operating features of this type of device has been generated, some of which is applicable to the modeling of dielectric arc discharges due to spacecraft charging.

Basically, the solid teflon PPT consist of a high voltage supply (1.3 to 3 kV) and energy storage capacitor (2 to 200 μf) and a spark plug ignition system. Figure A-1 is a schematic drawing of the PPT taken from the reference by Vondra, Thomasson and Solbes. The spark ignition initiates a discharge across the surface of the solid teflon which burns off approximately 400 Å of the dielectric material. A combination of $\vec{v} \times \vec{B}$ forces, $\vec{B}$ being due to the discharge current, and gas dynamic forces accelerate the ablated ionized and neutral particles out of the thruster nozzle at high speed (3000 to 40,000 m/s) providing the desired impulse or thrust (4 micropounds to 1 millipound). PPT parameters are shown in Table A-1.

As compared to the dielectric surface discharge, there are a number of features which are different on the PPT·

- The energy, stored in a physical capacitor, does not require a propagation mechanism as does a dielectric surface discharge of the kind that is of concern for spacecraft charging effects.
- The energy expended per unit area is much greater, 0.10 to 23 J/cm^2 as compared to approximately 10^{-3} J/cm^2 for spacecraft charging types of discharges.

---

*(1) R.J. Vondra, K. Thomasson and A. Solbes, "Analysis of Solid Teflon Pulsed Plasma Thruster," J. Spacecraft and Rockets Vol. 7 No. 12 December, 1970.

(2) D.J. Palumbo, W.J. Guman and M. Begun, "Pulsed Plasma Propulsion Technology," AFRPL-TR-74-SO, July, 1974.

(3) R.J. Vondra, "US Air Force Programs in Electric Propulsion" Paper No. 79-212 Princeton AIAA/DGLR 14th International Electric Propulsion Conference, October 30 to November 1, 1979.

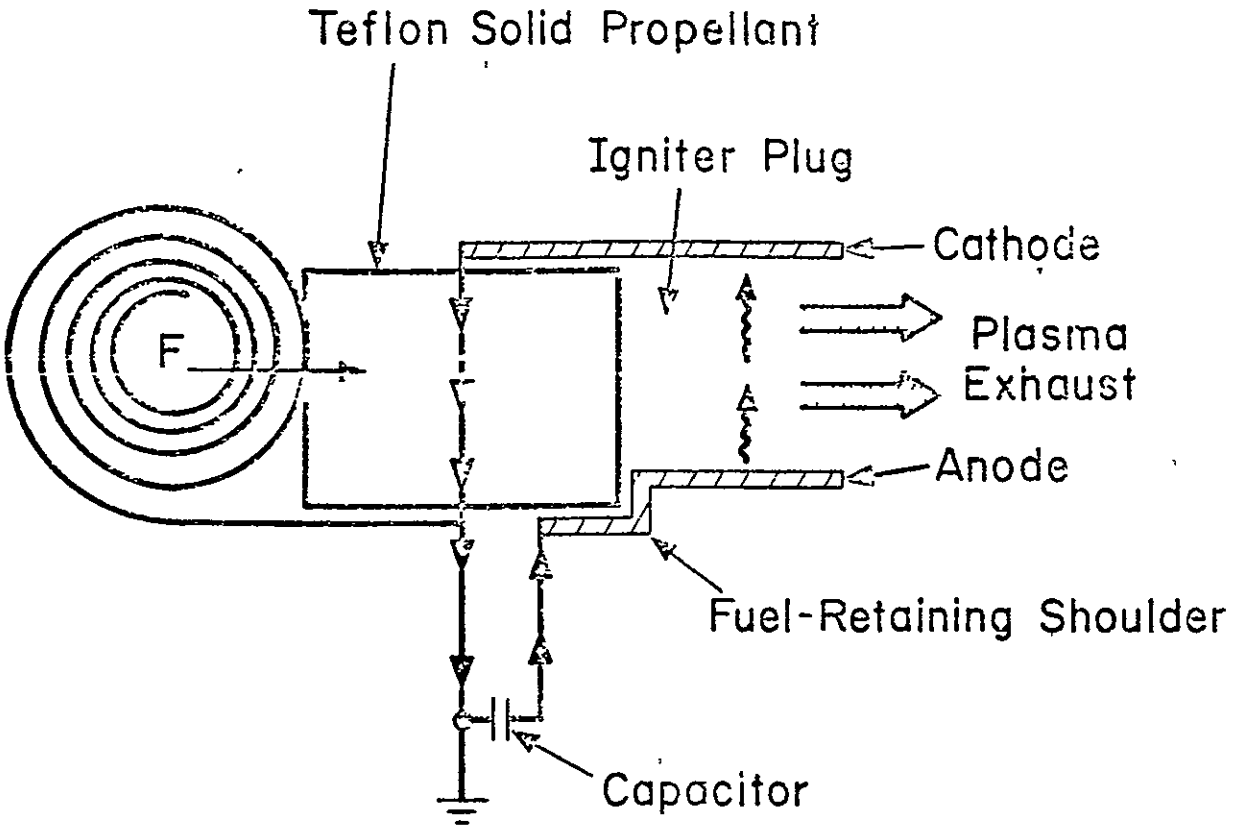

Figure A-1. Solid Fuel Microthruster (Schematic)

Table A-1. Comparison of 4 Micropound and 1 Millipound PPT EMI Parameters

	1 Millipound PPT	4 Micropound PPT
I_{max} (A)	120,000	5,800
Capacitor Voltage (V)	2,740	1,360
Capacitance (μf)	200	2.0
Energy (J)	750	1.85
Current Pulsewidth (μs)	12	1.0
Current Risetime (μs)	2.0	0.17
Length, ℓ, of Current Loop (m)	0.04	0.006
Height, h, of Current Loop (m)	0.083	0.03
*Microwave Power Density at 1 m ($mW/m^2/GHz$)	325	25

*Computed from $S = 6.859.10^{-14}\ V^3.687\ mW/m^2/MHz$ at 1 m (from Reference 2)

- The amount of surface material ablated per discharge is correspondingly greater.

Taking the 4 micropound PPT for example, the data available are shown in Table A-2.

Table A-2. Micropound PPT Data

Voltage on capacitor	1,360 V
Capacitance	2.0 μF
Stored energy, W_s	1.85 J
Electrical circuit losses	0.592 J (32 percent of W_s)
Energy into plasma	1.26 J (68 percent of W_s)
Kinetic energy	0.555 J (3 percent of W_s)
Electrode loss, ionization, plasma heating and electromagnetic radiation	1.20 J (65 percent of W_s)
Solid teflon surface area	0.6 x 3 cm = 1.8 cm^2
Energy density in plasma	0.668 J/cm^2
Mass ablated/pulse	10^{-5} gram/pulse
Mass ablated/J	$8.32 \cdot 10^{-6}$ gram/J· $10^{-5}/(0.65 \cdot 1.85)$

Assuming a density of 1.3 grams/cc for the dielectric material, the thickness of material, d, ablated per J is

$$d = 8.32 \cdot 10^{-6}/1.3 = 6.4 \cdot 10^{-6} \text{ cm}/(J/cm^2) = 640 \text{ Å}/(J/cm^2)$$

extrapolating this value to our spacecraft charging problem, the stored energy is

$$W_s = \frac{1}{2} CV^2 = \frac{1}{2} \cdot 52 \cdot 10^{-2} \cdot 25 \cdot 10^6 = 6.5 \cdot 10^{-4} \text{ J/cm}^2.$$

Assuming that half of the stored charge, 25 percent of W_s, remains after the discharge, the energy input into the plasma is

$$W_p = 0.75\ W_s = 4.88 \cdot 10^{-4}\ J/cm^2.$$

Thus, the thickness, d, of dielectric ablated per discharge is

$$d = 6.4 \cdot 10^{-6} \cdot 4.88 \cdot 10^{-4} = 3.10 \cdot 10^{-9}\ cm = 0.31\ \mathring{A}.$$

This thickness ablated is smaller than the 427$\mathring{A}$ ablated on the PPT.

APPENDIX 2 - DIELECTRIC HEATING BY A SURFACE PLASMA

This appendix considers the heating of the dielectric by the hot plasma at its surface. The effects of heating are:

- Power loss from the cooling of the plasma
- Heat input energy loss to the dielectric and the rise of dielectric temperature
- Ablation of dielectric surface material and absorbed gas molecules.

The problem considered is that of a semi-infinite dielectric slab whose surface is exposed to a step-function increase of temperature. Typical dielectric parameters assumed are shown in Table B-1.

Table B-1. Typical Dielectric Thermal Properties*

	Typical Dielectric	Copper
Density	2 grams/cc	8.9 grams/cc
Specific heat	0.2 Cal/gram	0.092 Cal/gram
Thermal conductivity, $\frac{1}{R}$	0.032 Cal/cm-s-3°K	0.96 Cal/cm-s-°K
Thermal capacitance, C	0.4 Cal/cc	0.82 Cal/cc
Diffusion coefficient, $D = \frac{1}{RC}$	0.005 cm^2/s	1.17 cm^2/s

*1 calorie = 4.187 J = 4.187 W/s

Table B-1 includes the thermal parameters for copper for comparison with the typical dielectric. In contrast with electrical conductivity, the ratio of thermal conductivity of a good conductor to a poor conductor, 480, is not nearly as large. The thermal capacitance, comparable to the dielectric constant in the electrical analogy, is similar to electrical capacitance in that it does not vary greatly from material to material.

The applicable equations leading to the 1-dimensional diffusion equation are:

$$\frac{-\partial V}{\partial X} = RI, \quad \frac{\partial I}{\partial X} = C\,\frac{\partial V}{\partial t}, \text{ giving}$$

$$\frac{\partial V}{\partial T} = \frac{1}{RC}\,\frac{\partial^2 V}{\partial X^2} = D\,\frac{\partial^2 V}{\partial X^2}$$

The above equations are written using equivalent electrical terms:

V (Voltage) ——————→ Temperature (°K or °C)
I (Current) ——————→ Heat flux ($Cal/cm^2/s$)
Q (Charge/cm) ——————→ Heat/cm ($\int Idt$)
R (Resistance/cm) ——————→ Thermal resistance/cm (V/I)
C (Capacitance/cm) ——————→ Thermal capacitance/cm (Q/V)

The solution to the diffusion equation for a step-function change in the temperature, V_0, at the surface of the dielectric for the boundary condition, V(x,0=0) for X >0 at t=0, V(0,t) = V_0 for all t is:

$$V(x,t) = V_0\left[1\text{-erf}\left(\frac{x^2}{4Dt}\right)^{0.5}\right]$$

where the error function,

$$\text{erf } x = \frac{2}{\pi}\int_0^x e^{-y^2} dy,$$

is a tabulated function. A more commonly tabulated function is the normal probability integral, P(x), which is simply related to the error function:

$$P(x) = \frac{1}{\sqrt{2\pi}}\int_{-x}^{x} e^{-y^2/2} dy = \text{erf}\left(\frac{x}{\sqrt{2}}\right);$$

$$\therefore \text{erf}(x) = P(\sqrt{2}x).$$

Figure B-1 shows a plot of temperature versus time for a fixed distance, x, into the surface of the dielectric. Because of the error function dependence on $x^2/4Dt$, the shape of the curve remains the same if the time scale were varied in proportion to x^2. At any x, the temperature eventually approaches the surface temperature, T_0. Figure B-2 shows a plot of the falloff of temperature with distance into the dielectric surface at a fixed instant of time. The temperature drops off to 50 percent of its surface value at x/x_0 equal to about 0.5:

$$\frac{x}{x_0} = 0.5 \text{ for } T(x) = 0.50T_0;\ x = 0.5x_0 = 0.5\sqrt{4Dt}.$$

For t = 100 ns or 10^{-7} second, using the value of D of 0.005 cm^2/s, the distance, x, at which the temperature is 50 percent of T_0, is $2.2.10^{-5}$ cm or 0.22 micron. By comparison, if the material were a good conductor such as copper (D = 1.17 cm^2/s), the corresponding distance, x_0, is 3.4 microns for a change in temperature equal to 50 percent of T_0 at 100 ns. The distance at which the temperature is 90 percent of the surface temperaure (t = 100 ns) is about an order of magnitude less, or 0.054 microns for the dielectric as compared to 0.82 micron for copper. The point to note here is that the depth of the dielectric which gets heated to the vaporization regime of temperatures is somewhat less than the approximately 1 micron penetration depth of 20 keV electrons.

The rate of heat input to the dielectric surface is the "current," I, at x equal to zero. The general expression for I is obtained by partial differentiation of the expression for V (x,t)·

$$I\ (x,t) = -\frac{1}{R}\frac{\partial V}{\partial X} = \left(\frac{1}{\pi D}\right)^{0.5}\frac{V_o}{R}\,t^{-0.5}e^{-X^2/(4Dt)},$$

$$I\ (0,t) = \left(\frac{1}{\pi D}\right)^{0.5}\frac{V_o}{R}\,t^{-0.5}\ (cal/cm^2/s)$$

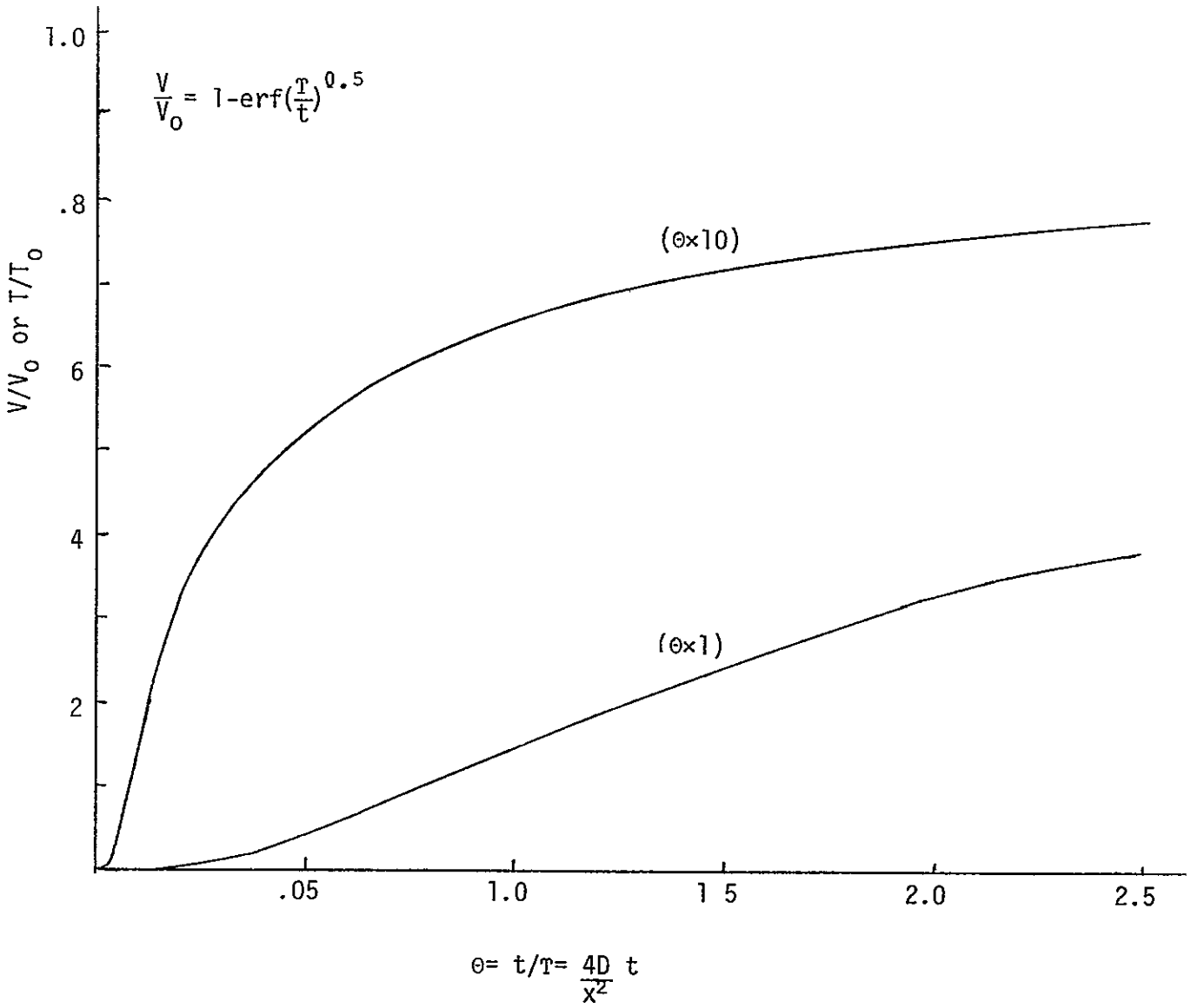

Figure B-1. Diffusion Equation Solution· Temperature versus Time* for a Fixed Distance**

*θx10 means "multiply abscissa by 10"

θx1 means: "use abscissa directly"

**The same curves apply if the "time" scale varies as x^2.

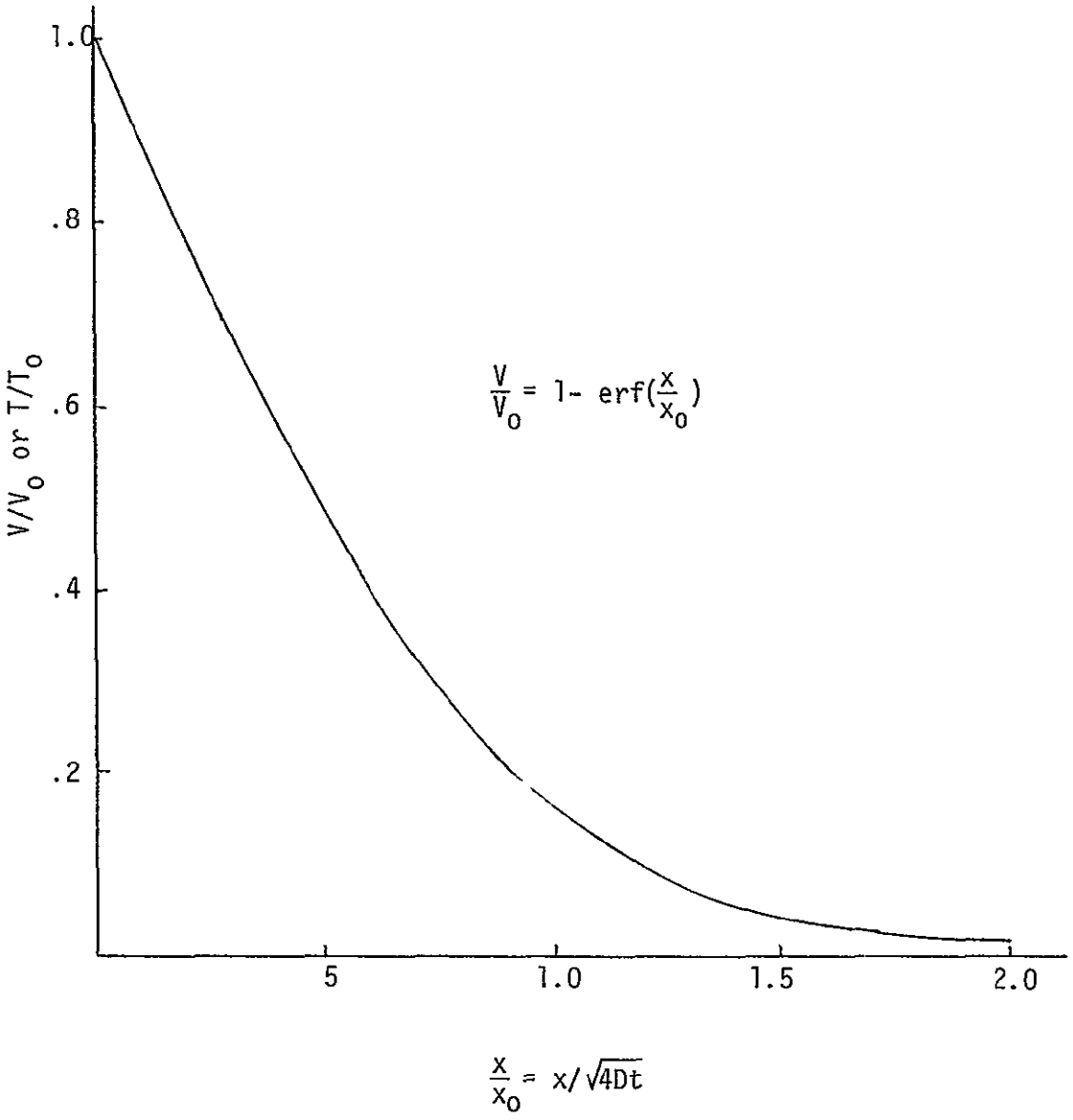

Figure B-2. Temperature versus Distance into Dielectric at a Fixed Instant of Time

The rate of heat input decreases as the inverse square root of time. The total heat or energy input, W at any time, t, is

$$W = \int I dt = 8.38 \left(\frac{1}{\pi D}\right)^{0.5} \frac{V_o}{R} t^{0.5} \ (J/cm^2)$$

where the J equivalent of the calories has been incorporated. The total energy input continually increases with time, as it must, to heat up the semi-infinite dielectric slab. In 100 ns, using a V_o of 3000°K, the energy input is

$$W = 8.38 \left(\frac{1}{\pi \cdot 0.005}\right)^{0.5} \cdot 3000 \cdot 0.002 \cdot 10^{-7/2} = 0.127 \ J/cm^2 \ .$$

Putting in the thermal parameters for copper for comparison, the energy input for 100 ns is 3.98 J/cm^2 which is 31.4 times larger than for the dielectric material. This is because of the much larger thermal conductivity of copper as well as its somewhat larger thermal capacitance. The energy input into the dielectric heats up a thinner surface layer, a fraction of a micron, in 100 ns.

The energy, W_s, stored in the dielectric surface per unit area is

$$W_s = \frac{1}{2} C V^2$$

where C is the capacitance per unit area:

$$C = \varepsilon_0 \ \varepsilon_r / d.$$

For a 2 mil thickness, d, and a dielectric constant, ε_r of 3, C is 52 pf/cm^2. Taking a breakdown field strength of 10^6 V/cm, the breakdown voltage would be 5 kV, giving a stored energy of

$$W_2 = \frac{1}{2} .5210^{-12} 0.25 \cdot 10^6 = 6.5 \cdot 10^{-4} \ J/cm^2.$$

Considering the experimentally observed fact that about half of the stored charge remains on the dielectric surface after a discharge, the energy dissipated in the area, W_a, is about 3/4 of W_s.

$$W_a = 4.9 \cdot 10^{-4} \text{ J/cm}^2.$$

Comparing this energy with the 0.13 J/cm^2 value calculated for the energy absorbed in 10^{-7} second, it is smaller by a factor of 260. This means that the postulated temperature rise of 3000°K was too large by this factor, and therefore should have been 11.5°K. Even this temperature increment is too large if some of the available energy is to be dissipated in ionizing the ablated surface material.

Since the results of the foregoing analysis are so much of what was expected, we now consider a different set of boundary conditions:

$V(x,0) = 0$ for $x>0$

$V(0,t) = V_0$ for $0<t<t_0$

$V(0,t) = 0$ for $t>t_0$

The forcing function is now a rectangular impulse of amplitude V_0 (or T_0) and duration, t_0, rather than a step function. The solution to the 1-dimensional diffusion equation is

$$V(x,t) = V_0 \left(\text{erf} \left\{ x/[4D(t-to)]^{0.5} \right\} - \text{erf} \left[x/(4Dt)^{0.5} \right] \right)$$

The above solution applies for $t>t_0$, only, and simplifies to the solution for the step-function case considered previously, for $t<t_0$ in which the first term is unity. The temperature profiles as functions of time at two fixed depths, x, of 50Å and 100Å are shown in Figure B-3 for a t_0 of 0.3 ns and 0.5 ns. At these depths, the peak temperature gets to 60 to 80 percent of the surface temperature. At very small depths of a few angstroms, the temperature profile follows the forcing function nearly exactly. Figure B-4 shows the maximum temperature as a function of depth for the 0.3 ns pulse.

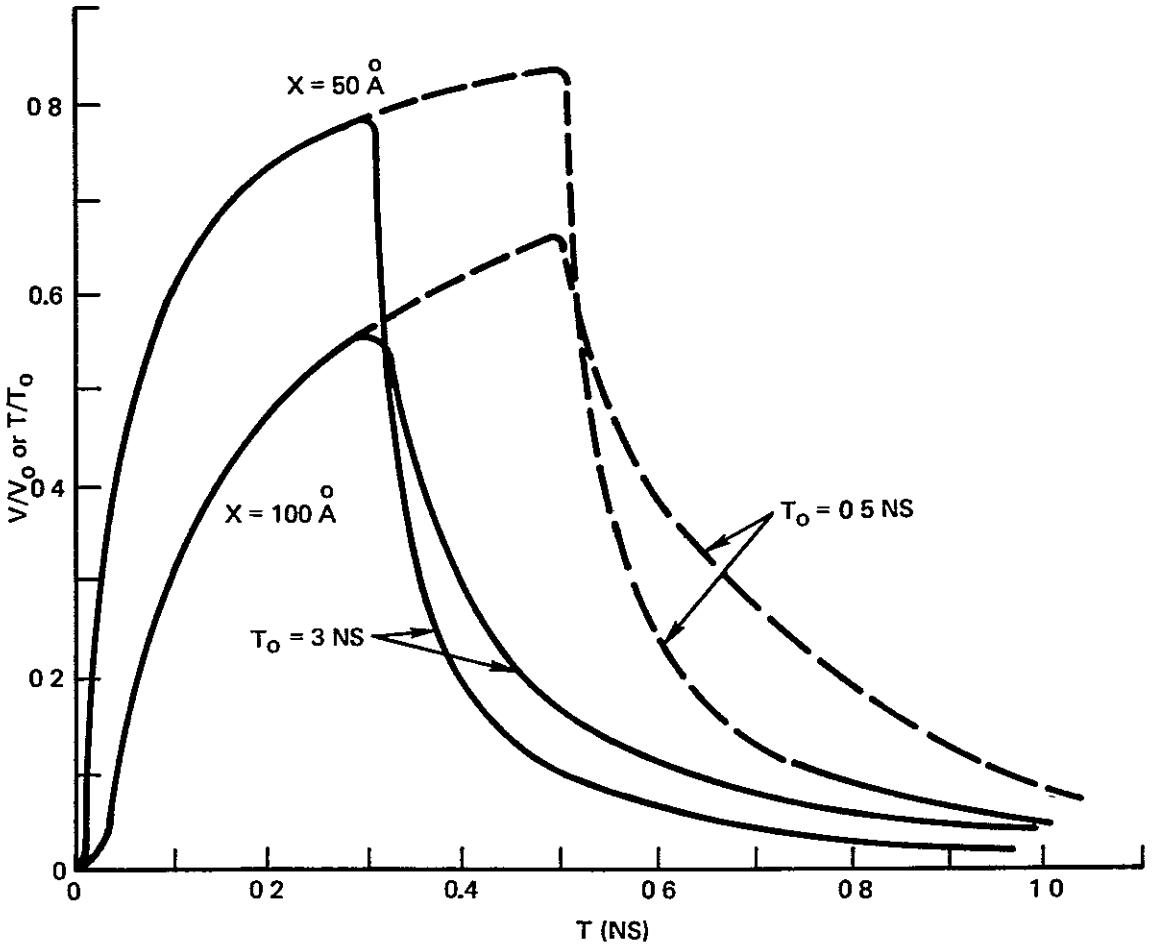

Figure B-3. Temperature-Time Profiles for a Rectangular Forcing Function

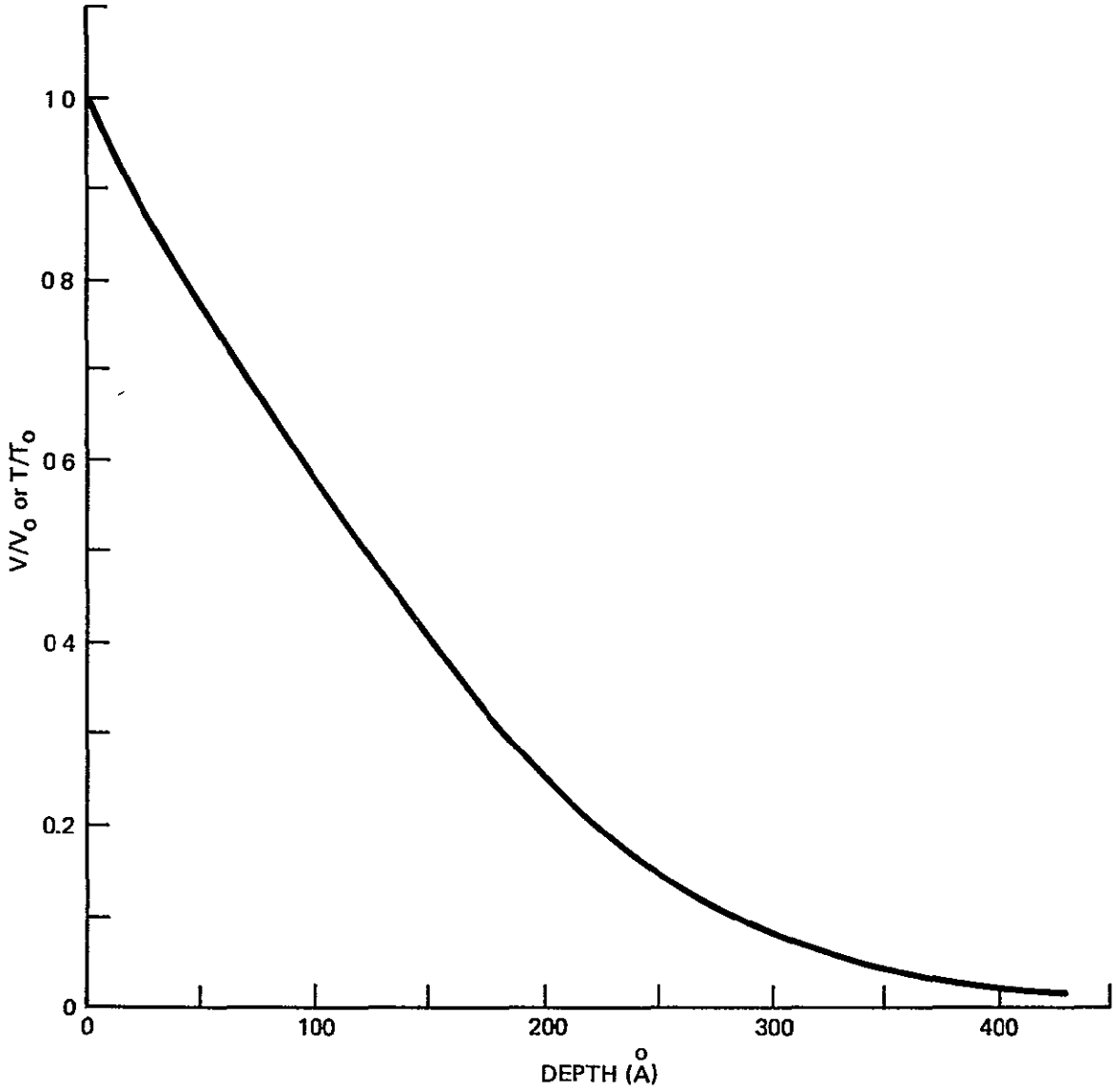

Figure B-4. Maximum Temperature Versus Depth for a 0.3 ns Wide Rectangular Temperature Pulse

The rate of heat flow is obtained as before by partial differentiation of V(x,t) with respect to x at the surface,

$$I\ (0,t) = \frac{1}{\sqrt{\pi D}} \frac{V_o}{R} t^{-0.5} \quad \text{for } o<t<t_o,$$

$$= \frac{-1}{\sqrt{\pi D}} \frac{V_o}{R} \left[(t-t_o)^{-0.5} - t^{0.5}\right] \text{for } t>t_o.$$

For $t>t_o$ heat flows back to the source and thus has a negative sign. The integral heat flux W is

$$W = \int I dt = \frac{2}{\sqrt{\pi D}} \frac{V_o}{R} t^{0.5} \text{ for } t<t_o;$$

$$= \frac{2}{\sqrt{\pi D}} \frac{V_o}{R} \left[t^{0.5} - (t-t_o)^{0.5}\right] \text{ for } t>t_o.$$

For $t>t_o$ the above equations reduce to

$$W = \frac{1}{\sqrt{\pi D}} \frac{V_o}{R} \left[t_o/(t)^{0.5}\right] .$$

The input heat energy is a maximum at t equal to t_o, and gets smaller as t increases beyond t_o. This is because some of the energy is fed back to the source after t_o. For t equal to 0.3 ns, the example of Figure B-3, the energy input is

$$W = \frac{2 \cdot 4.19}{\sqrt{\pi \cdot 0.005}} \cdot 3000 \cdot 0.002 \cdot (3 \cdot 10^{-10})^{0.5} = 6.95 \cdot 10^{-3} \text{ J/cm}^2$$

At t equal to 100 ns, however,

$$W = 2 \cdot 6.95 \cdot 10^{-3} \cdot \frac{0.3}{100} = 4.17 \cdot 10^{-4} \text{ J/cm}^2.$$

Compared to the available stored energy of $6.5 \cdot 10^{-4}$ J/cm^2 or the arc energy of $4.9 \cdot 10^{-4}$ J/cm^2, the heat input energy is in the right "ballpark."

Figure B-5 summarizes the results of the computations using the 1-dimensional diffusion equation, and Figure B-6 summarizes the conclusions for the analysis. An extensive body of work on the solid propellant (Teflon) pulsed plasma thruster was found in the literature. An empirical relation is presented between mass ablated per unit energy in the plasma discharge:

Mass ablated = $8.32 \cdot 10^{-6}$ grams/J.

This relation is used in the arc discharge analysis of Task 1.

- Stored energy - $6.5 \cdot 10^{-4}$ J/cm^2 (52 pf/cm^2, 5 kV breakdown)
- Arc energy - $4.9 \cdot 10^{-4}$ J/cm^2 (half of the stored charge remains)
- Step Function 3000°K Surface Temperature Rise
  - 0.13 J/cm^2 absorbed in 100 ns
  - 0.22 micron depth is heated to 1500°K in 100 ns
- Rectangular Forcing Function 0.3 ns wide, 3000°K
  - $6.95 \cdot 10^{-3}$ J/cm^2 absorbed at 0.3 ns
  - $4.2 \cdot 10^{-4}$ J/cm^2 net absorbed at 100 ns
  - Maximum temperature at 100°A depth is 1700°K
  - Maximum temperature at 60°A depth is 2300°K.

Figure B-5. Summary of Heat Flow Energy Calculation

- The available stored energy is insufficient, on an uniform per unit area basis, to account for the heat absorbed by the dielectric.

- Depths into the dielectric surface of the order of a fraction of a micron are heated to temperatures comparable to that at the surface in 10^{-7} second.

- A more comprehensive analysis is required involving the latent heat of vaporization of the dielectric material and the transport of heat from the plasma to the surface of the dielectric. Empirical data on ablation is available from pulsed plasma thruster (PPT) studies

  Mass Ablated = $8.32 \cdot 10^{-6}$ (grams/cm^2)/(J/cm^2)

  Ablated material is approximately 10 percent ionized

- The ablation process provides the materials for the off-surface plasma, and at the same time, modifies the conduction heat loss processes by cooling the dielectric surface so that it does not "soak up" excessive amounts of the available energy. The PPT technology data indicates that only a small fraction of the arc energy goes into ablation. The major portion goes into heating, ionzing and propelling of the plasma.

Figure B-6. Conclusions from the Heat Flow Analysis

APPENDIX 3. EFFECTS OF MAGNETIC FORCES ON G'

The trajectory of the arc discharge surface current density, J_s, is calculated here assuming that the only force of consequence is the magnetic force, v x B. The magnetic field, B, is that due to the return current, also J_s, flowing in the substrate, and may be obtained by applying Ampere's Law

$$\Phi\ H \cdot d\ell = 0.4\ \pi\ I,\quad B = H\ \frac{0.4\ \pi\ J_s}{2} = 0.2\ \pi\ J_s$$

where J_s is in A/cm. It should be noted that B is independent of the height of the arc discharge current sheet above the return current sheet. For the maximum J_s, 3.18 A, B is 2.0 gauss at x equal to ℓ. This is because we are considering the 1-dimensional case in which the current is flowing in the x-direction in an infinitely wide sheet (in the y-direction).

The force per cm of width, w, on a segment of length, dx, in MKS units is

$$dF = BJ_s\ dx$$

The force, F, is in the z direction, away from the surface, as shown in Figure C-1.

Equating this to the mass times acceleration gives:

$$dF = BJ_s dx = M\ \dot{v}_z\ dx\ (MKS)$$

where M is the mass per unit area. Converting to cgs units gives

$$B\ (gauss) \cdot 10^{-4} \cdot J_s\ (A/cm) \cdot 10^2 = M\ (grams/cm^2 \cdot 10 \cdot v_z\ (cm/s^2) \cdot 10^{-2}$$

$$\dot{v}_z = \frac{BJ_s}{10M} = 0.02\pi J_s^2\ /M\ (cm/s^2)$$

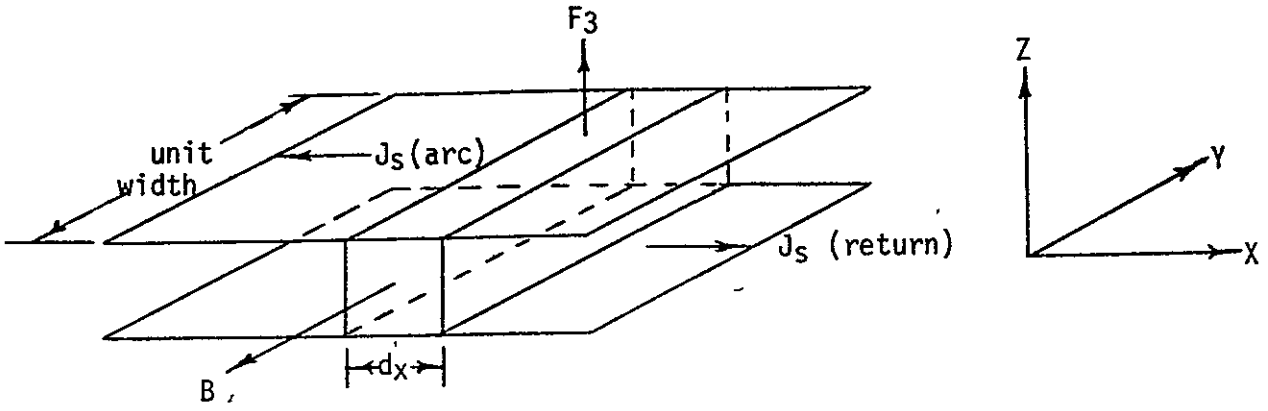

Figure C-1. Magnetic Force J_s and the Coordinate System

Since we are evaluating the displacement of the arc discharge current sheet for the region in which the brushfire wavefront is propagating with velocity, v_b, the time derivative is replaced with the space derivative:

$$\frac{dv_z}{dt} = v_b \frac{dv_z}{dx}$$

The mass and current densities, from our simplified analysis, are assumed to be given by·

$$10\ M = gCE_b^2\ x^2/2 + M_o,\ J_s = Cv_bE_bx.$$

The factor of 10 in the expression for M is to account for the fact that only 10 percent of the ablated mass is ionized according to pulsed plasma thruster technology data. The differential equation and its solution for v_z become

$$\frac{dv_z}{dx} = \frac{0.4\pi C v_b}{g} \frac{x^2}{x^2 + 2M_o/gCE_b^2}$$

$$v_z = \frac{0.4\pi C v_b}{g}\left[x - a \cdot \tan^{-1}\left(\frac{x}{a}\right)\right] \text{where } a^2 = \frac{2M_o}{gCE_b^2}$$

Using the space-time equivalence again.

$$v_z = \frac{dz}{dt} = v_b \frac{dz}{dx} = \frac{0.4\pi C v_b}{g}\left[x - a \cdot \tan^{-1}\left(\frac{x}{a}\right)\right]$$

$$= \frac{0.4\pi C}{q}\left[\frac{x^2}{2} - ax \tan^{-1}\left(\frac{x}{a}\right) + \frac{a^2}{2} \ln\left(1 + \frac{x^2}{a^2}\right)\right]$$

Figure C-2(a) shows v_z and z for x = 0 to x = ℓ = 0.25 cm, and Figure C-2(b) shows v_z and z for x = 0 to x = 20 cm. For Figure 6b ablation was assumed to have ceased and therefore J_s and M remain constant at their values at x = ℓ, 3.18 amp/cm, and $1.35 \cdot 10^{-9}$ grams/cm^2 respectively.

At x = ℓ, the end of the voltage gradient region, the distance off of the surface, z, is only $2.45 \cdot 10^{-7}$ cm. Even at x = 20 cm, v_z is only 3,850 cm/s, and z is only $1.57 \cdot 10^{-3}$ cm, which is only 63 percent of the assumed plasma thickness, d, of $2.5 \cdot 10^{-3}$ cm.

Because of these small z and v_z values, it is unlikely that v x B forces contribute appreciably to G', the ratio of blowoff to flashover arc discharge currents.

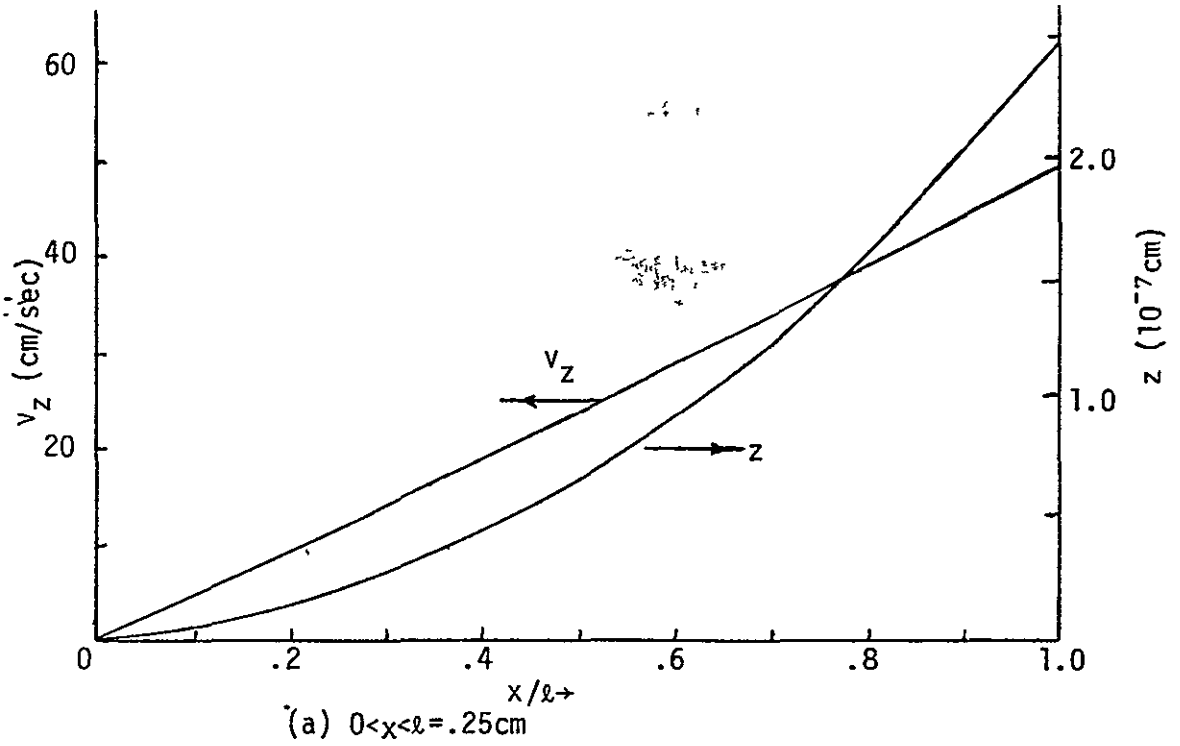

(a) $0<x<\ell=.25$cm

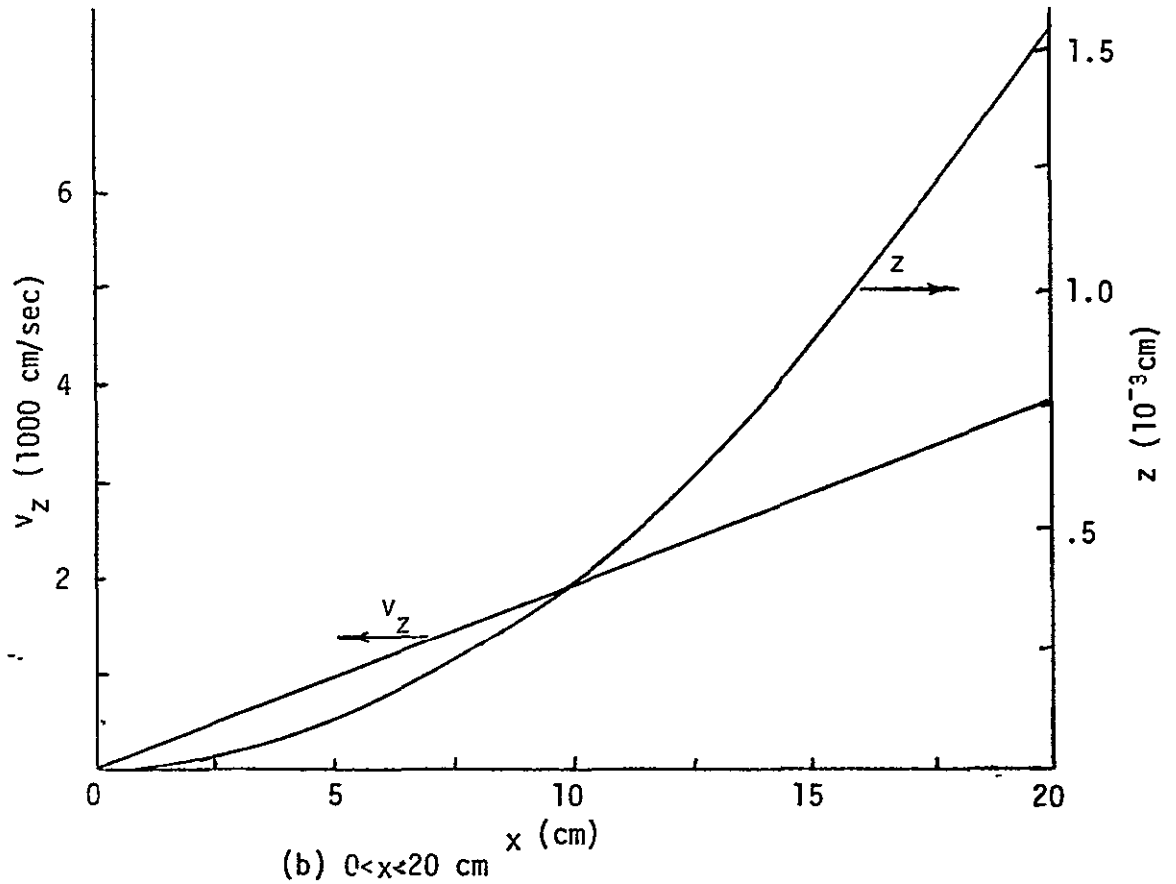

(b) $0<x<20$ cm

Figure C-2. z and v_z for Magnetic vxB Force

APPENDIX 4

BRUSHFIRE ARC DISCHARGE MODEL*

G. T. Inouye
TRW Defense and Space Systems Group, Redondo Beach, California

ABSTRACT

A 1-dimensional arc discharge model incorporating a brushfire-type propagation of a discharge wavefront has been investigated. A set of equations, somewhat similar to those leading to the diffusion equation, has been developed which includes electrical, thermal, and plasma parameters. The solutions of these equations are shown, under simplifying assumptions, to be consistent with a propagating brushfire wavefront. Voltage, current, plasma density, temperature, and resistivity profiles are obtained.

Mechanical, magnetic, and electrostatic forces are considered in evaluating the flashover to blowout current ratio, G', for arc discharges with the brushfire parameters developed in the model. This ratio is an important factor in determining the electromagnetic interference (EMI) impact of arc discharges on spacecraft electrical subsystems. The conclusion of the analysis is that electrostatic forces are much more important than magnetic forces. The magnitude of the G' factor obtained, 58.5 percent, is within the range of those obtained by experimental means. Improvements in the analytical model as well as in the experimental approach are recommended.

*This work was supported under National Aeronautics and Space Administration Contract NAS 3-21961.

INTRODUCTION

The problem of characterizing dielectric surface arc discharges due to spacecraft charging has been approached mainly by experimental means in the past because of the lack of an analytical model. A number of recent papers have presented analytical approaches to the problem. [1,2] The work presented here is a continued development of the concept of a brushfire propagation model developed by J. M. Sellen Jr. and the author.[3,4]

From the viewpoint of the implications of arc dischrges on the immunity of spacecraft to the EMI generated, the question of where the arc discharge currents flow is a critical factor. This problem has been formulated by defining a factor, G', which is defined as the ratio of the blowout to flashover currents. The flashover component is viewed as that which flows essentially from the dielectric surface through a breakdown region, perhaps an edge with high electric fields, directly back to the metallized backing of the dielectric surface. Flashover currents, because their geometrical extent is limited, are not expected to be a major source of spacecraft EMI. Blowout currents, on the other hand, may have a large impact on electrical subsystems because they result in replacement currents flowing through the spacecraft structure which must be of a magnitude equal to the blown off electron current. The density of replacement current flowing in the spacecraft structure is highly dependent on the location of the arcing source and on the particular configuration of the spacecraft. An arc on a boom mounted object, for example, may result in boom currents which couple very well into cabling along the boom. A spacecraft body-mounted source, on the other hand, may be so well grounded and shielded that only currents very close to the source are of sufficient magnitude to be of concern. Thus, the determination of a representative value of G', and its dependence on the size of the arcing source and any other parameters is of prime concern for spacecraft design. Any analytical arc discharge model should provide results that are consistent with experimental data. In addition, however, the work presented here predicts facets of the experimental approach, such as the spatial distribution of blowout currents and the dependence of G' on the sample grounding impedance, which were not adequately considered previously.

ARC DISCHARGE OVERVIEW

The brushfire propagation model addresses only the latter portion of the evolutionary processes involved in an arc discharge. The scenario would be as follows:

1. Differential chargeup by the environmental plasma and solar ultraviolet radiation
2. Edge breakdown at a weak point
3. Surface breakdown
   - High field emission
   - Avalanching processes
4. Brushfire propagation
   - Blowout and flashover currents; G'
   - Dependence on spacecraft potential
   - Limiting mechanisms on propagation.

The question of how external dielectric surfaces charge up differentially with respect to the grounded underlying vacuum deposited aluminum (VDA) or to structural metal is a complex problem which is not addressed here. Generally, the most hazardous situation exists when a dielectric surface is charged negatively with respect to the underlying metals by an excess of impinging electrons over postive ions. This is because with a reverse polarity, i.e., when the metals are negative and the dielectric surface is more positive because of photoemission or secondary emission, a field emission/secondary electron avalanche process tends to limit the magnitude of the differential potential to below 1000 V.

For the purposes at hand of developing an arc discharge model, the chargeup process is important in that negative chargeup potentials of 5 kV to 20 kV have been measured experimentally. The other important feature of chargeup for our present purpose is that theory and experimental evidence[5] indicate that significant densities of electrons may be buried at depths of the order of 1 micron below the surface at the time of the discharge. This feature of buried electronic charge should also exist on dielectric surfaces which have no net surface

charge because of photoemission or secondary emission. In fact, the buried charge should be somewhat deeper and more dense since retarding potentials are not present.

Dielectric breakdown due to high differential voltage stresses generally occurs for electric fields in the range of 10^5 to 10^6 V/cm at the edges of thin ($\sim$50 microns or 0.005 cm) insulating sheets. Punch-through far from the edges occurs with fields of the order of 10^7 V/cm. In practice, even punch-throughs probably occur at weak points where slight imperfections or irregularities exist in the material. Edges consist of exaggerated irregularities because they are created by slicing with a knife edge or by punching with stitching needles, and thus, are subject to high field emission and avalanche breakdown in a manner similar to that which will be discussed for surface breakdown. The similarity to surface breakdowns probably goes even further in that this type of breakdown is associated with surface and off-surface processes rather than those within the bulk of the material.

The net effect of an edge breakdown is that the potential of the surface near the edge goes to nearly 0 V, assuming that the thin dielectric is over a conducting plate which is at voltage reference, 0 V. Taking a singly-ionized particle of atomic weight 16 (oxygen) as being typical, the velocity associated with a 10 kV voltage drop is $3.5 \cdot 10^5$ m/s. Starting at zero velocity, the time for such an ion to traverse the 2 mils or 50 micron thickness of the dielectric is 0.3 ns. This order of magnitude time span, a fraction of a ns, is much shorter than the tens to hundreds of ns duration of vacuum dielectric surface arcs.

Assuming that a 2-mil thick sheet of Kapton, $\epsilon_r = 3$, breaks down at 10 kV over a semicircular area with a radius equal to its thickness, the capacitance is 52 pf/cm^2 or $2 \cdot 10^{-3}$ pf, and the charge stored is $2 \cdot 10^{-11}$ Coulomb. Assuming that all of this charge is dissipated in 0.3 ns, the corresponding current would be 0.068 A. Thus, the current, charge, time span, and energy ($\sim 10^{-7}$ joule) involved in the initial edge breakdown are quite small and negligible compared to those in the events that follow. The main effect of the initial edge breakdown is to create a plasma cloud and a surface electric field which initiates a subsequent surface discharge.

Dielectric surface breakdown has been reported to occur more readily, at 10^4 to 10^5 V/cm surface electric fields, than breakdown in the bulk of dielectric materials. The surface breakdown fields are expected to be highly dependent on surface conditions such as cleanliness, smoothness and absorbed gases.

BRUSHFIRE PROPAGATION MODEL

The experimentally observed "wipeoff" of charge over many hundreds of cm^2, and possibly greater areas of dielectric surface, requires either some mechanism for propagation of an initial surface breakdown in a brushfire mode, or that somehow all of the participating charge release occurs simultaneously over a large area. The propagation mode seems more plausible and is discussed further here. The source of discharging energy, the stored charge per unit area, is depleted, and the discharge must be fed by a forward propagation of the brushfire periphery into the still-charged regions of the dielectric. To discuss the brushfire propagation process, some of the basic equations are presented first. Then, a simplistic piecemeal solution of various aspects of the problem is presented to provide an insight into the quantitative aspects of the problem. Even the basic relations such as those for ablation and ionization are not developed from first principles, but rather, are taken from existing experimental data and theoretical work found in the literature. Figure 1 provides an overview of the brushfire propagation analysis.

The basic equations to be satisfied for the brushfire propagation problem are:

$$\frac{\partial V}{\partial t} = -\frac{1}{C}\frac{\partial J_s}{\partial x} \quad \text{and} \quad J_s = -\frac{1}{\rho_s}\frac{\partial V}{\partial x} \qquad (1,2)$$

Where the potential, V, and surface current density, J_s, are functions of horizontal distance, x, and time, t. The two other parameters of this 1-dimensional formulation are the capacitance per unit area, C, which is 52 pf/cm^2 for a 2 mil thick dielectric with a dielectric constant of 3, and the surface resistivity, ρ_s (ohms-per-square), of the plasma sheet that conducts the arc discharge current, J_s. The geometry of the problem is shown in Figure 2. The initial voltage, -5 kV was selected to give a 10^6 V/cm electric field bulk breakdown for the 2 mil dielectric thickness. A final voltage of -2.5 kV was assumed on the basis that about 50 percent of the initial voltage has been observed

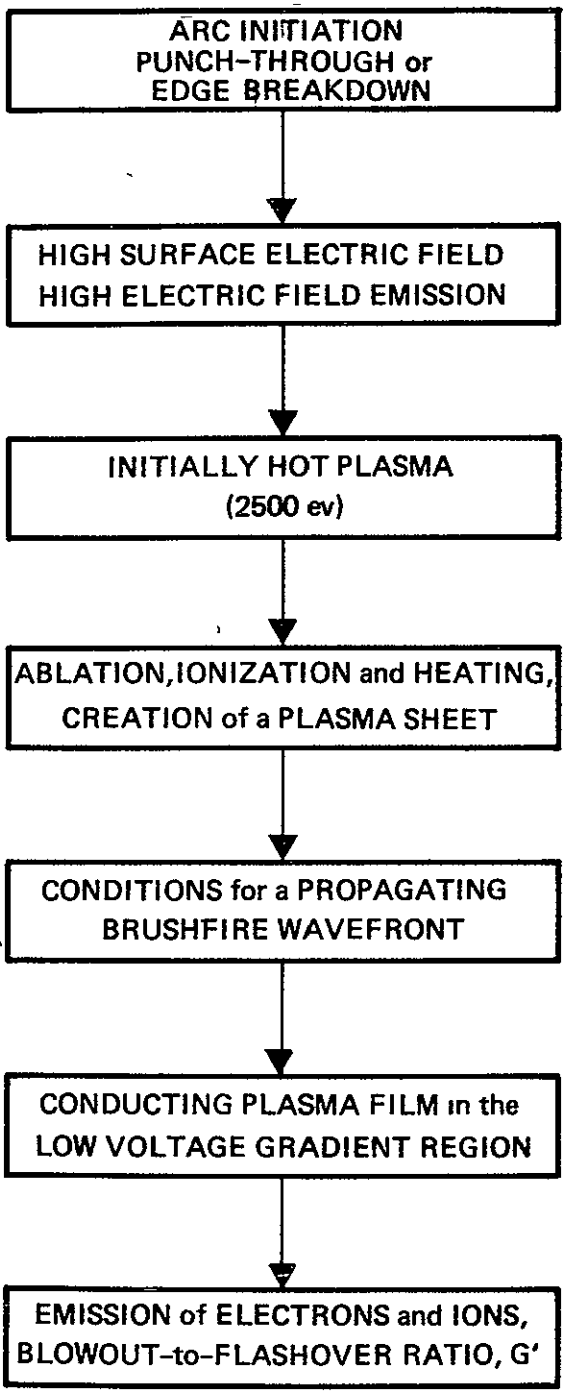

Figure 1. Overview of the Brushfire Propagation Analysis

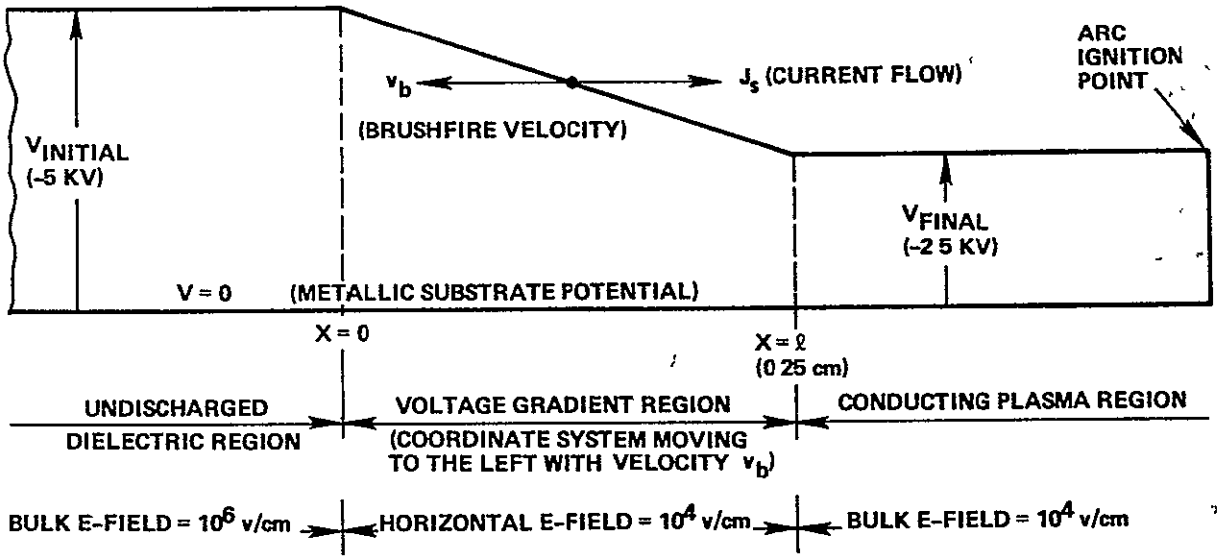

Figure 2. Voltage Profile of a Propagating Brushfire Wave Front

experimentally to remain after the discharge. As an initial guess, the voltage is assumed to decrease linearly with distance providing an electric field of 10^4 V/cm. The voltage gradient region is therefore 0.25 cm long. Combining equations (1) and (2) to eliminate J_s gives

$$\frac{\partial V}{\partial t} = \frac{1}{C\rho_s} \frac{\partial^2 V}{\partial x^2} \qquad (3)$$

This would be the diffusion equation with the diffusion coefficient, D:

$$\frac{\partial V}{\partial t} = D \frac{\partial^2 V}{\partial x^2} \quad \text{where } D = \frac{1}{C\rho_s} ,$$

except that ρ_s is not a constant in our problem. This is fortunate because the diffusion equation does not lead to a propagating mode with a constant velocity.

The plasma resistivity, ρ, and surface resistivity, ρ_s, are functions of the temperature, T: [6]

$$\rho = \frac{K}{T^{3/2}} \text{ ohm - cm, where } K = 0.03 \text{ ohm-cm-eV}^{3/2}, \qquad (4a)$$

$$\rho_s = \rho/d = \frac{K}{d} T^{-3/2} \text{ ohms}, \qquad (4b)$$

where d is the thickness of the plasma sheet. It is of interest to note that ρ is independent of the density of the plasma particles.

T is governed by a set of equations similar to those for V:

$$\frac{\partial T}{\partial t} = - \frac{1}{cM} \frac{\partial H}{\partial x}, \; H = - \frac{1}{} \frac{\partial T}{\partial x}, \qquad (5,6)$$

where H is the heat flux, c is the specific heat, M is the mass density, and is the thermal resistivity. For our problem here we neglect thermal conductivity, because of the short time spans involved, and assume that is infinite. The rate of heat energy deposition in an incremental distance, dx, in equation (5) is the power density, P_s:

$$- \frac{\partial H}{\partial x} = P_s = -J_s \frac{\partial V}{\partial x} \text{ watts/cm}^2 \qquad (7)$$

The specific heat, c, is obtained using the gas constant, R, by assuming that the plasma consists of neutrals, ions and electrons, each with 3 degrees of freedom:

$$c_m = \frac{1}{2} \cdot 9R = 4.5R = 4.5 \cdot 8.314 = 37.41 \text{ joule/(deg-mole)}. \qquad (8a)$$

Assuming the dielectric material has a molecular weight, G_m, of 16, c is given by:

$$c = c_m/G_m = 2.34 \text{ joule/(deg-gram)} = 2.71 \cdot 10^4 \text{ joule/(ev-gram)} \qquad (8b)$$

Where c_m is defined as the specific heat per mole

and G_m is defined as the mass density per mole.

The mass density, M, to be used in equation (5) is composed of two components, M_a, due to ablation because of the power dissipation, P_s, and M_o which is due to the initial field emission electrons:

$$M = M_a + M_o \text{ grams/cm}^2 \tag{9}$$

The ablated mass density, M_a, is assumed to be proportional to the time-integrated powwer density, P_s:

$$M_a = \int g\, P_s\, dt \text{ grams/cm}^2 \tag{10}$$

The proportionality constant, g, is taken from the pulsed plasma thruster technology data.[7]

$$g = 8.32 \cdot 10^{-6} \text{ grams/joule}$$

We view ablation as being due to "pounding" of the surface by ions which are accelerated by the electric field due to the electrons which have been stored (buried) by the basic spacecraft charging process.

M_o is not due to heating in the thermal sense but rather is due to collisions between the initial electrons, that are emitted or "pulled-out" by high field emission at localized regions of high electric field, and the dielectric surface atoms. The high field emission current density, J, is described in terms of the electric field, E, by:[8]

$$J = 6.5 \cdot 10^{-7} E^2 e^{-6.5 \cdot 10^9 / E}$$

According to this equation, J has a nearly step-function increase at

$$E = 6.5 \cdot 10^9 \text{ volt/meter} = 6.5 \cdot 10^7 \text{ V/cm}$$

The experimentally observed threshold electric field intensity of 10^4 V/cm, nearly four orders of magnitude less, must be due to the fact that localized regions of high electric fields exist on a sufficiently small microscopic scale.

M_o may be evaluated by equating the energy gained by these field-emitted electrons to an inital temperature, T_1:

$$k\, \Delta T_1 = e \Delta V = e E_b\, \Delta \lambda$$

Where k is the Boltzmann constant and e is the electronic charge.

We take the characteristic distance, λ, to be the Debye shielding distance:

$$\lambda = 6.9 \sqrt{\frac{T_1}{n}}$$

Where T_i is the temperature in °K, and n is the plasma density in number/cc. E_b is the surface breakdown electric field of 10^4 V/cm. These equations may be integrated to give:

$$T_1 = \frac{A^2}{n+n_o} \text{ °K, where } A^2 = \left(\frac{6.9eE_b^2}{2k}\right) = 1.602 \cdot 10^{17},$$

$$T_1 = \frac{1.381 \cdot 10^{13}}{n + n_o} \text{ eV where n and } n_o \text{ are in particles/cm}^3 \quad (11)$$

The constant of integration, n_o, has been introduced approximately in the form of additional number density where T_i varies inversely as the total density, by taking T_1 as 2500 eV when n is zero. Recall that n is the number density due to ablation.

This density, n, is evaluated from the ablated mass density, M_a, by

$$n = 6.02 \cdot 10^{23} \frac{\text{molecules}}{\text{mole}} \left(\frac{1 \text{ mole}}{16 \text{ grams}}\right) M_a \frac{\text{grams}}{\text{cm}^2} \cdot \frac{1}{d \text{ cm}} =$$

$$3.76 \cdot 10^{22} \frac{M_a}{d} \frac{\text{molecules}}{\text{cm}^3}$$

The parameter, d, is the thickness of the plasma film or sheet and is assumed to be 1 percent of the voltage gradient region or 0.0025 cm. The number density, n_o, is

$$n_o = \frac{1.38 \cdot 10^{13}}{2500} = 5.523 \cdot 10^9 \text{ particles/cm}^3 \quad (12a)$$

The corresponding mass density, M_o is:

$$M_o = n_o d \cdot \frac{16}{6.02 \cdot 10^{23}} = 3.67 \cdot 10^{-16} \text{ grams/cm}^2 \quad (12b)$$

SIMPLIFIED ANALYSIS

The simultaneous solution of all of the equations presented up to now is rather complex and requires a computer solution.

Here, some quantitative feeling for the results is obtained by a piecemeal approach with simplifying assumptions.

The first assumption is that there <u>is</u> a solution in which a constant brushfire propagation velocity, v_b, is appropriate. With this assumption, time variables may be replaced with space variables:

$$x = v_b t; \quad \frac{\partial f}{\partial t} = v_b \frac{\partial f}{\partial x} \tag{13}$$

Equations (1) and (2) may then be integrated to give:

$$J_s = C v_b (V_m - V), \text{ and} \tag{14}$$

$$V = V_m (1 - \ell^{-f(x)}), \text{ where } f(x) = C v_b \int_x^{\ell} \rho_s \, d_x \tag{15}$$

Where V_m is the maximum voltage change (2500 volts), and V is the voltage at any point x in the voltage gradient region. For this part of the analysis the zero reference voltage is taken to be the potential at the bottom of the voltage falloff region; i.e., $V = 0$ at $x = \ell$.

A further simplification of the problem is obtained by assuming that the voltage profile is known, a linear dropoff to $V_{final} = 0$ as shown in Figure 2. Temperatures, resistivities, particle densities, current densities as well as a new voltage profile can then be calculated. Consistency of the new voltage profile with the assumed profile will put constraints on the possible values of the parameters involved.

The assumed voltage profile is given by

$$V = V_m \left(1 - \frac{x}{\ell}\right) = V_m - E_b x$$

The breakdown value of the surface electric field, E_b, is assumed to be 10^4 V/cm.

The plasma parameters for the voltage gradient region may be calculated and are shown in the table below.

Table 1. Plasma Parameter Resulting from a Linear Voltage Gradient

$J_s = Cv_bV_mx/\ell = Cv_bE_bx$	$\rho_s = \frac{K}{d} T^{3/2} = 12(\frac{cg}{h})^{3/2}[\ell n(1+\frac{x^2}{A})]^{-3/2}$
$P_s = J_s \frac{\partial V}{\partial x} = J_sE_b = Cv_bE_b^2x$	$T_h = -\frac{h}{cm}\int P_s dt = \frac{h}{cg}(1 + x^2/A)$
$M_a = \int gP_s dt = gCE_b^2x^2/2$	where $A = 2M_o/(gCE_b^2) = 1.70 \cdot 10^{-8} cm^2$
$n = 3.76 \cdot 10^{22} gCE_b^2x^2/(2d)$	and T_h is the temperature due to heating.

The parameter, h, is included in the equation for T_h to account for the fact that not all of P_s goes into heating the plasma and raising the temperature. A heat absorption calculation shows that the heat loss into the dielectric surface constitutes a major sink for the energy in the plasma. The plasma thickness, d, was assumed to be 0.0025 cm, or 1 percent of the length of the voltage gradient region, ℓ. M_a and T_h do not depend on d, but n and ρ_s do. It should also be noted that all four of these parameters are independent of the brushfire velocity, v_b. This is because they all depend on the time-integrated power density, P_s, i.e., the energy, which is independent of velocity. The temperature, T, in the equation for surface resistivity, ρ_s, is a composite of the initial field emission/low collisional plasma temperature, T_i, and the temperature due to heating, T_h. These two temperature profiles have been combined in the root-sum-square sense:

$$T = (T_i^2 + T_h^2)^{0.5}$$

Since only the T_h component of T depends on h and the T_1 component does not, h was selected to give the most reasonable voltage profile, V(x) (see Figure 3a), when computed using equation (15). The value selected was

$\frac{h}{cg} = 8.71 \cdot 10^{-4}$, $h = 1.964 \cdot 10^{-4}$, where $c = 2.71 \cdot 10^{4}$ joules/(ev-gram), and

$g = 8.32 \cdot 10^{-6}$ grams/joule

As noted previously, h is a very small fractional number. The term in the expression for f(x) defined in equation (15) and in Table 1:

$$12\left(\frac{cg}{h}\right)^{3/2} Cv_b$$

must be a constant.

This means that the individual parameters may change as long as the value of the above combination remains constant. For example, if the per unit area capacitance C is doubled, the propagation velocity, v_b, is halved. There is no reason to expect c, g, or h to change when C is doubled by halving its thickness. It is possible, however, that c, g, or h may have values different from those assumed here, but the combination, cg/h, must remain at the same value.

For all of the computations and parametric curves which will be presented next, the brushfire propagation velocity, v_b, was selected to correspond to that of an ion of mass 16 (oxygen) accelerated through the breakdown voltage, V_b, of a 2 mil sheet of Kapton. The bulk breakdown electric field is assumed to be 10^6 V/cm:

$$v_b = \sqrt{2eV_b/m} = 2.45 \cdot 10^7 \text{ cm/sec for } V_b = 5000 \text{ V}$$

Figure 3a shows the assumed voltage profile, V(x), which is moving to the left at a velocity, v_b, equal to $2.45 \cdot 10^7$ cm/sec. V drops linearly from 2500 V at x = 0 to zero at x = ℓ where ℓ was chosen to be 0.25 cm in order to give the surface breakdown electric field of 10^4 V/cm. Figure 3a also shows the current density, J_s, which increases linearly from zero at x = 0 to 3.18 A/cm at x = ℓ. Figure 3b shows the power density, P_s, which increases linearly from zero at x = 0 to $3.18 \cdot 10^4$ W/cm^2 at x = ℓ. The plasma ion and electron density, n_1, is also shown in Figure 3b. It varies parabolically from zero at x = 0 to $2.03 \cdot 10^{15}$

particles/cm^3 at $x = \ell$. The ionization is assumed to be 10 percent of the total and therefore the neutral particle density is $1.83 \cdot 10^{16}$ particles/cc at $x = \ell$.

Figure 4a shows the temperature, T, and surface resistivity, ρ_s, as a function of x/ℓ.

Figure 4b shows the originally assumed linearly falling voltage profile and the voltage profile computed by using the ρ_s integral in equation (15). It can be noted that V(o) is only 90 percent of V_m at $x = 0$. However, the voltage gradient is greater than the surface breakdown electric field of 10^4 V/cm when x/ℓ is greater than about 0.5. The temperature in Figure 4a is extremely "hot" for small x/ℓ values but cools down quickly as the plasma density increases. A minimum is reached at x/ℓ equal to about 0.4 where the heating effect takes over, and the temperature rises slowly as x/ℓ increases beyond this point. The surface resistivity profile in Figure 4a varies as the inverse three-halves power of T.

In order for the computed voltage to be identical to the assumed voltage profile, the surface resistivity would have to be an inverse function of x:

$$\rho_s = \frac{1}{Cv_b x}, \quad Cv_b \int_x^{\ell} \rho_s dx = \ell n \frac{\ell}{x}, \quad \text{where } e^{-f(x)} = \frac{x}{\ell}.$$

The physics of the problem requires initially a very hot plasma and therefore a very small resistivity, rather than the initially very large surface resistivity required by the assumed linear voltage profile. What this says is that the linear voltage profile was <u>not</u> a good assumption. The computed profile of Figure 4b is presumably a better approximation to the "real" propagating brushfire voltage profile. In principle, iteration of the computations performed here with the computed voltage should provide a better solution. This is not done here, and a more thorough analysis using a computer is recommended.

BLOWOUT AND FLASHOVER CURRENTS; G'

The ratio of blowout to flashover currents, G', is a very important parameter in defining the EMI margin of immunity of a spacecraft to arc discharges. The current density, J_s, of 3.18 amp/cm calculated in the previous section is

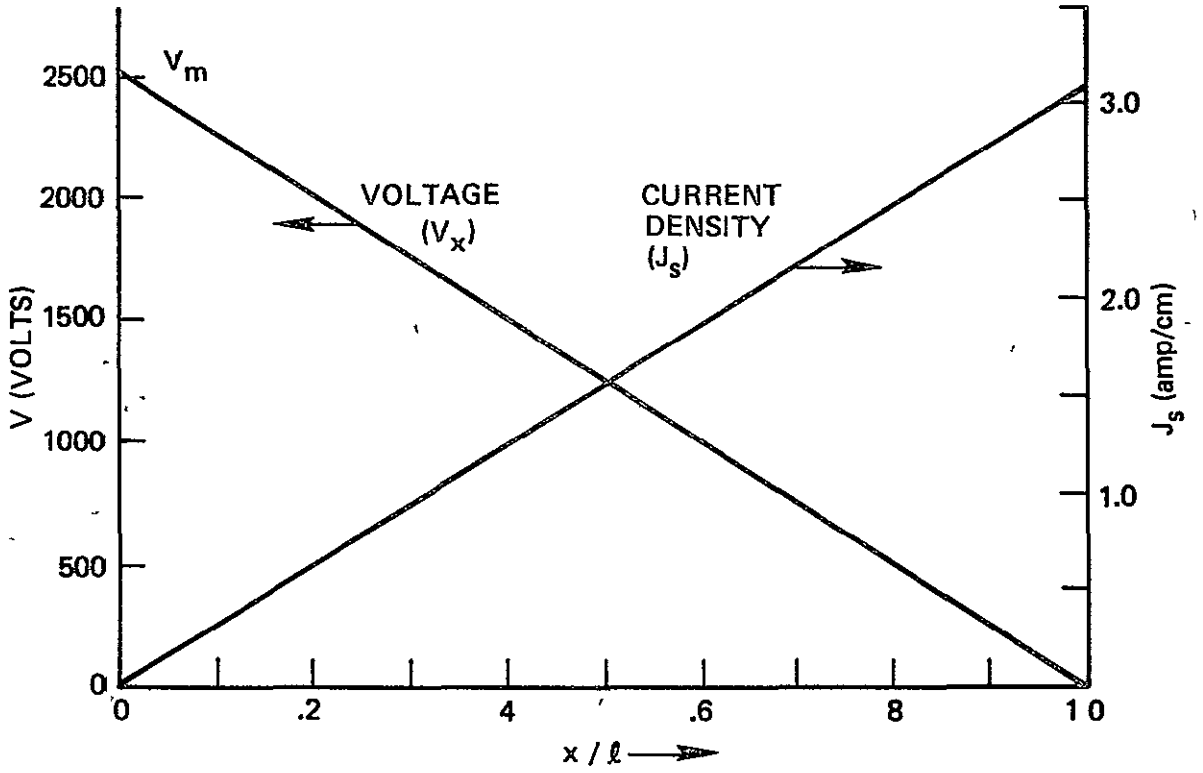

(a) VOLTAGE and CURRENT DENSITY

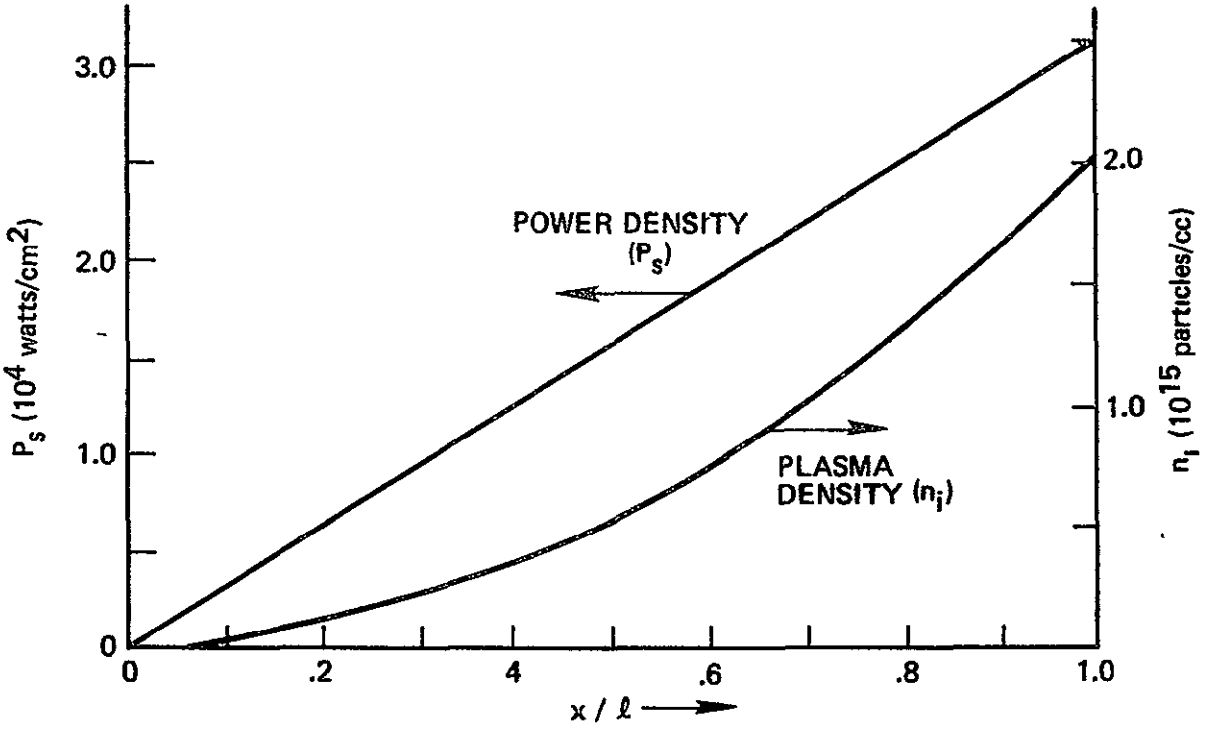

(b) POWER and PLASMA DENSITIES

Figure 3. Plasma Parameters Resulting from an Assumed Linear Voltage Profile

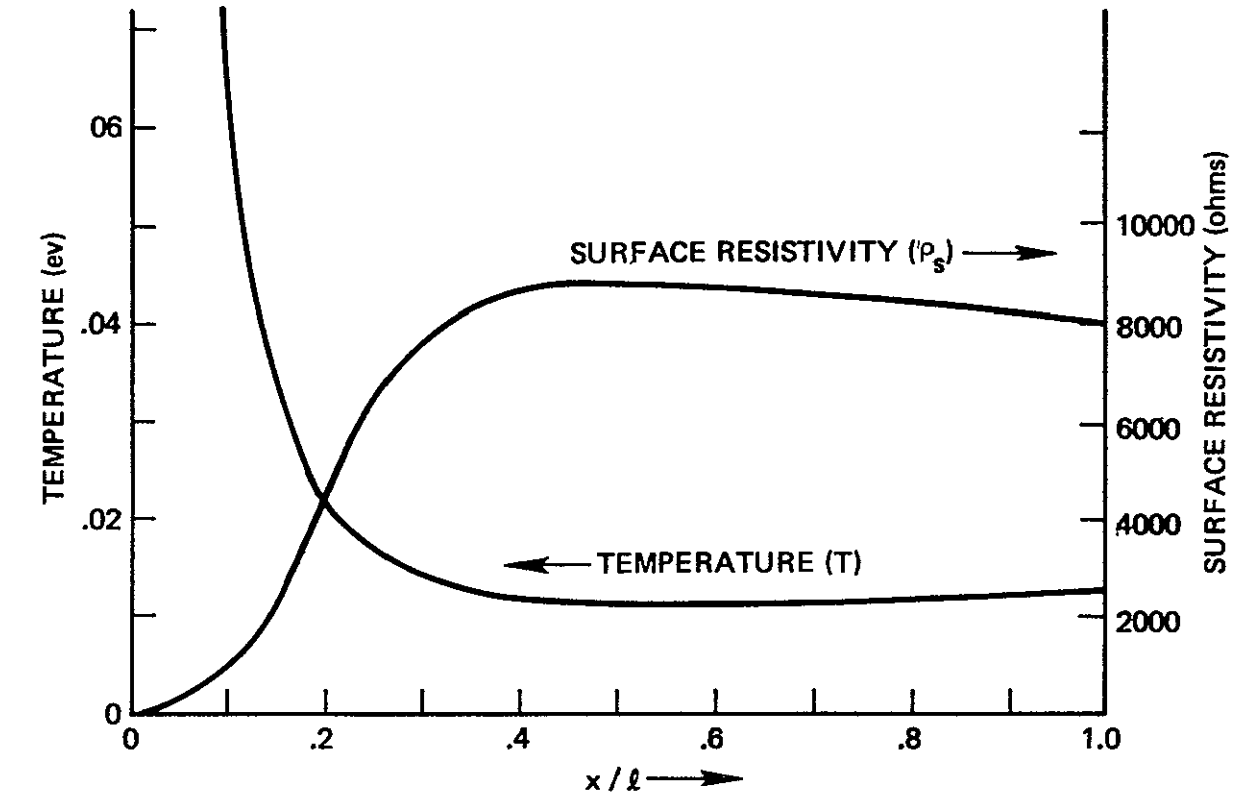

(a) TEMPERATURE and SURFACE RESISTIVITY PROFILES

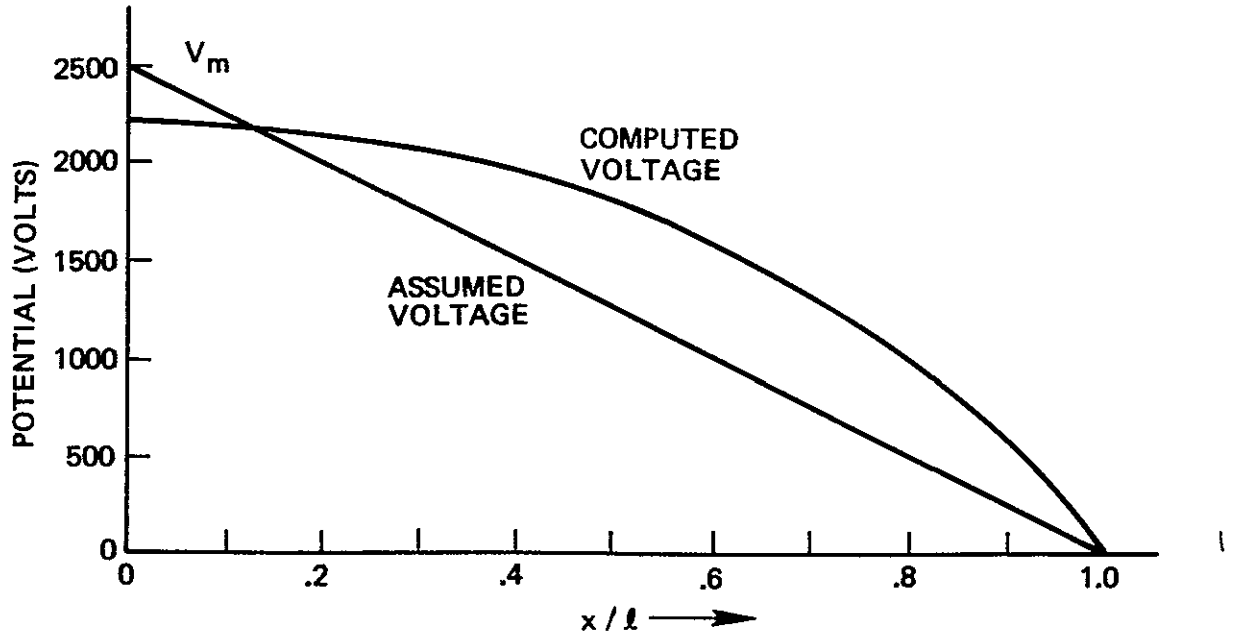

(b) ASSUMED and COMPUTED VOLTAGE PROFILES

Figure 4. Additional Plasma Parameters Resulting from a Assumed Linear Voltage Profile

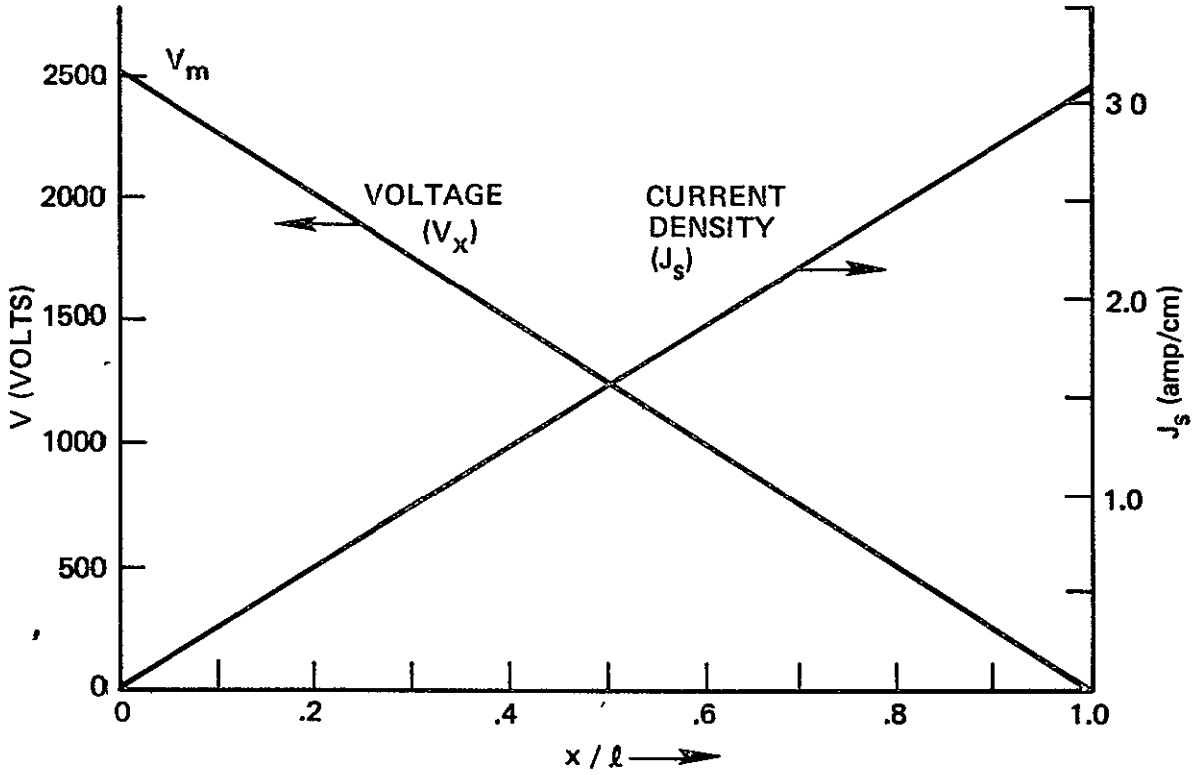

(a) VOLTAGE and CURRENT DENSITY

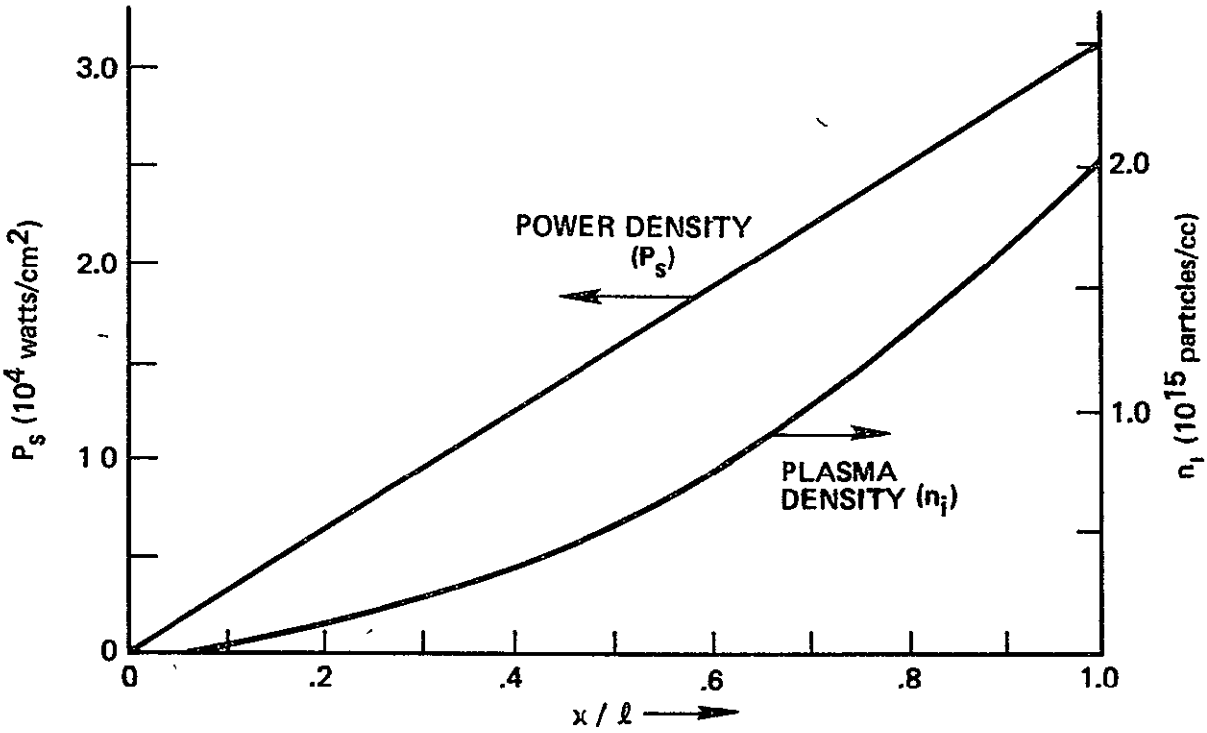

(b) POWER and PLASMA DENSITIES

Figure 3. Plasma Parameters Resulting from an Assumed Linear Voltage Profile

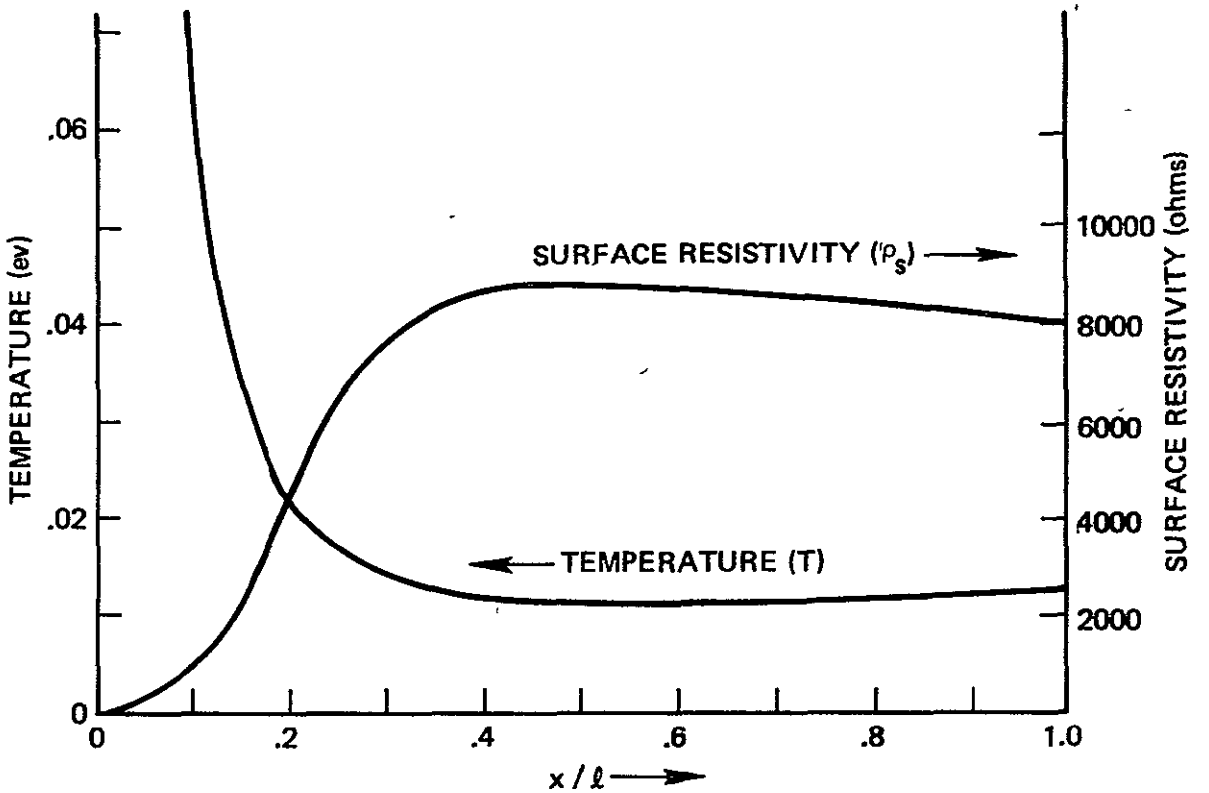

(a) TEMPERATURE and SURFACE RESISTIVITY PROFILES

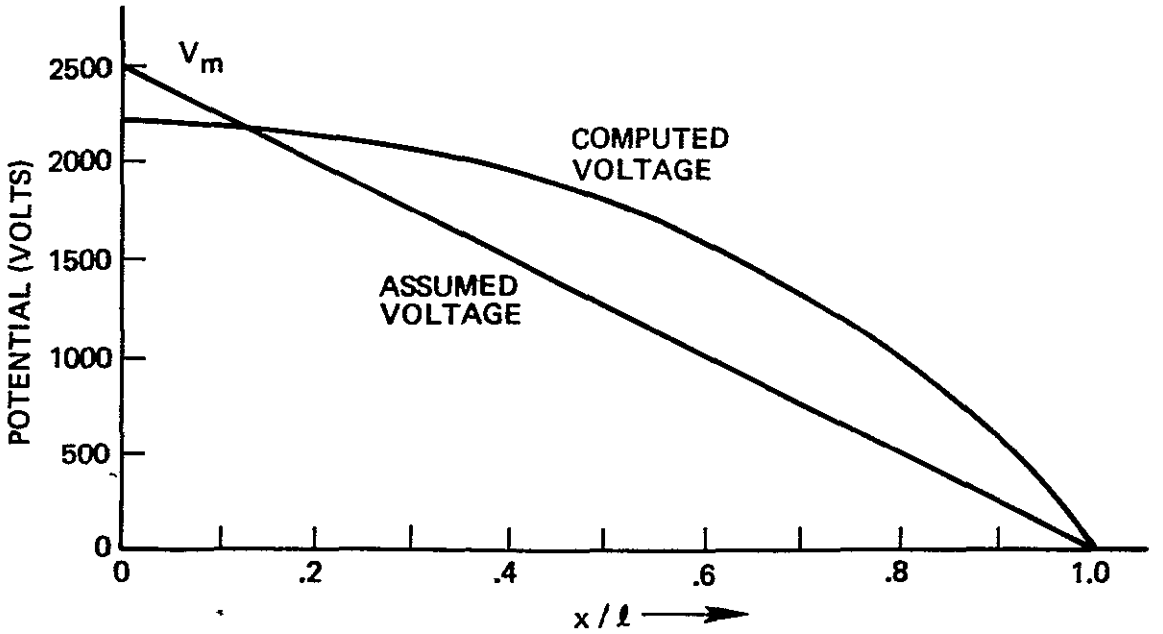

(b) ASSUMED and COMPUTED VOLTAGE PROFILES

Figure 4. Additional Plasma Parameters Resulting from a Assumed Linear Voltage Profile

that which flows to the point of arc discharge initiation in a plasma sheet and thence directly to the conductive substrate below. This is what has been termed the flashover current. Because of the localized nature of this component, the electric and magnetic field effects are also expected to be localized. Previously, the only long range effect considered was that due to the displacement current, CdV/dt where C is effectively the capacitance to space of the arcing element, and dV/dt is the time rate of change of the surface voltage. Because C is very small (~pf/cm^2) the corresponding currents are very small, and the voltages induced into cable harnesses were very small and at nonhazardous levels. Blowout currents are additional to the displacement currents discussed above. If they are of appreciable magnitude, they could be a serious source of hazard to spacecraft electrical subsystems.

In this section the results of the previous section on brushfire propagation are used to estimate the blowout current. Both magnetic and electrostatic forces were examined, and the conclusion was reached that only the latter is of consequence. Electric fields normal to the dielectric surface will force electrons to move away in the z direction. The overwhelming majority of electric field lines emanating from the electrons collected from environmental charging land on positive charges induced on the substrate. A few field lines, however, must go off to space to account for the voltage fall-off (or rise) from the dielectric surface potential to the space plasma potential (zero). Thus, it is already clear that the dielectric surface potential, through its associated electric field, plays an important role in determining the blowout to flashover arc discharge current ratio, G'. The magnitude of the electric field for a conducting sphere is

$$E_{radial} = \frac{Q}{4 \pi \varepsilon_0 a^2} = \frac{V_s}{a} \text{ (MKS units)}$$

where a is the radius of the sphere, V_s is the surface potential, and Q is the charge. For an arcing dielectric surface on a real spacecraft, a is not an easily defined parameter and requires a time-dependent, NASCAP-type, 3-dimensional LaPlace's equation solution in an arc whose discharge charge time is measured in nanoseconds.

We know that a is not as large as the spacecraft dimension and not as small as the dielectric thickness. For our purposes here, we assume that it is comparable to the size of a typical spacecraft box (or 20 cm), but keeping in mind that E_{radial} varies inversely as a.

The fact that edge or punch-through breakdown occurs at -5 kV, but -2.5 kV remains after the discharge, has been ignored up to now except to take the 2.5 kV differential as the voltage which "drives" the brushfire.

Thus:

$$V_s = V_o + V_r + V_m \left(1 - \frac{x}{\ell}\right),$$

where V_o is the spacecraft ground potential, V_r is the remaining voltage after the discharge (2500 V) and V_m is the maximum brushfire driving potential (2500 V). The proper signs have to be used to account for the fact that we are considering forces which drive electrons off of the surface. Ions are pulled harder against the surface. For the time being V_o will be assumed to be zero.

The velocity and displacement in the off-surface z-direction for an electron released at z = o and t = o are given by

$$F_z = eE_z = e\, V_s/a = m \frac{dv_z}{dt}$$

Incorporating, as before, the space-time equivalence via the brushfire propagation velocity v_b:

$$v_z(x) = \int_o^x \frac{2eV_m}{mav_b} \left(1 - \frac{x}{2\ell}\right) dx = \frac{2eV_m}{mav_b}\, x \left(1 - \frac{x}{4\ell}\right)$$

$$z(x) = \frac{2eV_m}{mav_b^2} \int_o^x \left(x - \frac{x^2}{4\ell}\right) dx = \frac{eV_m}{mav_b^2}\, x^2 \left(1 - \frac{x}{6\ell}\right)$$

The above equations apply in the MKS system of units. If a, v_b, and x are in cgs units, v_z and z may be obtained in cgs units by multiplying both of the above equations by 10^4.

Figure 5 shows v_z and z plotted as functions of x/ℓ. At $x = \ell$, v_z is $3.37 \cdot 10^9$ cm/sec and z is 19.1 cm. These values for electrostatic deflection are about eight orders of magnitude greater than the comparable values caused by magnetic forces on the plasma current.

To calculate the off-surface surface current density, J_{sz}, an integration over x has to be performed:

$$J_{sz}(x_1) = \int_0^{x_1} e\, n(x)\, v_z(x_1 - x)\, dx$$

$$\text{where } v_z(x_1 - x) = \frac{2eV_m}{mav_b}(x_1 - x)\left(1 - \frac{x_1 - x}{4\ell}\right) \cdot 10^4 \text{ cm/sec}$$

$$n(x) = Ax^2 \text{ electrons/cm}^3 \text{ (x in cm)}$$

$$A = 0.1 \cdot 3.76 \cdot 10^{21}\, gCE_b^2/2d = 3.25 \cdot 10^{16} \text{ cm}^2$$

$J_{sz}(x_1)$ is plotted in Figure 8 for $0<x<0.05\ell$.

$$J_{sz}(x_1) = 3.04 \cdot 10^4 \left(\frac{x_1}{\ell}\right)^4 \left(1 - \frac{2x_1}{5\ell}\right) \text{ amp/cm}$$

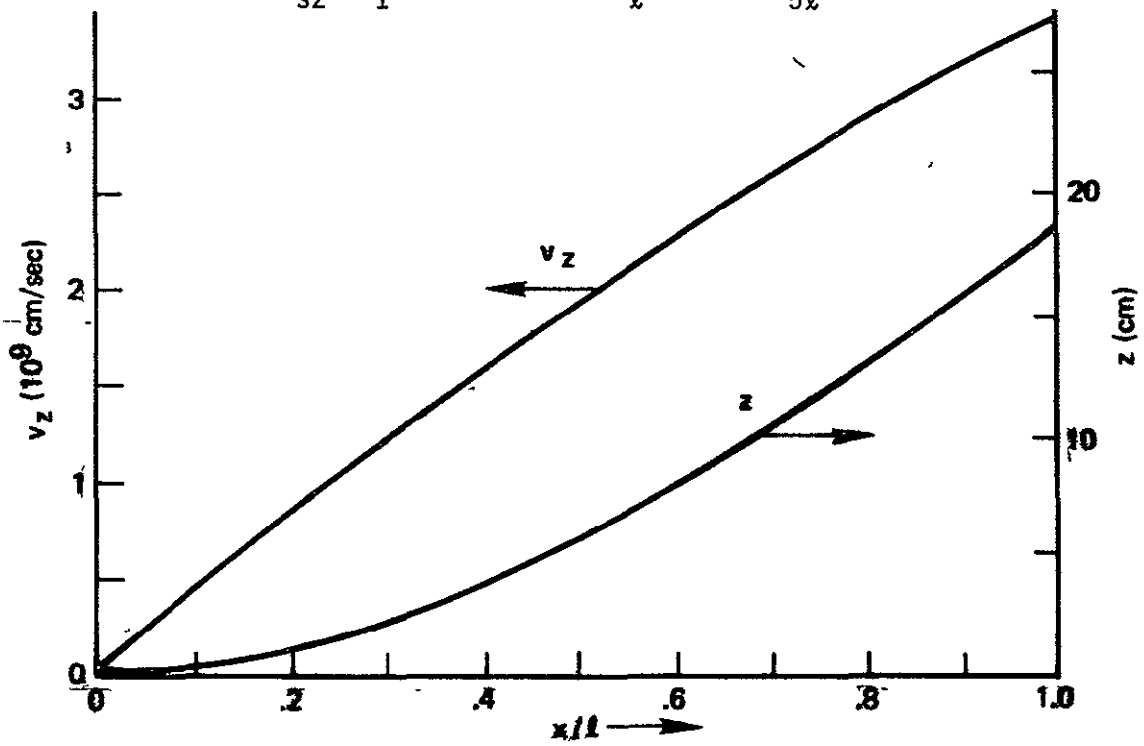

Figure 5. v_z and z for Electron at x = o (No Plasma Shielding)

At $x_1 = \ell = 0.25$ cm, J_{sz} would be 18,240 amp/cm, which is much too large in view of the 3.18 amp/cm value for J_s (in the x-direction) in the plasma sheet at $x = \ell$. There is, however, a mechanism whereby J_{sz} is cut off at a much smaller value. The situation is that at the same time as the off-surface charge is being elevated by electrostatic forces, the charge finds itself above a plasma whose Debye length is shorter than its height above the surface of the dielectric. At some height, z, and Debye length, λ, the electric field due to the charges below becomes completely blocked off, and the effective electric field becomes zero. We assume that this height, z, is equal to 4.6λ; i.e., when the electric field is shielded by 99 percent.

The effective height $\bar{z}(x)$ is calculated by averaging the z - distance travelled by all of the particles released from $x = o$ to $x = x_1$.

$$\bar{z}(x_1) = \frac{1}{\int_o^{x_1} n(x)\,dx} \int_o^{x_1} n(x)\, z(x_1 - x)\,dx$$

where $z(x_1 - x) = \frac{2eV_m}{mav_b^2}(x_1 - x)^2 \left(1 - \frac{x_1 - x}{6\ell}\right) \cdot 10^4$ cm

$$\bar{z}(x_1) = \frac{eV_m \ell^2}{mav_b^2}\left(\frac{x_1}{\ell}\right)^2 \left(1 - \frac{x_1}{12\ell}\right) \cdot 10^3 = 2.29\left(\frac{x_1}{\ell}\right)^2 \left(1 - \frac{x_1}{12\ell}\right) \text{ cm}$$

The Debye length is given by

$$\lambda = 6.9\,(T/n)^{0.5} \text{ cm}$$

where T is the temperature in °K and n is in electrons/cm^3.

Figure 6 shows z and λ plotted for $0 < x < \ell$ (where $\ell = 0.25$ cm). It can be seen that z is much greater than λ for most of the range of x/ℓ except near $x = o$. At $x = \ell$, z is about 2 cm, which is about 10 percent of the value for z, the height of a single electron released at $x = o$. Since the temperature for small

values of x is nearly completely dominated by the initial high-field-emitted electrons which are cooling off:

$$T \cong T_1 = \frac{1.381 \cdot 10^{13}}{n + n_o} \text{ ev} \cong \frac{1.60 \cdot 10^{17}}{n} {}^{o}K,$$

and $$\lambda = \frac{6.9.4.00 \cdot 10^{8}}{n} = \frac{2.76 \cdot 10^{9}}{3.25 \cdot 10^{16} x^2} = \frac{8.49 \cdot 10^{-8}}{x^2} = \frac{1.36 \cdot 10^{-6}}{(x/\ell)^2} \text{ cm}$$

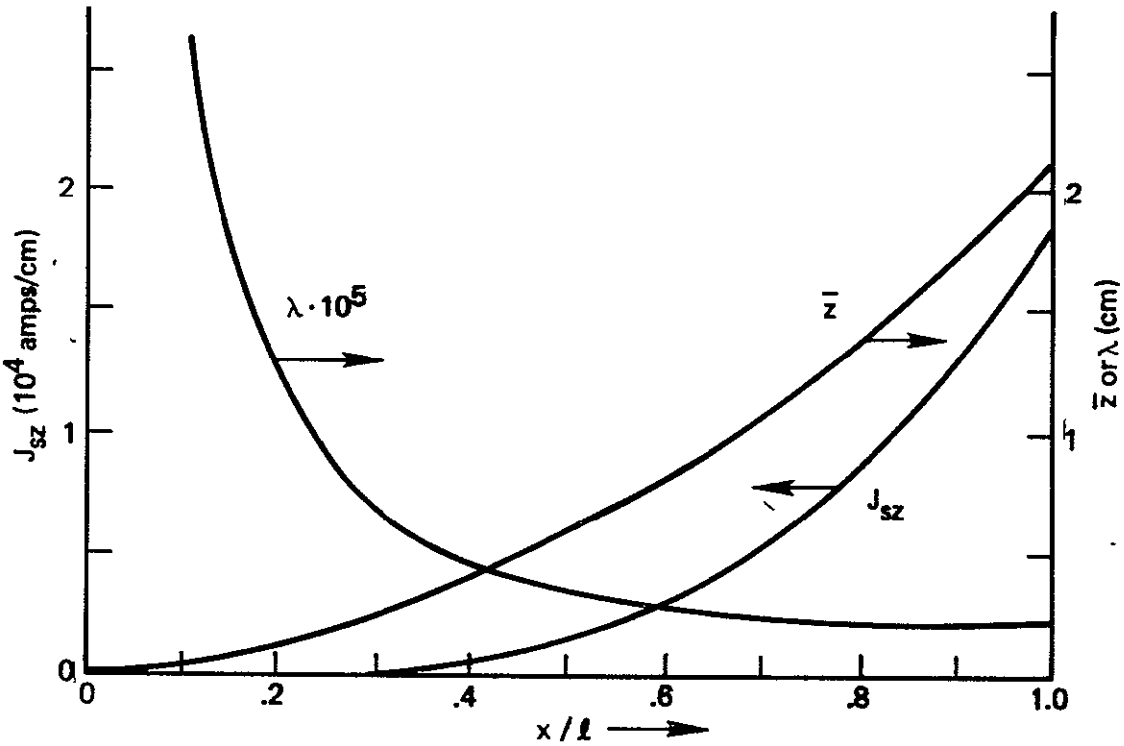

Figure 6. Debye Length (λ), J_{sz} and z (No Plasma Shielding)

Equating z to 4.6λ:

$$(x_1/\ell)^4 = 2.73 \cdot 10^{-6}, \quad x_1/\ell = 0.0407, \quad x_1 = 0.0102 \text{ cm}$$

Putting this value for x_1 into the equation for J_{sz} (x_1):

$$J_{sz}(x_1) = 3.04 \cdot 10^{4} \cdot 2.73 \cdot 10^{-6} = 0.083 \text{ A/cm}$$

The blowout to flashover current ratio G', taken to be the ratio of J_{sz} (x_1) to the maximum value of the plasma sheet current, J_s, (at x = ℓ) is then G' = J_{sz} (x_1)/J_s(ℓ) = 0.083/3.18 = 0.026 or 2.6 percent. Figure 7 shows z and 4.6λ plotted versus x/ℓ and their intersection at x/ℓ = 0.041.

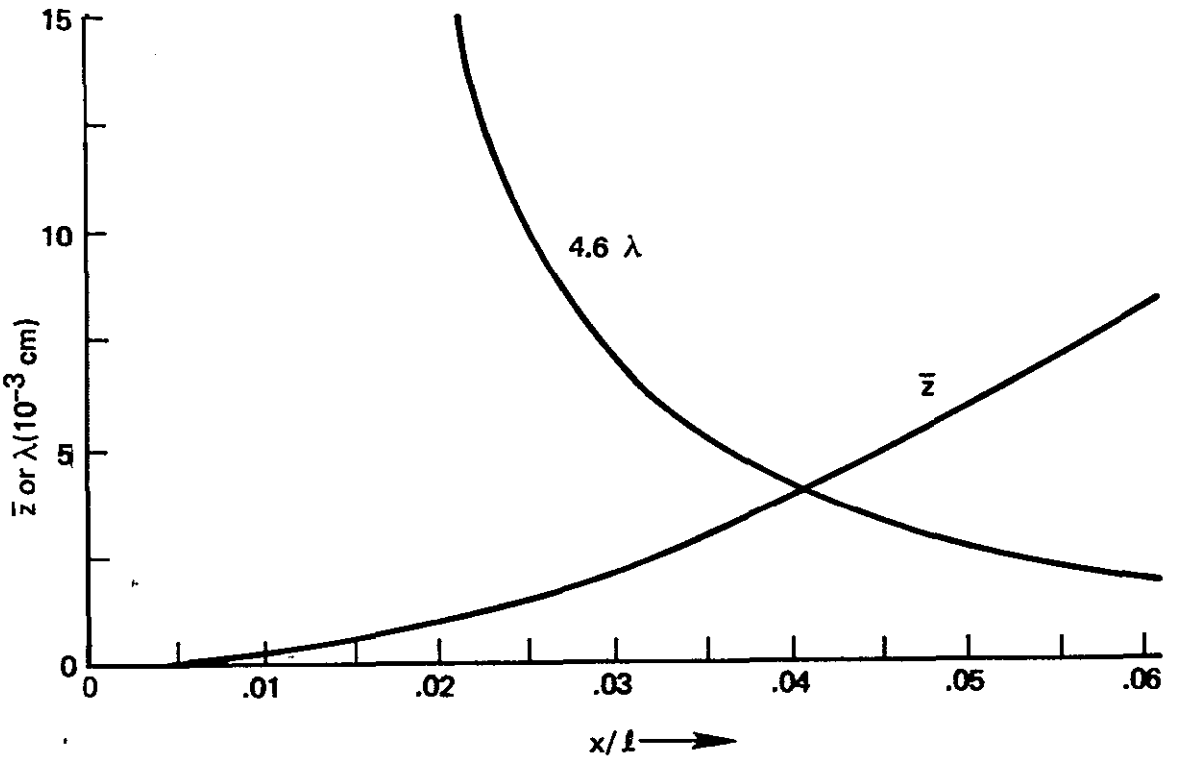

Figure 7. 4.6λ and z versus x/ℓ

A more nearly correct calculation for J_{sz} involves inserting the Debye shielding effect into the expression for v_z. We consider the shielding to apply to the external electric field by multiplying the potential by the exponential factor so that the corrected off-surface velocity, v_z^* is given by:

$$v_z^*(x_1) = \int_x^{x_1} \frac{2\,e\,V_m\,(1-\frac{x}{\ell})}{mav_b}\, e^{-\bar{z}/\lambda}\, dx.$$

Since the x values of consequence are very small ($x/\ell < 0.05$), the above expression may be simplified to

$$v_z^* \cong \frac{2eV_m}{mav_b} \int_x^{x_1} e^{-\bar{z}/\lambda}\, dx.$$

From the previous analysis,

$$\bar{z}/\lambda = 2.29\ (x/\ell)^2/(1.36\cdot10^{-6}x^2/\ell^2) = 1.68\cdot10^6\ (x/\ell)^4$$

Figure 8 shows v_z^* computed numerically and plotted as a function of x/ℓ. It starts at about 10^8 cm/sec at x=0 and drops to nearly zero by the time that x/ℓ = 0.04. The expression for J_{sz} now is

$$J_{sz}\ (x_1) = \int_0^{x_1} en\ (x)v_z^*\ (x)\ dx = \frac{2e^2V_mA}{mav_b} \int_0^{x_1} x^2\ dx \int_x^{x_1} e^{-1.68\cdot10^6(x/\ell)^4}\ dx$$

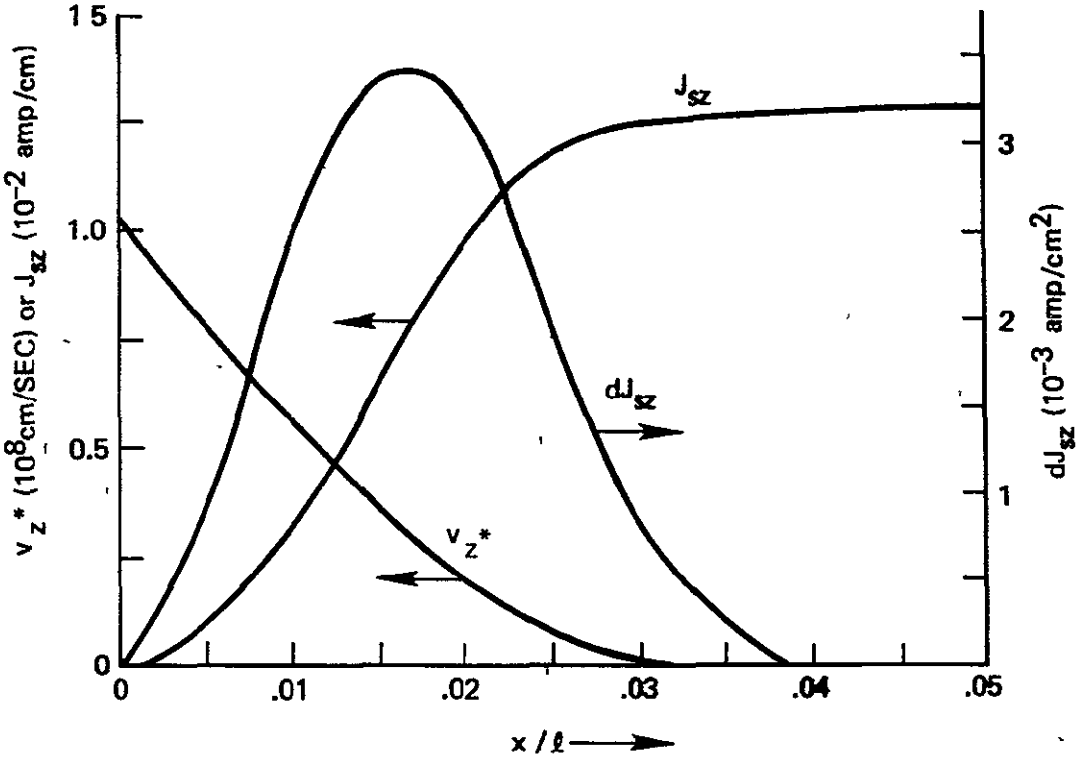

Figure 8. v_z^*, dJ_{sz} and J_{sz} Versus x/ℓ (Shielding by Plasma)

independent of the upper limit of the integral, x_1, for values of x/ℓ greater than about 0.04. This value is

$$J_{sz} = 0.0126 \text{ amp/cm},$$

and the ratio of blowout to flashover currents, G', is

$$G' = J_{sz}/J_z = 0.0126/3.18 = 0.40\%$$

Comparing Figures 7 and 8, it is clear that cutting off J_{sz} at $z = 4.6\lambda$ gives too large a value of x/ℓ and hence too large a value for J_{sz} and G'. From Figure 8, the "correct" values of the parameters for Figure 7 should have been:

$$x_1/\ell = 0.0254,\ \lambda = 2.11 \cdot 10^{-3}\ \text{cm},\ z = 1.47 \cdot 10^{-3}\ \text{cm},$$

$$z/\lambda = 1.43,\ \text{and}\ e^{-z/\lambda} = 0.24.$$

The Debye shielding effect has reduced J_{sz} from an excessively large value, 18,240 A/cm, to a value of 0.0216 A/cm. This latter value leads to a G' of 0.40 percent, which is much smaller than those that have been previously reported by us as well as by others. Another "correction" that should be applied is the fact that Debye shielding does cut off the electrons that are leaving the plasma sheet due to electric fields. However, the potential of the plasma remains unchanged, and thus the electric fields beyond the plasma remain unchanged. Therefore the "escaped" electrons continue to be accelerated by the surface potential even through their number is fixed. Since cutoff occurs at a very small x value ($x/\ell = 0.0254$, $\ell = 0.25$ cm), the accelerating potential is very nearly:

$$V_m + V_r = 2500 + 2500 = 5000\ \text{volts}$$

Where V_m is the maximum voltage change, and V_r is the remaining voltage after the discharge.

The surface current density, J_{sz}, by the time the escaped electrons have traversed the whole arcing source, then is given by:

$$J_{sz} = Nev_z \text{ where } v_z = \left[\frac{2e(V_m + V_r)}{m}\right]^{0.5} = 4.19 \cdot 10^9\ \text{cm/sec}$$

N is the number of released electrons per cm^2, and is obtained from n(x) by integration from x = 0 to x = x_1 or $x/\ell = 0.0254$:

$$n(x) = 3.25 \cdot 10^{16} x^2 \text{ electrons/cm}^3$$

$$N = \int_0^{x_1} n(x)dx = 2.774 \cdot 10^9 \text{ electrons/cm}^2$$

Therefore:

$J_{sz} = Nev_z = 1.86$ amp/cm, and $G' = J_{sz}/J_x = 1.86/3.18 = 58.5\%$

Since the electrons, in increasing their kinetic energy by 5 keV, have been accelerated in the x-direction as well as the z-direction, the use of the full 5 keV in calculating J_{sz} is not valid. A particle pushing trajectory calculation for the electrons in the presence of existing electric fields is required. Figure 9 is the author's conception of how the equipotential and electric field lines should appear. The escaping electrons do accelerate through the full 5 kev but the current, properly, should not be termed J_{sz}. From the "guessed" field configuration it appears that the blowout currents should be travelling at about a 45 degree angle to the surface in the direction of the ignition point.

EFFECT OF SPACECRAFT POTENTIAL ON G'

The importance of external electric fields in determining the blowout to flashover current ratio, G' has been discussed in the previous section. In the analysis, the change in the surface electric field due to the arc discharge was taken into account by the space and time dependence of the surface potential, V_s. However, the reference voltage, the spacecraft potential, V_0, was assumed to be constant at zero volts. In orbit, the blowout of the arc discharge electrons must be compensated by the recollection of an equal number of electrons if the spacecraft potential is to be unchanged. Any inequality between blowout

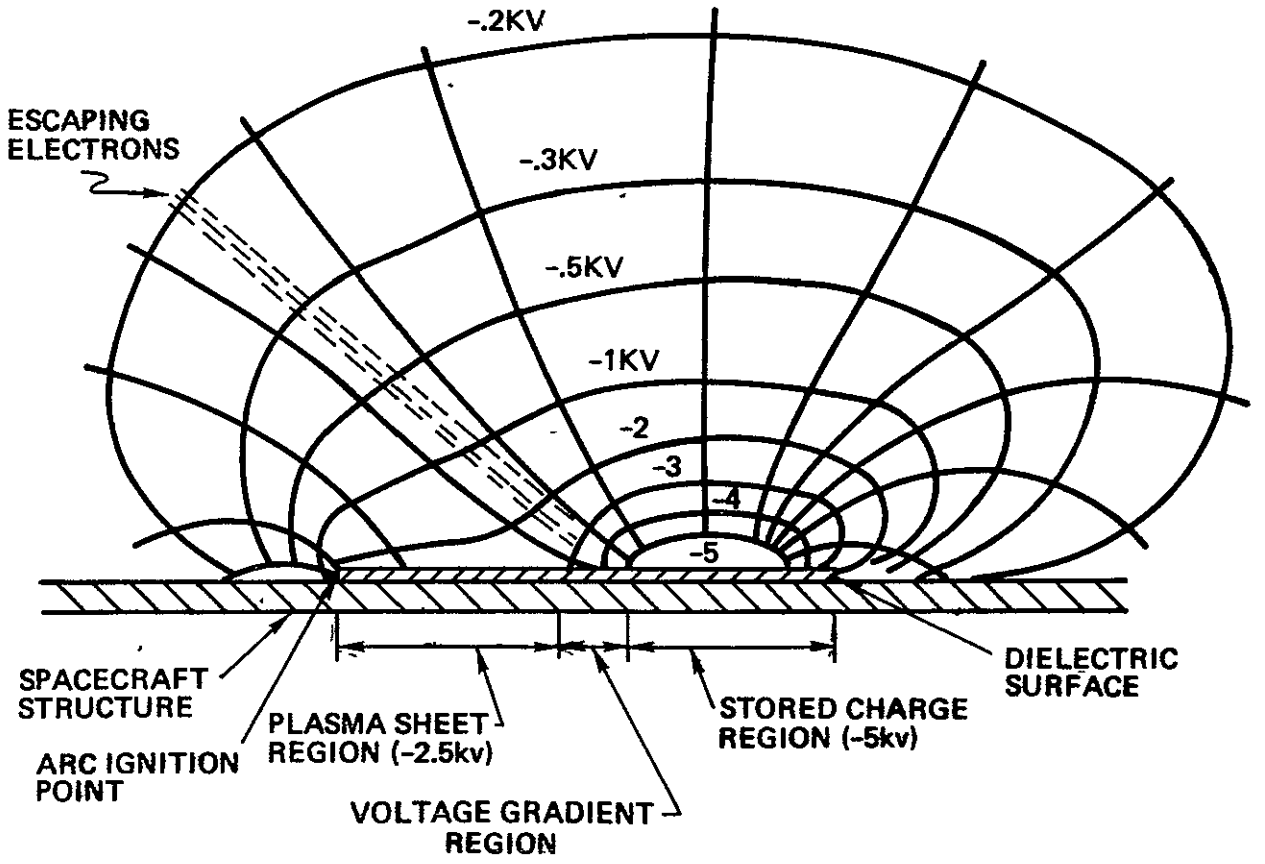

Figure 9. Brushfire Equipotential and E-field Lines

currents and return currents must be "made up" by displacement currents in the following charge balance equation:

$$C_s\Delta(V_s + V_o) + \int_o^t I_z dt = C_o\Delta V_o + \int_o^t I_r dt$$

In the above equation C_s is the capacitance of the arcing element to the remainder of the spacecraft (or to space), and C_o is the capacitance of the spacecraft to space. I_z is the blowout current from the arcing element, and I_r is the replacement current to the remainder of the spacecraft. Taking the derivative of the equation gives the current balance equation which must be satisfied during the arc discharge:

$$C_s \frac{d}{dt}(V_s + V_o) + I_z = C_o \cdot \frac{d}{dt} V_o + I_r$$

I_z is the blowout current density, J_{sz}, computed in the preceding section, multiplied by an appropriate width dimension. I_r is the integral of all of the replacement current densities collected over the entire exposed surface of the spacecraft. As I_r is collected, it returns to the arcing element via various structural paths on the spacecraft. Obviously, the structural current density is low at remote portions of the spacecraft, and becomes greater as the current flow paths converge towards the arcing element. For this reason, it is to be expected that the potential victims of EMI closest to the arcing source would be the most susceptible.

The point here is that V_o adjusts itself in a time dependent manner to assure that the current continuity equation is satisfied. Since electrons are leaving, V_o will go more positive. If, as assumed, V_o is initially near zero, V_o will become absolutely positive and attract electrons from the environment surrounding it, and repel ions. How far positive it becomes is a function of the surface area of the whole spacecraft, and the accessibility of replacement electrons. The problem is similar to that of computing the spacecraft charging potentials, but on a much shorter time scale--tens of ns rather than minutes.

The availability of electrons in the ambient plasma may be estimated as follows: Assume that electrons may take as long as 1 μs to reach the spacecraft,

a sphere of radius, R, of one meter at a potential, V_o, of 1 kV. The radius, r, from which electrons can arrive at the surface in 1μs is given by:

$$\frac{dr}{dt} = v(r) = \left[\frac{2e}{m} V(r)\right]^{0.5} = \left[\frac{2e}{m} \cdot \frac{Q}{4\pi\varepsilon_o r}\right]^{0.5}$$

$$\frac{2}{3}(r^{1.5} - R^{1.5}) = \frac{2e}{m} \cdot \frac{Q}{4\pi\varepsilon_o} t = \frac{2e}{m} V_o R \quad {0.5}_t$$

$$r = \left\{\frac{3}{2}\left[\frac{2e}{m} V_o R\right]^{0.5}{}_t + R^{1.5}\right\}^{2/3} = 9.47 \text{ meters for } t = 1\mu s.$$

For t = 100 ns, r is 2.44 meters. Assuming that the electron density is $1/cm^3$, a spherical volume, for 1μs, contains $3.20 \cdot 10^{10}$ electrons or a charge of $5.12 \cdot 10^{-9}$ coulombs. By comparison, a 10 cm wide arcing source, grounded, would have a current I_z of 19 A, and would emit, in 1μs, a charge of $1.9 \cdot 10^{-5}$ coulombs. This is more than three orders of magnitude more charge than is available.

Another calculation which indicates that the current available is insufficient to "clamp" V_o, utilizes the Langmuir - Mott Smith equation for the attraction of electrons at a Maxwellian temperature, T, to a conducting sphere of radius R:

$$I = 4\pi R^2 J_o\left(1 + \frac{V_o}{T}\right) = 22.5 \cdot 10^{-4} \text{ A}$$

for R = 1, V_o = T = 1 kV, and J_o = 1 na/cm^2 = 10^{-5} A/m^2

a "resistance," R_o, may be calculated from $R_o = \frac{V}{I} = 4 \cdot 10^6$ ohms.

The solution for the blowout current, I_z, in the presence of a variable time dependent V_o may be obtained from the following

$$I_z = J_{sz}w;\ J_{sz} = Nev_z;\ v_z = \sqrt{\frac{2eV_s}{m}},\ V_s = V_r - V_o$$

$$V_o = I_r R_o,\ V_o = \frac{1}{C_o}\int I_c dt.$$

In the above equations, w is the width of the arcing source, N is the number of electrons that have been ejected before the Debye shielding cutoff, V_s is the surface potential, V_r is the remaining voltage after the discharge (2500 V), I_r is the resistive replacement current flowing in R_o, and I_c is the displacement current flowing in the capacitance of the spacecraft to space, C_o. The electrical circuit is shown below in Figure 10.

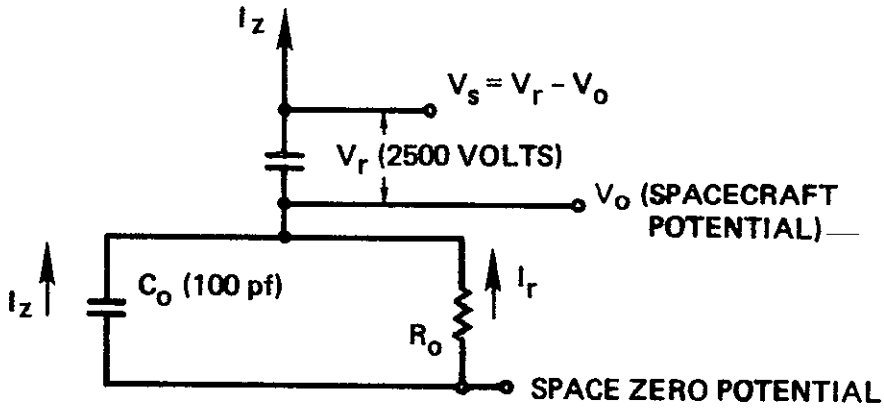

Figure 10. Electrical Circuit Defining I_z and $V_o(t)$

The above equations lead to the following result:

$$\frac{t}{\tau} = \frac{1}{p-q}\,\ln\left(\frac{x-p}{x-q}\cdot\frac{1-q}{1-p}\right) - \ln\left(\frac{x^2+Bx-1}{B}\right)$$

where p and g are roots of $x^2 + Bx - 1 = 0$,

$$\tau = R_o C_o,\ x = I_z/I_{zo},\ I_{zo} = A/V_r^{0.5} = 1.316 \cdot w(cm) \text{ amperes},$$

$$A = Ne(2e/m)^{0.5} \cdot 100\ w = 0.0236\ w,\ B = R_o I_{zo}/V_r = w \cdot R_o/1900.$$

Figures 11 and 12 show $I_z(t)$ and $V_0(t)$ for w = 10 cm. and various values of R_0. The time constant, $\tau = R_0C_0$, varies from 1 ns to 1 μs on the assumption that the C_0 is 100 pf. For R_0 large, V_0 approaches V_r and I_z decreases because V_s becomes small. For R_0 small, as in many vacuum tank experiments, V_0 never gets very large, and I_z remains near I_{zo}. Figure 13 shows the steady state I_z and V_0 plotted as a function of R_0.

The preceding discussion about R_0 indicates that it is quite large. For the approximation that $I_r \ll I_c$, the solutions for I_z and V_0 are:

$$\therefore I_z = I_{zo}\,[1-t/(2\tau_0)],\quad V_0 = V_r[1-(1-\frac{t}{2\tau_0})^2].$$

I_z decreases linearly to zero in a time $2\tau_0 = 2C_0V_r/I_{zo} = 3.8\cdot10^{-7}/w$ seconds or 38 ns for w = 10 cm. V_0 rises parabolically to V_r in the same time period. For a 10 cm square sample, then, the brushfire propagates according to our model in a time, t, of:

$$t = \frac{10\text{ cm}}{2.45\cdot10^7\text{ cm/sec}} = 408\text{ ns}\ .$$

I_z, however, lasts for only 38 ns or about 10 percent of the discharge time with an "average" G' of 29 percent rather than the peak value of 58 percent. Thus, the in-orbit G' is of shorter duration and of lower average magnitude as compared to a laboratory determination with R_0 shorted to ground. A proper laboratory experiment should incorporate a high R_0 but should also include an appropriate C_0.

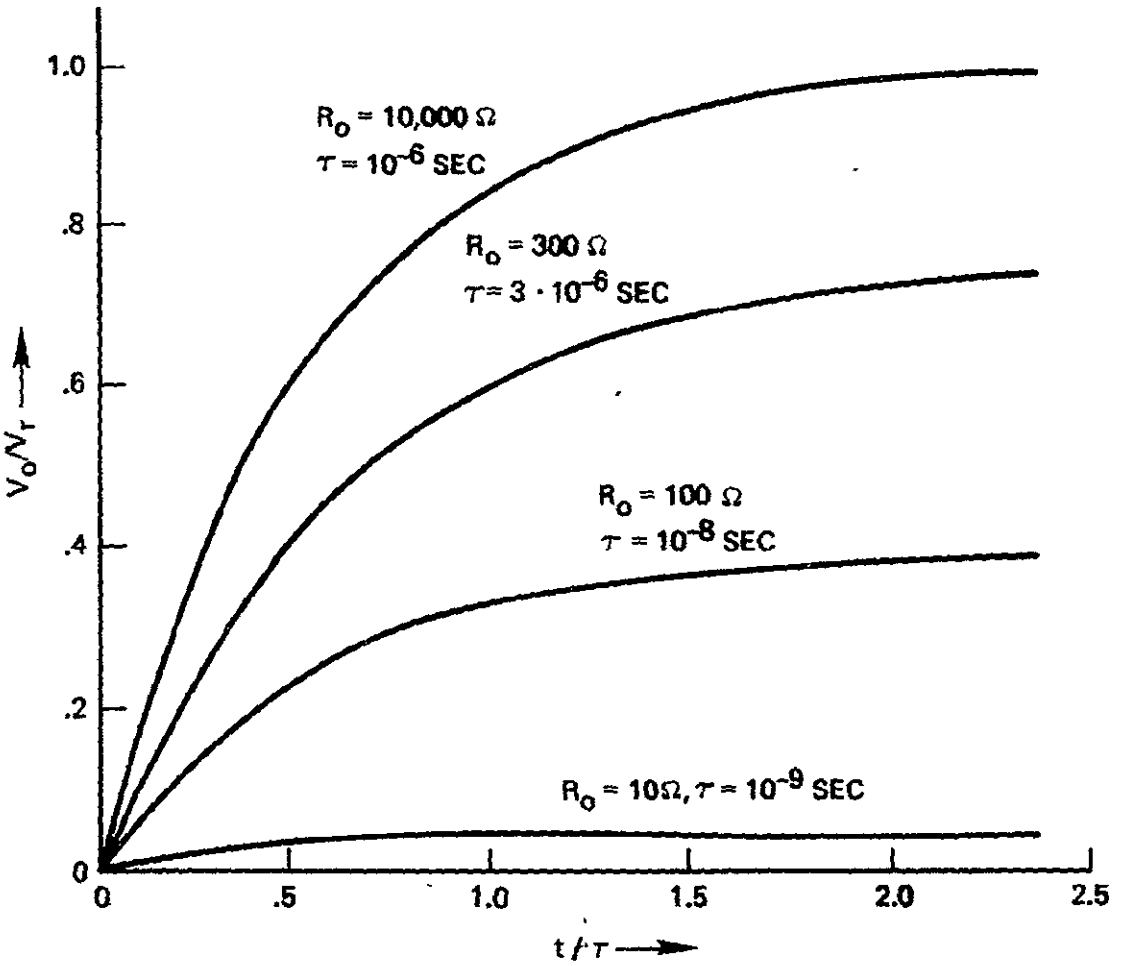

Figure 11. V_o/V_r as a Function of t/τ

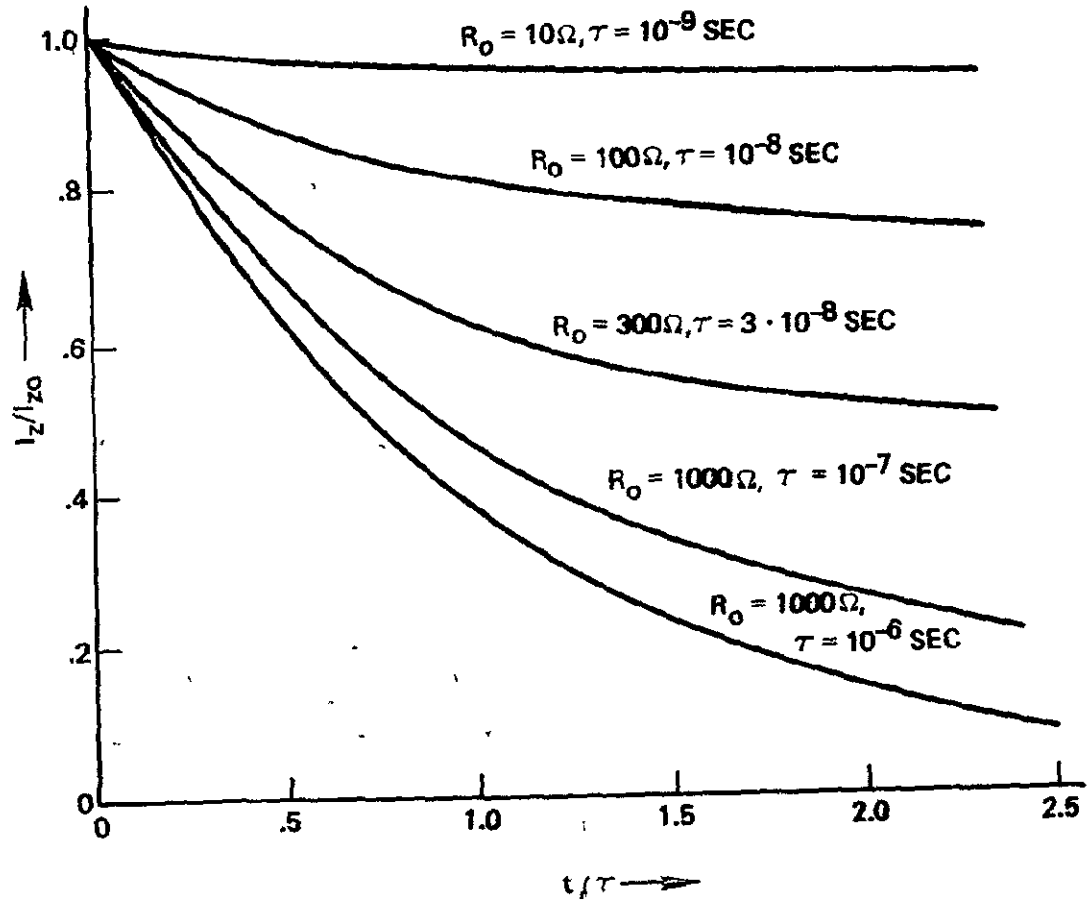

Figure 12. I_z/I_{zo} as a Function of t/τ

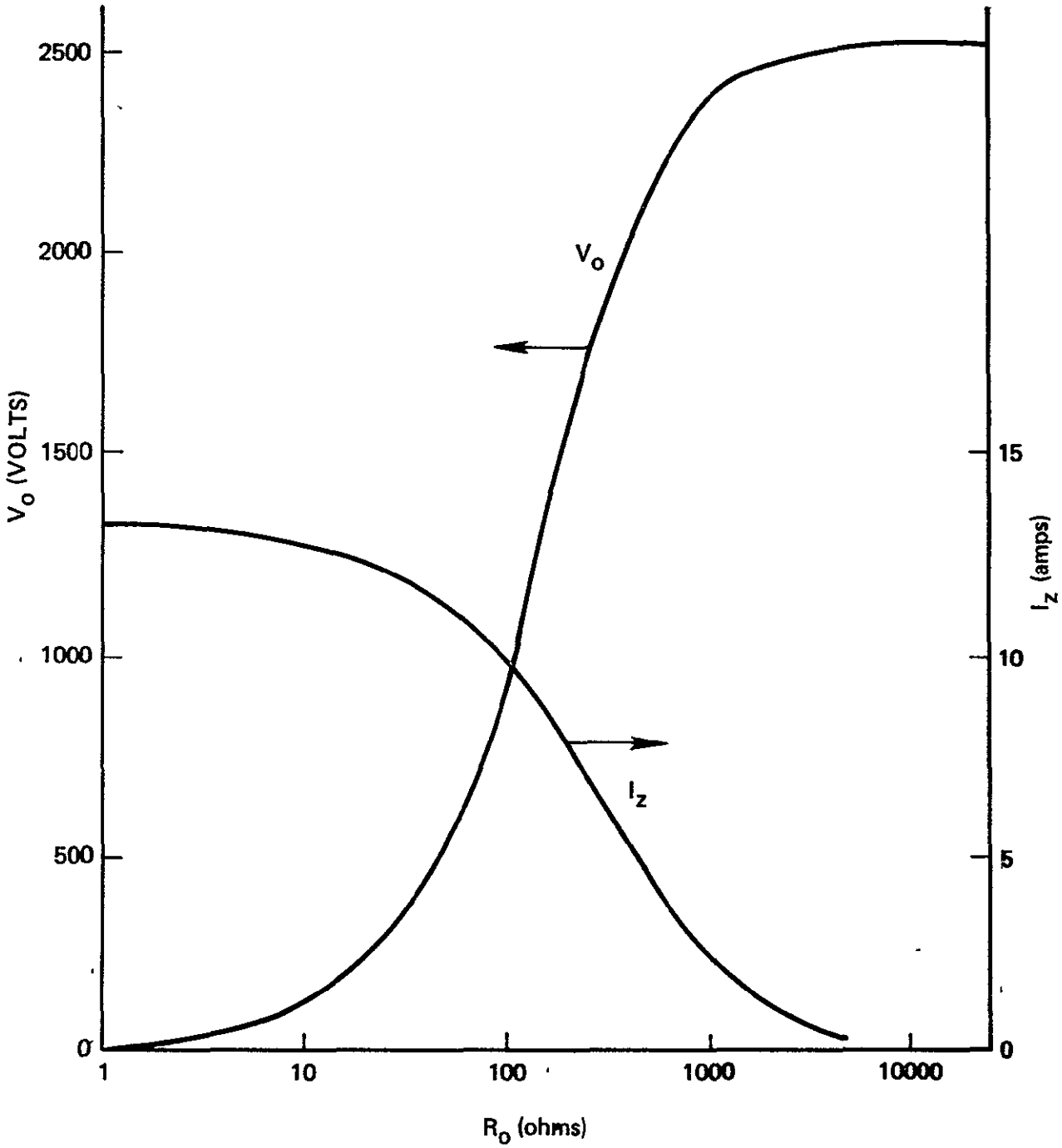

Figure 13. Steady State V_o and I_z Versus R_o for W = 10 cm

LIMITING MECHANISMS ON BRUSHFIRE PROPAGATION

The question arises as to whether some processes exist whereby the brushfire propagation might be limited. The paper by Aron and Staskus[9] seems to indicate that propagation continues for samples as large as 5058 cm^2. Their samples (4 mil teflon) were laid on an aluminum plate that was 0.313 cm thick. This seems to indicate that the plasma sheet resistance, the part behind the voltage gradient region, is not a problem.

In some applications, the dielectric sheet with the vacuum deposited aluminum (VDA) is not over a good conducting ground plane. In these cases the surface resistivity of the VDA film becomes important. Typical values are in the order of 1 ohm-per-square, but this may be exceeded by more than a factor of 10 after handling and during the installation process. A 100 cm long sample, then will develop more than 1 kV with a 1 A/cm arc discharge surface current density, J_s. If one considers then that arc discharge surface currents are really not 1-dimensional, but rather flow from the whole surface towards a single breakdown point, the surface current density increases greatly and therefore the voltage drop may become comparable to the voltage across the dielectric before breakdown. Although the brushfire propagation as developed depends only on the electric field at breakdown, E_b, rather than the voltage, V_b, a dependence on the latter may develop in a more critical analysis.

Figure 14 shows an example of a set of surface voltage measurements before and after an arc discharge. The discharge clearly did not wipe off the stored charge uniformly. The charge seems to have flowed towards the edge at which breakdown occurred, but was slowed down as the distance from that location increased. This particular sample was mounted on an aluminum substrate. However, the VDA was sandwiched with a Kapton sheet between the VDA and the aluminum substrate. Thus, resistive currents were forced to flow through the VDA rather than through the substrate.

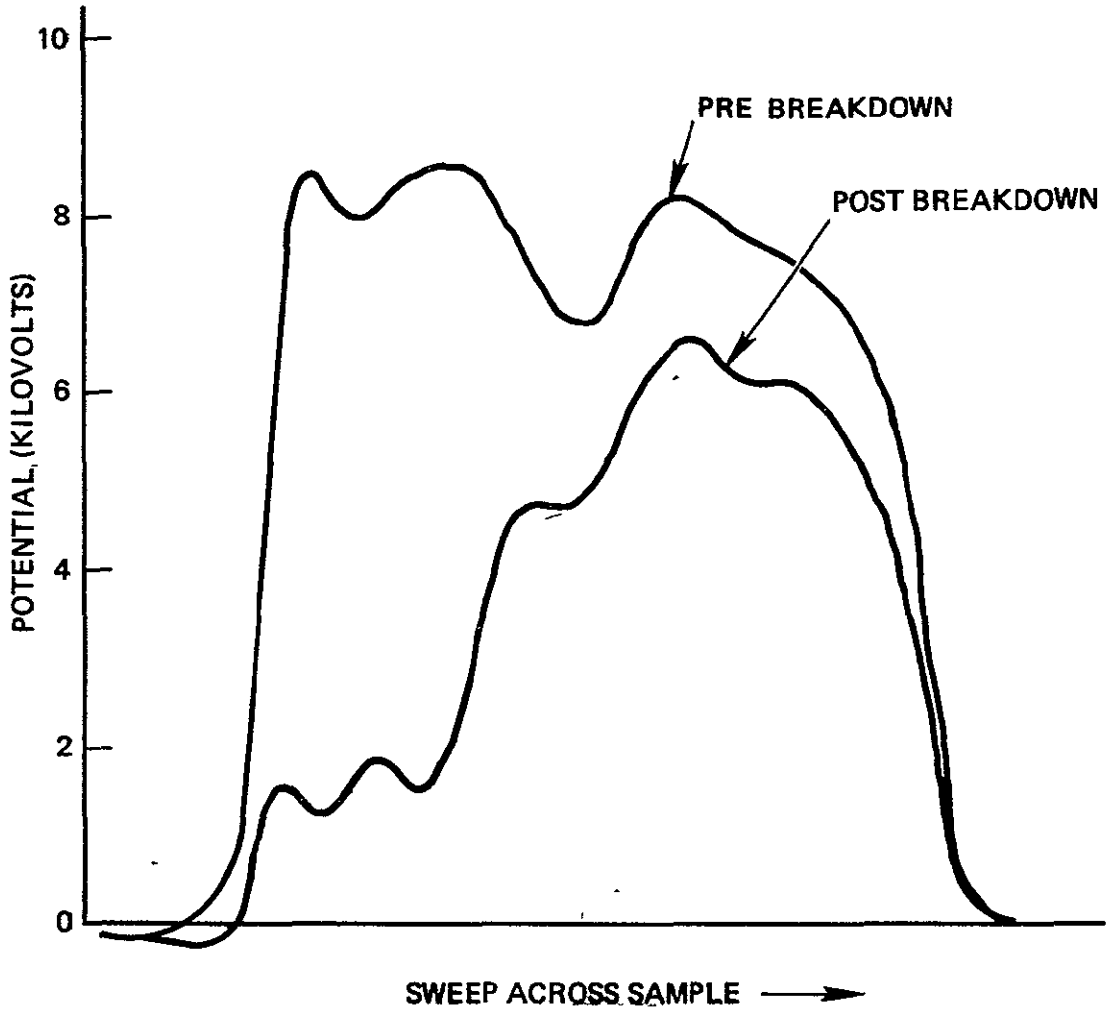

Figure 14. A Potential Profile of 6 x 6 inch Kapton Laminate Sample Before and After a "Relatively" Low Voltage Breakdown Near Edge of Sample

SUMMARY AND CONCLUSIONS FROM THE BRUSHFIRE ARC DISCHARGE MODEL ANALYSIS

Summarizing the analytical development of the arc discharge brushfire propagation model should begin with noting the many deficiencies. The first is that the analysis is 1-dimensional while most arcing configurations are 2-dimensional. Thus, no account is taken of the "sidewards" propagation effect both as it affects the brushfire wavefront steepness requirements, and the greater concentration of plasma sheet currents as they converge towards the arc initiation point. There are many assumptions which may or may not be justified such as the ignoring of thermal conductance, and the assumption that the plasma thruster data, $8.32 \cdot 10^{-6}$ grams per joule of material ablated, was applicable. The assumption of a plasma sheet thickness, 1 percent of the length of the voltage gradient region, was not derived from physical principles, but rather, from an idea of what a "sheet" should be. The gram-molecular-weight of the dielectric material, 16, also was a guess, and the specific heat depends on this number. The plasma properties which would clearly identify the time dependent roles of electrons, ions and neutrals have not been carefully treated. In particular, the inertial/collisional role of ions in determining the brushfire velocity should be included in the basic equations so that the velocity is consistent with the other physical processes involved. The areas of improvements that are needed in the present analysis are summarized below. As stated previously, there are many improvements that can be made in the analytical model as presented here, and it is hoped that this work will provide some insight into how a more nearly correct model should be formulated.

- Many assumptions need to be examined
  - Thermal conductivity, mass ablated, plasma sheet thickness, etc
- More physical processes need to be included
  - Role of ions in determining brushfire velocity, ablation, ionization and radiation processes
  - "Mechanical" processes of particle acceleration and collisions

- Self-consistent solutions are needed
  - Computerized approach
- Model should be expanded to include the 2-dimensional problem.

The analysis has provided a first-cut solution to voltage, current, plasma density, temperature and resistivity profiles associated with the plasma sheet of a propagating brushfire wavefront. The flashover surface current density associated with the discharge rises linearly with distance away from the head of the wavefront as

$$J_{sx} = Cv_b V_m x/\ell.$$

At the bottom of the voltage falloff region J_s reaches a maximum value:

$$J_{sx} = Cv_b V_m = 3.18 \text{ A/cm, for } V_m = 2500 \text{ V}$$

which is proportional to the breakdown voltage V_m. The duration of the arc discharge is simply the sample size (linear dimension) divided by the brushfire propagation velocity, v_b. To the extent that the theory is applicable to the 2-dimensional case, the duration should be proportional to the square-root of the area. The following combination of parameters for a given dielectric material must be a constant:

$$\left(\frac{cg}{h}\right)^{3/2} Cv_b,$$

where c is the specific heat, g is the mass ablated per joule, h is the fraction of the power expended in raising the plasma temperature, C is the dielectric capacitance per unit area and v_b is the brushfire propagation velocity. The above combination of parameters must be a constant for a given dielectric material except that C also depends on the thickness. Thus, increasing the thickness decreases C, and hence v_b should decrease correspondingly.

Another result of the analysis is that magnetic V X B forces are much less effective in producing blowout currents than electric field forces. Debye shielding of electric fields limits the blowout electrons to the very tip of the brushfire wavefront. An analogy for the blowout current would be the smoke puffing out of the smokestack of the locomotive of a train as

it moves forward -- not the whole train burns. The blowout electrons are accelerated by the chargeup potentials and the ratio of blowout to flashover currents, G', has been calculated to be

$$G' = 58.5\%$$

This value of G' takes into account the experimentally observed fact that about one-half of the stored charge (1/4 of the stored energy) remains after the discharge. If the fraction of remaining charge were lower, the flashover current would be proportionately larger, but the blowout current would be about the same since the number of electrons remains nearly the same and the total accelerating potential also remains the same. Thus G' would decrease, but only by a factor of about two. From the results of the above analysis, G' is independent of the size of the arcing source. The surface voltage at breakdown affects G' as its square-root.

The dependence of the blowout current, and therefore G', on the spacecraft potential is rather drastic, and depends on the capability of the spacecraft to collect return currents, either from the surrounding plasma or from the blowout current itself. The spacecraft potential rises in order to compensate for the blown off charges and to collect the required number of electrons, or to make up the deficiency via displacement currents. Because the spacecraft capacitance to space, C_o, is small ($\sim$100 pf), the accelerating potential for the blowout electrons is quickly cancelled -- in 38 ns out of a total of 408 ns for the whole brushfire process to take place -- in our example of a 10 cm square arcing source. Most laboratory experiments in the past have grounded the arcing source to the vacuum system ground through a low resistance of a few ohms. A more proper simulation of in-orbit conditions for arc discharges would be to increase the grounding resistance to greater than 10,000 ohms, and add a parallel capacitance of about 100 pf. The conclusions resulting from the brushfire model analysis are summarized below:

- The flashover surface current density, J_{sx}, (3.18 A/cm), is proportional to V_m.
- $\left(\frac{h}{cg}\right)^{3/2} \cdot Cv_b$ is a constant (see text for definition of parameters).
- The discharge duration is proportional to the length of a 1-dimensional source.

- And is proportional to the square-root of the area of a 2-dimensional source.

- The blowout surface current density, J_{sz}, (1.86 A/cm), is proportional to the square-root of the surface potential at breakdown.

- G' (58.5 percent) is independent of the area of the arcing source.

  - Depends on electric field forces; magnetic forces are negligible.

- G' is grossly affected by how the spacecraft potential varies during the discharge.

  - J_{sz} is cut off by positive spacecraft potentials (smaller net potentials) during the discharge.

- Laboratory measurements of G' should take into account conditions on orbit.

The author acknowledges the contributions of two colleagues to the present analysis of the arc discharge brushfire propagation model. M. J. Sellen Jr. coined the term, "brushfire," and formulated the initial concepts on the steepness requirements for a propagating wavefront. R. L. Wax critiqued many aspects of the model. In particular, his insight into the plasma physical processes was invaluable.

REFERENCES

(1) R. Leadon and J. Wilkenfeld, "Model for Breakdown Process in Dielectric Discharges," Spacecraft Charging Technology - 1978. NASA Conference Publication 2071, AFGL-TR-79-0082.

(2) I. Katz, M. J. Mandell, D. E. Parks and G. W. Schnuelle, "A Theory of Dielectric Surface Discharges," 1980 IEEE Annual Conference on Nuclear and Space Radiation Effects, July 1980.

(3) A. Rosen, N. L. Sanders, J. M. Sellen, Jr. and G. T. Inouye, "Final Report - Effects of Arcing Due to Spacecraft Charging on Spacecraft Survival," NASA/LeRC Report No. CR 159593, November 14, 1978.

(4) G. T. Inouye and J. M. Sellen, Jr., "A Proposed Mechanism for the Initiation and Propagation of Dielectric Surface Discharges," Proc. 1978 Symposium on Effects of the Ionosphere on Space and Terrestrial Systems.

(5) K. G. Balmain "Scaling Laws and Edge Effects for Polymer Surface Discharges," Spacecraft Charging Technology - 1978, NASA Conference Publication 2071, AFG-TR-0082.

(6) L. Spitzer, Jr., "Physics of Fully Ionized Gases" Interscience Publishers, Ltd., 1956, pp. 82-86.

(7) R. J. Vondra, K. Thomasson and A. Solbes, "Analysis of Solid Teflon Pulsed Plasma Thruster," J. Spacecraft and Rockets, Volume 7 No. 12, December 1970.

(8) J. Millman and S. Seeley, "Electronics" Second Edition McGraw-Hill Book Co., Inc., 1951, 111-112.

(9) P. R. Aron and J. V. Staskus, "Area Scaling Investigations of Charging Phenomena," Spacecraft Charging Technology - 1978, NASA Conference Publication 2071, AFGL-TR-0082.